EUMETSAT

AC SAF

ATMOSPHERIC COMPOSITION MONITORING

OPERATIONS REPORT

Issue 1/2022 rev. 2

Reporting period: January – June 2022

Authors			
Prepared by			
NAME			**INSTITUTE**
Jari Hovila			FMI
Contributions			
NAME			**INSTITUTE**
Jari Hovila, Jukka Kujanpää, Kaisa Lakkala			FMI
Axel Schmidt, Sander Slijkhuis, Pieter Valks			DLR
Olaf Tuinder, Robert van Versendaal			KNMI
Helge Jønch-Sørensen			DMI
Katerina Garane, MariLiza Koukouli			AUTH
Jeroen van Gent, José Granville, François Hendrick, Jean-Christopher Lambert, Bavo Langerock, Gaia Pinardi, Tijl Verhoelst			BIRA-IASB
Andy Delcloo			KMI
Peggy Tesche-Achtert			DWD
Anne Boynard, Cathy Clerbaux, Maya George, Camille Viatte			LATMOS
Rosa Astoreca, Pierre-François Coheur, Daniel Hurtmans, Catherine Wespes			ULB
Carlos Vicente			EUMETSAT
Approved by			
AC SAF Technical Manager	Jari Hovila / FMI	07/12/2022	*Signature*

Document change log

Revision	Date	Description of change
1	25/10/2022	Initial revision
2	07/12/2022	List of abbreviations: updated Sections 3.1.1 and 3.1.2: Cross-references corrected Section 7.1.1: Third paragraph added Section 7.2: Invalid cross-reference removed Section 7.3: Added description of the FRM4DOAS analysis chain Section 7.6.1: Statement of product quality/accuracy remaining stable during the reporting period added Section 7.7: Two paragraphs modified to indicate that IASI NRT O3 and HNO3 products have been released as operational Tables 3.1: Product IDs corrected Table 3.3: Product IDs corrected Table 3.5: The word “successful” removed from the title of EOWEB order statistics Table 7.1: Metop-A NRT total ozone product removed Table 7.3: Metop-A NRT tropospheric ozone product removed Table 7.10: Metop-A NRT trace gas products removed Table 7.13: Metop-A NRT ozone profile product removed Table 7.16: Metop-A NRT aerosol products removed Table 10.1: Outdated contents removed

List of abbreviations

AC SAF	Satellite Application Facility on Atmospheric Composition Monitoring
ARP	Absorbing Aerosol Index from PMDs data product
ARP-A	Absorbing Aerosol Index from PMDs data product from Metop-A
ARP-B	Absorbing Aerosol Index from PMDs data product from Metop-B
ARP-C	Absorbing Aerosol Index from PMDs data product from Metop-C
ARS	Absorbing Aerosol Height data product
ARS-A	Absorbing Aerosol Height data product from Metop-A
ARS-B	Absorbing Aerosol Height data product from Metop-B
ARS-C	Absorbing Aerosol Height data product from Metop-C
ATMOS	Atmospheric Parameters Measured by in-Orbit Spectroscopy (DLR data service)
ATO	Assimilated Total Ozone
AUTH	Aristotle University of Thessaloniki
BIRA-IASB	Belgian Institute for Space Aeronomy
BrO	Bromine Oxide
CDOP	Continuous Development and Operations phase
CO	Carbon Monoxide
DLR	German Aerospace Center
DMI	Danish Meteorological Institute
DWD	German Weather Service
ECMWF	European Centre for Medium-Range Weather Forecasts
EDC	EUMETSAT Data Centre
EDD	Erythemal Daily Dose
EOWEB	Earth Observation on the WEB
EPS	European Polar System
EUMETCast	EUMETSAT’s primary dissemination mechanism for the near real-time delivery of satellite data and products
EUMETSAT	European Organisation for the Exploitation of Meteorological Satellites
FMI	Finnish Meteorological Institute
GOME	Global Ozone Monitoring Experiment
H2O	Water Vapour
HCHO	Formaldehyde
HR	High resolution
KMI	Royal Meteorological Institute of Belgium
KNMI	Royal Netherlands Meteorological Institute
L1b	Level 1b data product
L1c	Level 1c data product
L2	Level 2 data product
L3	Level 3 data product

LATMOS	Laboratoire Atmosphères, Milieux, Observations Spatiales
LER	Lambertian-equivalent reflectivity data record
NHP	Near Real-time High-resolution Ozone Profile data product
NO2	Nitrogen Dioxide
NRT	Near Real-time
NTO	Near Real-time Total Column data product
NUV	Near Real-time UV index data product
O3	Ozone
O3M SAF	Satellite Application Facility on Ozone and Atmospheric Chemistry Monitoring
OHP	Offline High-resolution Ozone Profile data product
OHP-A	Offline High-resolution Ozone Profile data product from Metop-A
OHP-B	Offline High-resolution Ozone Profile data product from Metop-B
OHP-C	Offline High-resolution Ozone Profile data product from Metop-C
OEM	Optimal Estimation Method
OPERA	Ozone Profile Retrieval Algorithm
OTO	Offline Total Column data product
OUV	Offline Surface UV data product
OUV-A	Offline Surface UV data product from Metop-A
OUV-AB	Offline Surface UV data product from Metop-A and Metop-B
OUV-B	Offline Surface UV data product from Metop-B
OUV-BC	Offline Surface UV data product from Metop-B and Metop-C
PDU	Product Dissemination Unit
PGE	Product Generation Element
PMD	Polarisation Measurement Device
RD	Reference Document
RMS	Root Mean Square
RMSE	Root Mean Square Error
SO2	Sulphur Dioxide
TOC	Total Ozone Column data product
TrOC	Global Tropospheric Ozone Column data product
TTrOC	Tropical Tropospheric Ozone Column data product
ULB	Université libre de Bruxelles
UTC	Coordinated Universal Time

TABLE OF CONTENTS

1. Introduction

1.1. Scope

The scope of this document is to summarise the operational activities concerning the products in operation and the associated services during the reporting period to see that the general requirements applicable to these services and products of the AC SAF [RD1, RD2, RD3] are fulfilled. Intended readers of this document are the members of AC SAF project team, Review Board of the annual Operations Review, AC SAF Steering Group and EUMETSAT OPS/WG as well as the users of the AC SAF products.

Operations Reports include information about product availability/timeliness, quality assurance, website usage, and delivery statistics. Main events, major anomalies and software/hardware updates are reported also. AC SAF Operations Report is published twice a year.

1.2. Reporting period

This Operations Report covers the period January – June 2022.

1.2.1. Highlights

New products

- 27 January: Metop-C IASI near real-time CO and SO_2 products were upgraded from 'demonstrational' to 'operational' status
- 20 April: NRT UV index products (clear-sky and cloud-corrected), based on Metop-C data, available
- 18 May: NRT IASI HNO_3, total O_3 and O_3 profile products upgraded to ‘operational’ status

New data records

- 14 April: GOME-2A/B high-resolution ozone profile data record released
- 2 May: Tropospheric BrO data record released

1.3. Reference documents

Table 1.1. Operations Report reference documents

Reference	Title	Issued	Reporting period
RD1	Product Requirements Document (SAF/AC/FMI/RQ/PRD/001)	29/10/2021	N/A
RD2	Service Specification (SAF/AC/FMI/RQ/SESP/001)	22/09/2020	N/A
RD3	EUMETSAT Operational Services Specification (EUM/OPS/SPE/09/0810)	14/08/2015	N/A
RD4	EPS End User Requirements Document (EPS/MIS/REQ/93001)		N/A

Reference	Title	Issued	Reporting period
RD5	O3M SAF Validation Report for NRT, offline and reprocessed total ozone columns	11/12/2015	January 2007 – December 2014
RD6	AC SAF Validation Report for NRT, offline, reprocessed and level 3 total/tropospheric NO2 columns	10/11/2017	Metop-A: January 2007 – July 2015 Metop-B: January 2013 – July 2015
RD7	O3M SAF Validation Report for Metop-A NRT and offline coarse/high-resolution ozone profiles	20/02/2012	January 2007 – May 2011
RD8	O3M SAF Validation Report for Metop-B NRT and offline coarse/high-resolution ozone profiles	30/06/2013	December 2012 – April 2013
RD9	O3M SAF Validation Report for Metop-B NRT UV indexes	27/05/2013	May 2013
RD10	O3M SAF Validation Report for NRT, offline and reprocessed total SO2 columns	09/12/2015	January 2007 – December 2014
RD11	O3M SAF Validation Report for offline and reprocessed total BrO columns	09/12/2015	January 2007 – December 2014
RD12	O3M SAF Validation Report for NRT, offline and reprocessed total HCHO columns	30/10/2015	January 2007 – July 2015
RD13	O3M SAF Validation Report for offline and reprocessed total H2O columns	30/10/2015	January 2007 – August 2015
RD14	O3M SAF Validation Report for NRT and offline aerosol products	25/06/2013	January 2007 – May 2013
RD15	O3M SAF Validation Report for Metop-B offline UV products	03/02/2015	June 2012 – May 2013
RD16	O3M SAF Validation Report for Metop-A reprocessed total ozone columns	19/02/2010	January 2007 – June 2009
RD17	AC SAF Validation Report for GOME-2 surface LER product	27/03/2019	MSC: February 2007 – June 2018 PMD: April 2008 – June 2018
RD18	O3M SAF Validation Report for offline tropospheric ozone columns (cloud slicing)	03/07/2015	January 2007 – December 2014

Reference	Title	Issued	Reporting period
RD19	O3M SAF Validation Report for NRT and offline tropospheric ozone columns (ozone profiles)	09/09/2015	January 2007 – December 2014
RD20	O3M SAF Validation Report for NRT IASI CO	17/11/2015	September 2015 – November 2015
RD21	AC SAF Validation Report for OClO data record	29/05/2017	January 2007 – September 2016
RD22	AC SAF Validation Report for NRT IASI SO2	17/11/2017	Metop-A: January 2007 – December 2013 June 2017 – October 2017 Metop-B: June 2017 – December 2017
RD23	AC SAF Validation Report for level-3 total H2O data record	06/11/2017	Metop-A: January 2007 – December 2014 Metop-B: January 2013 – December 2014
RD24	AC SAF Validation Report for Metop-C offline tropical tropospheric ozone columns	05/06/2020	February – December 2019
RD25	AC SAF Validation Report for Metop-C NRT and offline global tropospheric ozone columns	05/06/2020	February – December 2019
RD26	AC SAF Validation Report for Metop-C NRT and offline high-resolution ozone profiles	05/06/2020	February – December 2019
RD27	AC SAF Validation Report for Metop-C NRT and offline total ozone columns	25/05/2020	February – July 2019
RD28	AC SAF Validation Report for Metop-C NRT and offline total/tropospheric nitrogen dioxide columns	25/11/2019	February – July 2019
RD29	AC SAF Validation Report for Metop-C NRT and offline total formaldehyde columns	19/05/2020	February – July 2019
RD30	AC SAF Validation Report for Metop-C offline total bromine monoxide columns	19/05/2020	February – July 2019
RD31	AC SAF Validation Report for Metop-C offline total water vapour columns	30/03/2020	February – July 2019

Reference	Title	Issued	Reporting period
RD32	AC SAF Validation Report for NRT, offline and reprocessed absorbing aerosol height products	03/07/2020	2007-2019
RD33	AC SAF Validation Report for Metop-C NRT and offline absorbing aerosol index from PMDs products	09/10/2019	January – October 2019
RD34	AC SAF Validation Report for Metop-C NRT and offline total sulphur dioxide products	21/01/2021	February – July 2019
RD35	AC SAF Validation Report for NRT IASI total O3 and O3 profiles	28/02/2022	December 2019 – November 2020
RD36	AC SAF Validation Report for NRT IASI HNO3	26/04/2022	December 2019 – December 2021

Online documents:

Service Specification, Validation Reports

1.4. Definition of terms

Availability is based on the definition in the EUMETSAT Operational Services Specification [RD3].

Product-specific clarifications:

- For NRT products, the monthly availability limit is 97.5 %. The availability is calculated as a “worst case scenario”:

$$\frac{\text{in time processed and disseminated L2 PDUs}}{\text{received L1b PDUs} + \text{missed L1b PDUs marked as “reception confirmed” in the EUMETCast sendlist}}$$

- For offline products, the monthly availability limit is 95.5 %. The availability is defined by the ratio of the number of in time processed, archived and quality-approved L2 products to the number of orbits for which L1b PDUs have been received per month.
- NUV and OUV are daily L3 products, and availability is defined as the fraction of days in a month with products fulfilling the timeliness requirements.

Timeliness defines whether the product is near real time (NRT) product which is disseminated or ready for download in three hours from sensing at the latest or offline product which is available for download in two weeks after sensing at the latest, during system availability. System unavailability will in most cases not lead to loss of data but to delays with respect to the specified timeliness. In practice, timeliness of a product is determined by calculating the time from sensing to EUMETCast or archive upload. In the Operations Reports, the timeliness is presented as monthly average, minimum and maximum values.

Accuracy is defined as in the EPS End User Requirements Document [RD4]: the values of accuracy “represent RMS values” taking as reference the ‘true value’ measured by ground based instruments.

1.5. Accuracy requirements of AC SAF products

The following table lists all operational AC SAF products and their accuracy requirements as defined in [RD2].

Table 1.2. Accuracy requirements of AC SAF products

Product identifier	Product name	Product acronym	Threshold accuracy	Target accuracy	Means of quality assurance
O3M-41.1	NRT total O3	MBG-N-O3	20 %	4 % (SZA < 80°) 6 % (SZA > 80°)	Validation report
O3M-300		MCG-N-O3			
O3M-50.1	NRT total NO2	MBG-N-NO2	20 % of annual mean	8-15 % of annual mean	Online monitoring Validation report
O3M-338		MCG-N-NO2			
O3M-52.1	NRT tropospheric NO2	MBG-N-NO2TR	50 %	30 %	Online monitoring Validation report
O3M-341		MCG-N-NO2TR			
O3M-55.1	NRT total SO2	MBG-N-SO2	100 %	50 % (SZA < 70°)	Online monitoring Validation report
O3M-374		MCG-N-SO2			
O3M-177	NRT total HCHO	MBG-N-HCHO	100 %	50 % (polluted)	Online monitoring Validation report
O3M-344		MCG-N-HCHO			

Product identifier	Product name	Product acronym	Threshold accuracy	Target accuracy	Means of quality assurance
O3M-47.1	NRT high-resolution ozone profile	MBG-N-O3HRPR	30 % in stratosphere 70 % in troposphere	15 % in stratosphere 30 % in troposphere	Online monitoring Validation report
O3M-311		MCG-N-O3HRPR			
O3M-78	NRT absorbing aerorol height	MBG-N-AAH	3 km (layer height < 10 km) 4 km (layer height > 10 km)	1 km (layer height < 10 km) 2 km (layer height > 10 km)	Online monitoring Validation report
O3M-364		MCG-N-AAH			
O3M-72.1	NRT absorbing aerosol index from PMDs	MBG-N-AAIPMD	1.0 index points	0.5 index points	Online monitoring Validation report
O3M-362		MCG-N-AAIPMD			
O3M-409	NRT UV index, clear-sky	MCG-NUV_CLEAR	20 %	10 %	Online monitoring Validation report
O3M-410	NRT UV index, cloud-corrected	MCG-NUV_CLOUD	20 %	10 %	Online monitoring Validation report
O3M-80	NRT IASI CO	MBI-N-CO	25 % (normal conditions) 50 % (high pollution or low signal)	12 % (normal conditions) 20 % (high pollution or low signal)	Validation report
O3M-352		MCI-N-CO			
O3M-57	NRT IASI SO2	MxI-N-SO2	200 % (below 10 km) 100 % (above 10 km)	100 % (below 10 km) 35 % (above 10 km)	Validation report
O3M-377					
O3M-81	NRT IASI HNO3	MxI-N-HNO3	50 %	35 %	Validation report
O3M-336					
O3M-44	NRT IASI total ozone	MxI-N-O3	10 %	5 %	Validation report
O3M-306					
O3M-49	NRT IASI ozone profile	MxI-N-O3PR	30 % in stratosphere 50 % in troposphere	15 % in stratosphere 30 % in troposphere	Validation report
O3M-315					
O3M-06.1	Offline total O3	MAG-O-O3	20 %	4 % (SZA < 80°) 6 % (SZA > 80°)	Validation report
O3M-42.1		MBG-O-O3			
O3M-301		MCG-O-O3			
O3M-07.1	Offline total NO2	MAG-O-NO2	20 % of annual mean	8-15 % of annual mean	Online monitoring Validation report
O3M-51.1		MBG-O-NO2			
O3M-339		MCG-O-NO2			
O3M-37.1	Offline tropospheric NO2	MAG-O-NO2TR	50 %	30 %	Online monitoring Validation report
O3M-53.1		MBG-O-NO2TR			
O3M-342		MCG-O-NO2TR			
O3M-09.1	Offline total SO2	MAG-O-SO2	100 %	50 % (SZA < 70°)	Online monitoring Validation report
O3M-56.1		MBG-O-SO2			
O3M-375		MCG-O-SO2			

Product identifier	Product name	Product acronym	Threshold accuracy	Target accuracy	Means of quality assurance
O3M-08.1	Offline total BrO	MAG-O-BrO	50 %	30 %	Online monitoring Validation report
O3M-82.1		MBG-O-BrO			
O3M-317		MCG-O-BrO			
O3M-10.1	Offline total HCHO	MAG-O-HCHO	100 %	50 % (polluted)	Online monitoring Validation report
O3M-58.1		MBG-O-HCHO			
O3M-345		MCG-O-HCHO			
O3M-12.1	Offline total H2O	MAG-O-H2O	25 %	10 %	Validation report
O3M-86.1		MBG-O-H2O			
O3M-386		MCG-O-H2O			
O3M-35	Offline tropical tropospheric ozone	MAG-O-O3TR	50 %	25 %	Validation report
O3M-43		MBG-O-O3TR			
O3M-302		MCG-O-O3TR			
O3M-39.1	Offline high-resolution ozone profile	MAG-O-O3HRPR	30 % in stratosphere 70 % in troposphere	15 % in stratosphere 30 % in troposphere	Online monitoring Validation report
O3M-48.1		MBG-O-O3HRPR			
O3M-312		MCG-O-O3HRPR			
O3M-172	NRT global tropospheric ozone	MAG-N-O3TROC	50 %	20 %	Validation report
O3M-174		MBG-N-O3TROC			
O3M-304		MCG-N-O3TROC			
O3M-173	Offline global tropospheric ozone	MAG-O-O3TROC	50 %	20 %	Validation report
O3M-175		MBG-O-O3TROC			
O3M-305		MCG-O-O3TROC			
O3M-69	Offline absorbing aerosol height	MAG-O-AAH	3 km (layer height < 10 km) 4 km (layer height > 10 km)	1 km (layer height < 10 km) 2 km (layer height > 10 km)	Online monitoring Validation report
O3M-79		MBG-O-AAH			
O3M-365		MCG-O-AAH			
O3M-63.1	Offline absorbing aerosol index from PMDs	MAG-O-AAIPMD	1.0 index points	0.5 index points	Online monitoring Validation report
O3M-73.1		MBG-O-AAIPMD			
O3M-363		MCG-O-AAIPMD			
O3M-450 – O3M-464	Offline surface UV	MM-O-UV_*	50 %	20 %	Online monitoring Validation report

Latest validation reports for all pre-operational and operational AC SAF products are listed in Section 1.3.

Online monitoring, when applicable, can be used to replace the regular validation reporting. Online monitoring results are found from dedicated sections “Online quality monitoring”, if the processing centre in question has such functionality.

2. Processing centre: FMI

2.1. Offline surface UV

Offline surface UV (OUV) product is a multi-mission (Metop-B+C) product consisting of 15 sub-products which are listed in Table 2.1. Since they are all archived in the same file, single entries in the tables in the following sections represent them all.

Table 2.1. OUV sub-products

Product Identifier	Product Name	Product Acronym
O3M-450	Offline UV daily dose, erythemal (CIE) weighting	MM-O-UV_DD_CIE
O3M-451	Offline UV daily dose, plant response weighting	MM-O- UV_DD_PLANT
O3M-452	Offline UV daily dose, DNA damage weighting	MM-O-UV_DD_DNA
O3M-453	Offline UV daily dose, UVA range (315-400 nm)	MM-O-UV_DD_UVA
O3M-454	Offline UV daily dose, UVB range (280-315 nm)	MM-O-UV_DD_UVB
O3M-455	Offline UV daily maximum dose rate, erythemal (CIE) weighting	MM-O-UV_MDSR_CIE
O3M-456	Offline UV daily maximum dose rate, plant response weighting	MM-O-UV_MDSR_PLANT
O3M-457	Offline UV daily maximum dose rate, DNA damage weighting	MM-O-UV_MDSR_DNA
O3M-458	Offline UV daily maximum dose rate, UVA range (315-400 nm)	MM-O-UV_MDSR_UVA
O3M-459	Offline UV daily maximum dose rate, UVB range (280-315 nm)	MM-O-UV_MDSR_UVB
O3M-460	Offline UV solar noon UV index	MM-O-UV_NOON_UVI
O3M-461	Offline UV daily maximum ozone photolysis rate	MM-O-UV_MPHR_O3
O3M-462	Offline daily maximum nitrogen dioxide photolysis rate	M-O-UV_MPHR_NO2
O3M-463	Offline UV daily dose, vitamin D weighting	MM-O-UV_DD_VITD
O3M-464	Offline UV daily maximum dose rate, vitamin D weighting	MM-O-UV_MDSR_VITD

2.1.1. Availability

Availability requirement for OUV has been defined in Section 1.4. The availability statistics of FMI products are presented in Table 2.2. If the availability requirement has been violated, those values are marked with red colour, identified by numbers and reported in Table 2.7.

Table 2.2. Availability of OUV product during the reporting period

1/2022	2/2022	3/2022	4/2022	5/2022	6/2022
100 %	100 %	100 %	100 %	100 %	100 %

2.1.2. Timeliness

Timeliness indicates the elapsed time between sensing and product dissemination. Timeliness requirement is 15 days for offline products. If the requirement has been violated, those values are marked with red colour. In addition, the violations are identified by numbers and reported in Table 2.7 if they have caused the availability values to drop below the allowed limits.

Note: timeliness violations are not listed as anomalies if the availability is above the limit.

The values in Table 2.3 indicate the elapsed times (days, hours and minutes in the format [ddT]hh:mm) from sensing to archive upload. In each cell, the values from top to bottom represent observed monthly average, minimum and maximum times.

Table 2.3. Timeliness of OUV product during the reporting period

1/2022	2/2022	3/2022	4/2022	5/2022	6/2022
avg: 04T01:47 min: 03T01:32 max: 12T08:36	avg: 03T01:38 min: 03T01:27 max: 03T01:42	avg: 03T01:39 min: 03T01:32 max: 03T01:47	avg: 03T02:48 min: 03T01:27 max: 04T10:52	avg: 04T00:54 min: 03T00:32 max: 08/06:02	avg: 03T02:27 min: 03T02:17 max: 03T02:37

2.2. Services, main events and anomalies

Table 2.4. FMI service statistics related to product archiving, ordering and AC SAF Helpdesk

Description of service / event	1/2022	2/2022	3/2022	4/2022	5/2022	6/2022
Product ordering [1]						
Number of users (cumulative)	537	547	554	565	574	577
Number of orders	9	5	12	21	15	2
Number of ordered products	OHP: 2 ARP: 140 OUV time-series: 31412	OHP: 10 ARP: 2779	OHP: 31 ARP: 171 OUV time-series: 1824	OOP: 3 OHP: 2 ARS: 17587 ARP: 187 OUV subset: 4018 OUV time-series: 35997	OHP: 1725 ARS: 13218 ARP: 74611	OHP: 1 ARP: 28
Ordered data volume	OHP: 503 MB ARP: 963 MB OUV time-series: 9.87 MB	OHP: 2.48 GB ARP: 19.3 GB	OHP: 7.57 GB ARP: 1.18 GB OUV time-series: 420 kB	OOP: 128 MB OHP: 745 MB ARS: 17.7 GB ARP: 1.28 GB OUV subset: 4.82 GB OUV time-series: 2.17 MB	OHP: 428 GB ARS: 13.3 GB ARP: 494 GB	OHP: 242 MB ARP: 192 MB
Number of bulk orders	0	0	0	0	0	0
Number of failed orders [2]	0	0	0	0	0	0
Archive statistics [3]						
Number of archived products (Metop-B)	OHP: 438 ARS: 438 ARP: 438	OHP: 397 ARS: 397 ARP: 397	OHP: 430 ARS: 430 ARP: 430	OHP: 425 ARS: 425 ARP: 425	OHP: 438 ARS: 438 ARP: 438	OHP: 426 ARS: 426 ARP: 426
Size of archived products (Metop-B)	OHP: 110 GB ARS: 449 MB ARP: 3.03 GB	OHP: 99.5 GB ARS: 406 MB ARP: 2.75 GB	OHP: 108 GB ARS: 440 MB ARP: 2.97 GB	OHP: 106 GB ARS: 436 MB ARP: 2.92 GB	OHP: 109 GB ARS: 451 MB ARP: 3.00 GB	OHP: 106 GB ARS: 440 MB ARP: 2.95 GB

Number of archived products (Metop-C)	OHP: 440 ARS: 440 ARP: 440	OHP: 396 ARS: 396 ARP: 396	OHP: 437 ARS: 437 ARP: 437	OHP: 425 ARS: 425 ARP: 425	OHP: 440 ARS: 440 ARP: 440	OHP: 424 ARS: 424 ARP: 424
Size of archived products (Metop-C)	OHP: 110 GB ARS: 451 MB ARP: 3.04 GB	OHP: 99.2 GB ARS: 406 MB ARP: 2.75 GB	OHP: 109 GB ARS: 447 MB ARP: 3.02 GB	OHP: 105 GB ARS: 436 MB ARP: 2.91 GB	OHP: 110 GB ARS: 454 MB ARP: 3.02 GB	OHP: 106 GB ARS: 439 MB ARP: 2.95 GB
Number of archived multi-mission products	OUV: 31	OUV: 28	OUV: 31	OUV: 30	OUV: 31	OUV: 30
Size of archived multi-mission products	OUV: 563 MB	OUV: 535 MB	OUV: 569 MB	OUV: 527 MB	OUV: 458 MB	OUV: 506 MB
GOME-2 L1b PDU rolling archive statistics [4]						
PDUs archived / PDUs “reception confirmed” (Metop-B)	13278/14879 89.2 %	13360/13437 99.4 %	13995/14657 95.5 %	13597/14365 94.7 %	13913/14865 93.6 %	14053/14367 97.8 %
PDUs archived / PDUs “reception confirmed” (Metop-C)	13114/14880 88.1 %	13276/13419 98.9 %	13987/14792 94.6 %	13486/14324 94.1 %	13888/14849 93.5 %	13896/14350 96.8 %
Helpdesk statistics						
Number of emails	1	1	7	2	6	0
Number of email threads	1	1	4	2	2	0
Average response time ([ddT]hh:mm)	00:15	01T11:14	02T03:30	01T07:15	04:54	-

1 More detailed information about the orders is available in Appendix 1
2 Failed orders are detailed in Appendix 2
3 Based on sensing start time
4 For Level 1b products, the availability is defined as the number of archived L1b PDUs divided by the number of L1b PDUs with status “reception confirmed” in the EUMETCast sendlist

Data archive statistics since 2008 are illustrated in Figure 2.1.

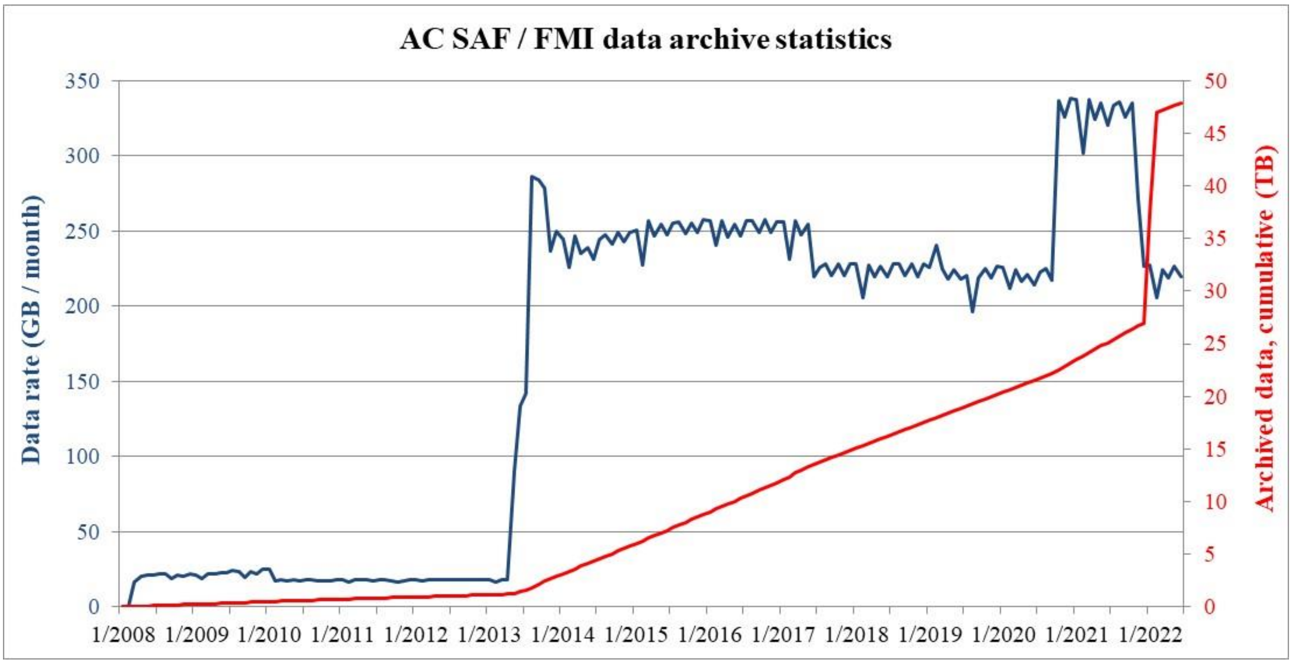

Figure 2.1. FMI data archive statistics: data rate and cumulative amount of data

Sudden increase in the cumulative amount of archived data in January – February 2022 is due to archiving of Metop-A/B high-resolution ozone profile data record R1.

Events affecting the data rate are presented in Table 2.5.

Table 2.5. Events affecting the FMI archive data rate

Date	Event	Data rate (GB/month)
03/2008	Archiving of OOP-A started	19.1 – 22.2
06/2009	Archiving of OUV-A started	19.2 – 23.8
11/2009	Archiving of ARS-A started	25.3
02/2010	Compression of OOP-A started	16.2 – 18.3
05/2013	Archiving of OHP-A started	133 – 142
08/2013	Archiving of OOP-B, OHP-B and ARS-B started	279 – 284
11/2013	Archiving of ARP-A and ARP-B started. KNMI implements shuffling algorithm in the hdf5 compression	226 – 250
03/2014	Archiving of OUV-A discontinued, archiving of OUV-B started	227 – 250
02/2015	OPERA algorithm update, tropospheric integrated profiles added	247-257
06/2017	Archiving of OOP-A and OOP-B discontinued	206-229
10/2020	Archiving of ARS-C, ARP-C and OHP-C started	302-338
11/2021	Archiving of OHP-A, ARS-A and ARP-A discontinued	206 – 227

Table 2.6 lists the main events (product/service/hardware/software updates etc.) at FMI during the reporting period.

Table 2.6. Main events at FMI during the reporting period

Date	Description
18 January – 23 February	Archiving of high-resolution ozone profile data record R1 (34.5 TB)
12 May	FMI data archive storage space increased to 75 TB

Table 2.7 lists the main local and external anomalies during the reporting period. Corrective and preventive actions should be provided also when applicable.

Table 2.7. Main local and external anomalies affecting FMI systems and performance during the reporting period

ID	Time period	Description
		Nothing to report.

3. Processing centre: DLR

3.1. NRT and offline total/tropospheric trace gas columns, tropical tropospheric ozone

This section reports availability and timeliness of the operational NRT and offline L2 products processed for GOME-2 on Metop-A, Metop-B and Metop-C.

3.1.1. Availability

For Level 1b products, the availability is defined as the number of L1b PDUs with status “reception confirmed”, i.e. EUMETSAT received these L1b PDUs through its EUMETCast reference receiving station, divided by the total number of L1b PDUs listed in the EUMETCast sendlist.

Availability for offline L2 products has been defined in Section 1.4. The availability statistics of DLR products are presented in Table 3.1 and Table 3.2. If the availability requirements have been violated, those values are marked with red colour, identified by numbers and reported in Table 3.7.

Table 3.1. Availability of Metop-B total and tropospheric trace gas column products during the reporting period

Product Identifier	Product Name	1/2022	2/2022	3/2022	4/2022	5/2022	6/2022
L1b	PDUs received / PDUs “reception confirmed”	14879/14879 100 %	13436/13437 100 %	14657/14657 100 %	14365/14365 100 %	13982/14865 94.1 %	14360/14367 99.9 %
O3M-41.1	NRT total O3	99.8 %	99.9 %	99.9 %	100 %	94.1 % (1)	99.9 %
O3M-50.1	NRT total NO2						
O3M-52.1	NRT tropospheric NO2						
O3M-55.1	NRT total SO2						
O3M-177.0	NRT total HCHO						
O3M-42.1	Offline total O3	100 %	100 %	100 %	100 %	100 %	100 %
O3M-51.1	Offline total NO2						
O3M-53.1	Offline tropospheric NO2						
O3M-56.1	Offline total SO2						
O3M-58.1	Offline total HCHO						
O3M-82.1	Offline total BrO						
O3M-86.1	Offline total H2O						
O3M-43	Offline tropical tropospheric ozone	100 %	100 %	100 %	100 %	100 %	100 %

Table 3.2. Availability of Metop-C total and tropospheric trace gas column products during the reporting period

Product Identifier	Product Name	1/2022	2/2022	3/2022	4/2022	5/2022	6/2022
L1b	PDUs received / PDUs “reception confirmed”	14879/14880 99.9 %	13417/13417 100 %	14790/14792 99.9 %	14324/14324 100 %	13957/14849 94.0 % (2)	14290/14350 99.6 %
O3M-300	NRT total O3	99.9 %	99.9 %	99.9 %	100 %	94.0 % (2)	99.6 %
O3M-338	NRT total NO2						
O3M-341	NRT tropospheric NO2						
O3M-374	NRT total SO2						
O3M-344	NRT total HCHO						
O3M-301	Offline total O3	100 %	100 %	100 %	100 %	100 %	100 %
O3M-339	Offline total NO2						
O3M-342	Offline tropospheric NO2						
O3M-375	Offline total SO2						
O3M-345	Offline total HCHO						
O3M-317	Offline total BrO						
O3M-386	Offline total H2O						
O3M-302	Offline tropical tropospheric ozone	100 %	100 %	100 %	100 %	100 %	100 %

3.1.2. Timeliness

Timeliness indicates the elapsed time between sensing and product dissemination. Timeliness requirements are 3 hours for NRT products and 15 days for offline products. If the requirements have been violated, those values are marked with red colour. In addition, the violations are identified by numbers and reported in Table 3.7 if they have caused the availability values to drop below the allowed limits.

Note: timeliness violations are not listed as anomalies if the availability is above the limit.

The values for NRT products in Table 3.3 and Table 3.4 indicate the elapsed times (days, hours and minutes in the format [ddT]hh:mm) from sensing to EUMETCast (NRT) upload. In each cell, the values from top to bottom represent observed monthly average, minimum and maximum times for NRT products.

Offline products (excluding the tropospheric product) are monthly aggregates and the reported value is the absolute time of archive upload to the EOWEB catalogue.

Table 3.3. Timeliness of Metop-B total and tropospheric trace gas column products during the reporting period

<table>
<tr><th>Product Identifier</th><th>Product Name</th><th>1/2022</th><th>2/2022</th><th>3/2022</th><th>4/2022</th><th>5/2022</th><th>6/2022</th></tr>
<tr><td>O3M-41.1</td><td>NRT total O3</td><td rowspan="5">avg: 00:51
min: 00:30
max: 02:09</td><td rowspan="5">avg: 00:51
min: 00:29
max: 01:45</td><td rowspan="5">avg: 00:51
min: 00:24
max: 01:49</td><td rowspan="5">avg: 00:51
min: 00:28
max: 01:49</td><td rowspan="5">avg: 00:50
min: 00:31
max: 01:49</td><td rowspan="5">avg: 00:52
min: 00:32
max: 02:05</td></tr>
<tr><td>O3M-50.1</td><td>NRT total NO2</td></tr>
<tr><td>O3M-52.1</td><td>NRT tropospheric NO2</td></tr>
<tr><td>O3M-55.1</td><td>NRT total SO2</td></tr>
<tr><td>O3M-177.0</td><td>NRT total HCHO</td></tr>
<tr><td>O3M-42.1</td><td>Offline total O3</td><td rowspan="7">2022-02-16T15:29:06</td><td rowspan="7">2022-03-12T14:22:08</td><td rowspan="7">2022-04-12T14:29:04</td><td rowspan="7">2022-05-12T14:27:37</td><td rowspan="7">2022-06-12T14:24:02</td><td rowspan="7">2022-07-12T14:36:06</td></tr>
<tr><td>O3M-51.1</td><td>Offline total NO2</td></tr>
<tr><td>O3M-53.1</td><td>Offline tropospheric NO2</td></tr>
<tr><td>O3M-56.1</td><td>Offline total SO2</td></tr>
<tr><td>O3M-58.1</td><td>Offline total HCHO</td></tr>
<tr><td>O3M-82.1</td><td>Offline total BrO</td></tr>
<tr><td>O3M-86.1</td><td>Offline total H2O</td></tr>
<tr><td>O3M-43</td><td>Offline tropical tropospheric ozone</td><td>N/A</td><td>N/A</td><td>N/A</td><td>N/A</td><td>N/A</td><td>N/A</td></tr>
</table>

Table 3.4. Timeliness of Metop-C total and tropospheric trace gas column products during the reporting period

<table>
<tr><th>Product Identifier</th><th>Product Name</th><th>1/2022</th><th>2/2022</th><th>3/2022</th><th>4/2022</th><th>5/2022</th><th>6/2022</th></tr>
<tr><td>O3M-300</td><td>NRT total O_3</td><td rowspan="5">avg: 01:41
min: 01:13
max: 02:09</td><td rowspan="5">avg: 01:41
min: 00:40
max: 02:21</td><td rowspan="5">avg: 01:45
min: 00:34
max: 00:12</td><td rowspan="5">avg: 01:42
min: 00:34
max: 02:12</td><td rowspan="5">avg: 01:41
min: 00:36
max: 02:43</td><td rowspan="5">avg: 01:43
min: 00:37
max: 02:47</td></tr>
<tr><td>O3M-338</td><td>NRT total NO_2</td></tr>
<tr><td>O3M-341</td><td>NRT tropospheric NO_2</td></tr>
<tr><td>O3M-374</td><td>NRT total SO_2</td></tr>
<tr><td>O3M-344</td><td>NRT total HCHO</td></tr>
<tr><td>O3M-301</td><td>Offline total O_3</td><td rowspan="7">2022-02-16T14:53:37</td><td rowspan="7">2022-03-12T13:36:28</td><td rowspan="7">2022-04-12T13:53:10</td><td rowspan="7">2022-05-12T13:51:18</td><td rowspan="7">2022-06-12T13:48:35</td><td rowspan="7">2022-07-12T13:56:00</td></tr>
<tr><td>O3M-339</td><td>Offline total NO_2</td></tr>
<tr><td>O3M-342</td><td>Offline tropospheric NO_2</td></tr>
<tr><td>O3M-375</td><td>Offline total SO_2</td></tr>
<tr><td>O3M-345</td><td>Offline total HCHO</td></tr>
<tr><td>O3M-317</td><td>Offline total BrO</td></tr>
<tr><td>O3M-386</td><td>Offline total H_2O</td></tr>
<tr><td>O3M-302</td><td>Offline tropical tropospheric ozone</td><td>N/A</td><td>N/A</td><td>N/A</td><td>N/A</td><td>N/A</td><td>N/A</td></tr>
</table>

3.2. Services, main events and anomalies

Table 3.5. DLR service statistics related to product archiving and ordering

Description of service / event	1/2022	2/2022	3/2022	4/2022	5/2022	6/2022
Archive statistics [2]						
Number of archived products (cumulative) – according to product insertion time	341712	359010	396037	522639	529377	530338
Size of archived products (TB, cumulative)	11.5	12.2	13.6	16.1	16.3	16.4
Number of missing orbit products – according to sensing time	539	1	13	0	4	0
Number of archived products with good/poor/error[3] quality assessed per month – according to product insertion time	875/0/3	788/4/2	843/0/17	845/0/8	840/4/27	837/4/15
Online Access [1]						
Number of searches in the GOME.TC collection	89	105	146	145	127	145
Number of FTP (ATMOS/VELA) subscribers	477	487	495	503	512	514
Number of FTP (ATMOS/VELA) downloads	111540	121420	283780	80130	102931	158944
Downloaded data volume (GB)	445.8	910.5	2918	254.8	668.0	1267
Product ordering						
Number of EOWEB orders	2	0	4	8	6	4
Delivered data volume (GB)	5.82	0	9.53	23.9	23.4	106

[1] NTO product and OTO product is stored at the DLR for external search and download
[2] O3MOTO product (collection GOME.TC, Metop missions) is archived and available to non-NRT users
[3] good: max. 2 PDUs missing, poor/error: more than 2 PDUs missing

Table 3.6 lists the main events (product/service/hardware/software updates etc.) at DLR during the reporting period.

Table 3.6. Main events at DLR during the reporting period

Date	Event
January	Completion of switch-over to the new EUMETCast reception system on DLR premises.

Table 3.7 lists the main and external local anomalies at DLR during the reporting period. Corrective and preventive actions should be provided also when applicable.

Table 3.7. Main local and external anomalies affecting DLR systems and performance during the reporting period

ID	Time period	Description
1	7-9 May	On 3 May, 06:26 local time, the license key on the reception server o3m4 was not recognized anymore, i. e. no data was received on this server. However, the outage was covered fully be the redundant reception server o3m1. The missing license key was not discovered immediately, since this was the first occurrence of this specific issue and no specific monitoring was in place. On 7 May, 15:37 local time, the tellicast receiving software on reception server o3m1 showed the state “Starting” instead of state “OK”, i. e. no data was received. First analysis pointed towards a faulty connection between the USB dongle and the server. Further detailed investigation showed that the issue was related to the demodulator hardware. Corrective actions: On 9 May the reception server o3m4 was rebooted, which solved the issue. The reception server o3m1 was powered off completely, uncabled, recabled and restarted, which solved the issue and re-established nominal operations. Preventive action: With regards to the root cause analysis on o3m1 and the relation to the demodulator hardware it is planned to exchange this piece of hardware in case the issue reoccurs. On o3m4 two preventive actions have been taken. Firstly, the procedure from the EUMETSAT User Help website to fix “EKU problems on Linux: ‘Found missing or wrong user key part’” was applied. Secondly, the EKU Monitoring Tool provided by EUMETSAT was installed. With the help of this tool the tellicast log file entries are read and evaluated and in case of a specific timeout message restarts the tellicast client automatically. As a more general measure the internal monitoring has been amended in order to cover such issues. In addition, the internal operations guide has been updated and the operations team is instructed accordingly.

4. Processing centre: KNMI

4.1. NRT and offline ozone profiles, absorbing aerosol height and index, global tropospheric ozone

4.1.1. Availability

For Level 1b products, the availability is defined as the number of unique L1b PDUs received either via EUMETCast Satellite or EUMETCast Terrestrial (demonstrational dissemination service), divided by the number of L1b PDUs not marked as “not sent” in the EUMETCast Satellite sendlist. This approximation presumes that all PDUs marked as “sent not confirmed” are still available via EUMETCast Terrestrial.

Availability for offline L2 products has been defined in Section 1.4. The availability statistics of KNMI products are presented in Table 4.1 and Table 4.2. If the availability requirements have been violated, those values are marked with red colour, identified by numbers and reported in Table 4.9.

Tropospheric ozone products are included in the ozone profile products and have the same statistics. The same applies to scattering aerosol index products which are included in the absorbing aerosol index products.

Table 4.1. Availability of Metop-B L1b PDUs, ozone profile products and aerosol products during the reporting period

Product Identifier	Product Name	1/2022	2/2022	3/2022	4/2022	5/2022	6/2022
EUMETCast							
L1b	PDUs received / sent	14892/14879 100.1 %	13437/13437 100 %	14657/14657 100 %	14365/14365 100 %	14870/14870 100 %	14383/14377 100 %
O3M-47.1	NRT high-resolution ozone profile	100 %	100 %	100 %	100 %	100 %	100 %
O3M-78	NRT absorbing aerosol height	100 %	100 %	100 %	100 %	100 %	100 %
O3M-72.1	NRT absorbing aerosol index from PMDs	100 %	100 %	100 %	100 %	100 %	100 %
WMO/GTS							
O3M-47.1	NRT high-resolution ozone profile	100 %	100 %	100 %	100 %	100 %	100 %
FMI archive							
O3M-48.1	Offline high-resolution ozone profile	100 %	100 %	100 %	100 %	100 %	100 %
O3M-79	Offline absorbing aerosol height	100 %	100 %	100 %	100 %	100 %	100 %
O3M-73.1	Offline absorbing aerosol index from PMDs	100 %	100 %	100 %	100 %	100 %	100 %

Table 4.2. Availability of Metop-C L1b PDUs, ozone profile products and aerosol products during the reporting period

Product Identifier	Product Name	1/2022	2/2022	3/2022	4/2022	5/2022	6/2022
EUMETCast							
L1b	PDUs received / sent	14880/14880 100 %	13417/13417 100 %	14798/14792 100 %	14324/14324 100 %	14872/14872 100 %	14378/14362 100.1 %
O3M-311	NRT high-resolution ozone profile	100 %	100 %	100 %	100 %	100 %	99.8 %
O3M-364	NRT absorbing aerosol height	100 %	100 %	100 %	100 %	100 %	99.8 %
O3M-362	NRT absorbing aerosol index from PMDs	100 %	100 %	100 %	100 %	100 %	99.8 %
WMO/GTS							
O3M-311	NRT high-resolution ozone profile	100 %	100 %	100 %	100 %	100 %	99.8 %
FMI archive							
O3M-312	Offline high-resolution ozone profile	100 %	100 %	100 %	100 %	100 %	100 %
O3M-365	Offline absorbing aerosol height	100 %	100 %	100 %	100 %	100 %	100 %
O3M-363	Offline absorbing aerosol index from PMDs	100 %	100 %	100 %	100 %	100 %	100 %

4.1.2. Timeliness

Timeliness indicates the elapsed time between sensing and product dissemination. Timeliness requirements are 3 hours for NRT products and 15 days for offline products. If the requirements have been violated, those values are marked with red colour. In addition, the violations are identified by numbers and reported in Table 4.9 if they have caused the availability values to drop below the allowed limits.

Note: timeliness violations are not listed as anomalies if the availability is above the limit.

The values in Table 4.3 and Table 4.4 indicate elapsed times (days, hours and minutes in the format [ddT]hh:mm) from sensing to EUMETCast and WMO/GTS (NRT) or archive upload (offline). In each cell, the values from top to bottom represent observed monthly average, minimum and maximum times.

Tropospheric ozone products are included in the ozone profile products and have the same statistics.

Table 4.3. Timeliness of Metop-B ozone profile and aerosol products during the reporting period

Product Identifier	Product Name	1/2022	2/2022	3/2022	4/2022	5/2022	6/2022
EUMETCast							
O3M-47.1	NRT high-resolution ozone profile	avg: 01:04 min: 00:43 max: 02:29	avg: 01:03 min: 00:30 max: 02:05	avg: 01:06 min: 00:29 max: 02:04	avg: 01:03 min: 00:29 max: 02:03	avg: 01:03 min: 00:31 max: 02:07	avg: 01:06 min: 00:33 max: 03:24
O3M-78	NRT absorbing aerosol height	avg: 00:50 min: 00:29 max: 02:08	avg: 00:50 min: 00:29 max: 01:45	avg: 00:52 min: 00:23 max: 01:48	avg: 00:49 min: 00:29 max: 01:48	avg: 00:49 min: 00:30 max: 01:47	avg: 00:51 min: 00:30 max: 03:17
O3M-72.1	NRT absorbing aerosol index from PMDs	avg: 00:50 min: 00:29 max: 02:08	avg: 00:50 min: 00:29 max: 01:45	avg: 00:52 min: 00:23 max: 01:48	avg: 00:49 min: 00:29 max: 01:48	avg: 00:49 min: 00:30 max: 01:47	avg: 00:51 min: 00:30 max: 03:17
WMO/GTS							
O3M-47.1	NRT high-resolution ozone profile	avg: 01:05 min: 00:43 max: 02:30	avg: 01:04 min: 00:31 max: 02:05	avg: 01:08 min: 00:30 max: 02:05	avg: 01:04 min: 00:30 max: 02:04	avg: 01:04 min: 00:32 max: 02:08	avg: 01:07 min: 00:34 max: 03:25
FMI archive							
O3M-48.1	Offline high-resolution ozone profile	avg: 07:27 min: 06:53 max: 08:29	avg: 07:28 min: 06:51 max: 08:18	avg: 07:31 min: 06:48 max: 08:57	avg: 07:24 min: 06:33 max: 08:15	avg: 07:18 min: 06:36 max: 08:00	avg: 21:31 min: 06:36 max: 02T03:09
O3M-79	Offline absorbing aerosol height	avg: 07:25 min: 06:47 max: 08:24	avg: 07:26 min: 06:52 max: 08:13	avg: 07:28 min: 06:43 max: 08:58	avg: 07:22 min: 06:34 max: 08:10	avg: 07:15 min: 06:34 max: 08:01	avg: 21:32 min: 06:37 max: 02T03:01
O3M-73.1	Offline absorbing aerosol index from PMDs	avg: 07:23 min: 06:45 max: 08:06	avg: 07:25 min: 06:49 max: 08:01	avg: 07:27 min: 06:37 max: 08:57	avg: 07:21 min: 06:31 max: 08:10	avg: 07:16 min: 06:31 max: 08:16	avg: 21:28 min: 06:31 max: 02T03:01

Table 4.4. Timeliness of Metop-C ozone profile and aerosol products during the reporting period

Product Identifier	Product Name	1/2022	2/2022	3/2022	4/2022	5/2022	6/2022
EUMETCast							
O3M-311	NRT high-resolution ozone profile	avg: 01:52 min: 00:55 max: 02:29	avg: 01:52 min: 00:37 max: 02:39	avg: 01:56 min: 00:34 max: 02:25	avg: 01:52 min: 00:35 max: 02:25	avg: 01:52 min: 00:38 max: 04:07	avg: 01:53 min: 00:39 max: 04:24
O3M-364	NRT absorbing aerosol height	avg: 01:39 min: 00:55 max: 02:08	avg: 01:39 min: 00:36 max: 02:18	avg: 01:43 min: 00:33 max: 02:09	avg: 01:39 min: 00:34 max: 02:11	avg: 01:38 min: 00:35 max: 02:10	avg: 01:39 min: 00:36 max: 04:13
O3M-362	NRT absorbing aerosol index from PMDs	avg: 01:39 min: 00:55 max: 02:08	avg: 01:39 min: 00:37 max: 02:17	avg: 01:43 min: 00:33 max: 02:08	avg: 01:39 min: 00:34 max: 02:11	avg: 01:38 min: 00:35 max: 02:10	avg: 01:39 min: 00:36 max: 04:13

Product Identifier	Product Name	1/2022	2/2022	3/2022	4/2022	5/2022	6/2022
WMO/GTS							
O3M-311	NRT high-resolution ozone profile	avg: 01:53 min: 00:56 max: 02:30	avg: 01:53 min: 00:38 max: 04:04	avg: 01:57 min: 00:35 max: 02:26	avg: 01:53 min: 00:36 max: 02:26	avg: 01:53 min: 00:39 max:02:42	avg: 01:54 min: 00:41 max: 04:25
FMI archive							
O3M-312	Offline high-resolution ozone profile	avg: 07:55 min: 07:17 max: 08:37	avg: 07:57 min: 07:21 max: 08:38	avg: 08:05 min: 07:21 max: 09:45	avg: 08:03 min: 07:12 max: 08:38	avg: 08:06 min: 07:18 max: 08:44	avg: 22:34 min: 07:33 max: 02T03:42
O3M-365	Offline absorbing aerosol height	avg: 07:52 min: 07:15 max: 08:30	avg: 07:55 min: 07:17 max: 08:34	avg: 08:03 min: 07:19 max: 09:45	avg: 08:01 min: 07:19 max: 08:40	avg: 08:06 min: 07:28 max: 08:49	avg: 22:35 min: 07:34 max: 02T03:46
O3M-363	Offline absorbing aerosol index from PMDs	avg: 07:51 min: 07:09 max: 08:47	avg: 07:52 min: 07:16 max: 08:49	avg: 08:02 min: 06:49 max: 08:40	avg: 08:00 min: 07:19 max: 08:39	avg: 08:04 min: 07:19 max: 08:43	avg: 22:30 min: 07:25 max: 02T03:42

4.2. Services, main events and anomalies

Tropospheric ozone products are included in the ozone profile products and have the same statistics.

Table 4.5. Number of products sent to FMI archive[1]

Product Identifier	Product Name	Metop satellite	1/2022	2/2022	3/2022	4/2022	5/2022	6/2022
O3M-48.1	Offline high-resolution ozone profile	B	438	397	430	425	438	426
O3M-312		C	440	396	437	425	440	424
O3M-79	Offline absorbing aerosol height	B	438	397	430	425	438	426
O3M-365		C	440	396	437	425	440	424
O3M-73.1	Offline absorbing aerosol index from PMDs	B	438	397	430	425	438	426
O3M-363		C	440	396	437	425	440	424

Table 4.6. Number of products stored locally at KNMI[2]

Product Identifier	Product Name	Metop satellite	1/2022	2/2022	3/2022	4/2022	5/2022	6/2022
O3M-47.1	NRT high-resolution ozone profile	B	8375	7596	8166	7997	8165	7887
O3M-311		C	8386	7570	8309	7953	8186	7882
O3M-78	NRT absorbing aerosol height	B	8375	7596	8166	7997	8165	7887
O3M-364		C	8386	7570	8309	7953	8186	7882

Product Identifier	Product Name	Metop satellite	1/2022	2/2022	3/2022	4/2022	5/2022	6/2022
O3M-72.1	NRT absorbing aerosol index from PMDs	B	8375	7596	8166	7997	8165	7887
O3M-362		C	8386	7570	8309	7953	8186	7882
O3M-48.1	Offline high-resolution ozone profile	B	438	397	430	425	438	426
O3M-312		C	440	396	437	425	440	424
O3M-79	Offline absorbing aerosol height	B	438	397	430	425	438	426
O3M-365		C	440	396	437	425	440	424
O3M-73.1	Offline absorbing aerosol index from PMDs	B	438	397	430	425	438	426
O3M-363		C	440	396	437	425	440	424

Table 4.7. EUMETCast and WMO/GTS uploads[3]

Product Identifier	Product Name	Metop satellite	1/2022	2/2022	3/2022	4/2022	5/2022	6/2022
O3M-47.1	NRT high-resolution ozone profile	B	8375/8364	7596/7596	8166/7500	7997/7997	8165/8165	7884/7884
O3M-311		C	8386/8386	7570/7569	8309/7631	7953/7953	8183/8186	7867/7866
O3M-78	NRT absorbing aerosol height	B	8375	7596	8166	7997	8165	7884
O3M-364		C	8386	7570	8309	7953	8186	7869
O3M-72.1	NRT absorbing aerosol index from PMDs	B	8375	7596	8166	7997	8165	7884
O3M-362		C	8386	7570	8309	7953	8186	7869

[1] Products are archived in HDF5 format.
[2] Products are stored for 3 years (in HDF5 and BUFR formats).
[3] NRT high-resolution ozone profile is disseminated via EUMETCast and WMO/GTS in BUFR format. NRT absorbing aerosol index and NRT absorbing aerosol index from PMDs are disseminated only via EUMETCast (in HDF5 and BUFR formats).

Table 4.8 lists the main events (product/service/hardware/software updates etc.) at KNMI during the reporting period.

Table 4.8. Main events at KNMI during the reporting period

Date	Description
	Nothing to report.

Table 4.9 lists the main local and external anomalies at KNMI during the reporting period. Corrective and preventive actions should be provided also when applicable.

Table 4.9. Main local and external anomalies affecting KNMI systems and performance during the reporting period

ID	Time period	Description
		Nothing to report.

5. Processing centre: DMI

5.1. NRT clear-sky and cloud-corrected UV index

5.1.1. Availability

NUV product is required to be produced every day, either on the basis of new GOME ATO input or in the case of ATO delivery failure based on back-up total ozone data (ECMWF or climatology).

Availability requirement for NUV has been defined in Section 1.4. The availability statistics of DMI products are presented in Table 5.1. If the requirement is violated, those values are marked with red colour, identified by numbers and reported in Table 5.5.

Table 5.1. Availability of NRT UV products during the reporting period

Product Identifier	Product Name	1/2022	2/2022	3/2022	4/2022	5/2022	6/2022
O3M-409	NRT UV index, clear-sky	100 %	100 %	100 %	100 %	100 %	96.7 % (1)
O3M-410	NRT UV index, cloud-corrected						

5.1.2. Timeliness

Timeliness requirement for NUV says that the final NUV product is to be delivered to users no later than two hours after receiving the ATO input and not later than 04:00 UTC. Processing is started at 02:45 UTC thus the maximum processing time allowed is 1 hour 15 min. If the timeliness requirement is violated, those values are marked with red colour. In addition, the violations are identified by numbers and reported in Table 5.5 if they have caused the availability values to drop below the allowed limits.

Days where no products are produced or could be delivered to users (as indicated in Table 5.1) are not included in Table 5.2.

Note: timeliness violations are not listed as anomalies if the availability is above the limit.

The values in Table 5.2 indicate elapsed processing times (hours, minutes and seconds in the format [hh:]mm:ss). In each cell, the values from top to bottom represent observed monthly average, minimum and maximum processing times.

Table 5.2. Timeliness of NRT UV products during the reporting period

Product Identifier	Product Name	1/2022	2/2022	3/2022	4/2022	5/2022	6/2022
O3M-409	NRT UV index, clear-sky	avg: 10:11 min: 09:06 max: 13:08	avg: 09:35 min: 08:56 max: 11:59	avg: 09:38 min: 08:47 max: 12:14	avg: 08:42 min: 05:46 max: 12:43	avg: 05:44 min: 05:35 max: 05:58	avg: 05:42 min: 05:26 max: 06:02
O3M-410	NRT UV index, cloud-corrected						

5.2. Services, main events and anomalies

Table 5.3. Number of products stored locally at DMI[1]

Description of service / event	1/2022	2/2022	3/2022	4/2022	5/2022	6/2022
Storage statistics						
Number of stored products (NRT UV index, clear-sky)	31	28	31	30	31	30
Number of stored products (NRT UV index, cloud-corrected)	31	28	31	30	31	30
Total size of stored products (MB)	248	224	248	240	248	240

[1] NUV products are stored at the DMI at least until the end of the Metop programs.

Table 5.4 lists the main events (product/service/hardware/software updates etc.) at DMI during the reporting period.

Table 5.4. Main events at DMI during the reporting period

Date	Event
19 April	Operation was moved to a new virtual machine. Upgrading from Ubuntu 8.04 to Ubuntu 20.04. Processing time reduced with approximately 50 %.

Table 5.5 lists the main local and external anomalies at DMI during the reporting period. Corrective and preventive actions should be provided also when applicable.

Table 5.5. Main local and external anomalies affecting DMI systems and performance during the reporting period

ID	Time period	Description
1	18 June	A minor update to the code was not properly tested. The products were delayed by 50 minutes.

6. Processing centre: EUMETSAT

6.1. NRT IASI CO, SO2, HNO3 and ozone profile

6.1.1. Availability

For Level 1c products, the availability is defined as the number of available PDUs divided by the number of maximum expected PDUs.

For NRT products, the availability requirement is 97.5 % and it is defined by the ratio of the number of in time processed and disseminated products to the number of maximum expected input products (L1c PDUs) per month.

The availability statistics of EUMETSAT products are presented in Table 6.1 and Table 6.2. If the availability requirements have been violated, those values are marked with red colour, identified by numbers and reported in Table 6.7 and Table 6.8.

Note that in the frame of this product processing centre being the EUMETSAT HQ in Darmstadt, the L1c data is directly available to the algorithm, i.e., its availability is not dependable of EUMETCast dissemination. Furthermore, since there is no relay of information from *Satellite* processing centres, the L2 product availability in the following tables concern the end-to-end availability as they were recorded in the EUMETSAT Reference Receiving Stations.

Metop-C NRT IASI CO (O3M-352) and NRT IASI SO2 (O3M-377), released with the "Operational" status on 18 May 2022 have been added to this report given that they were operationally distributed during the entire reporting period, even if holding the "Demonstrational" status. The same happens to HNO3 and ozone profile products for all satellites.

Table 6.1. Availability of Metop-B L1c PDUs and IASI NRT products during the reporting period

Product Identifier	Product Name	1/2022	2/2022	3/2022	4/2022	5/2022	6/2022
L1c	PDUs available / PDUs expected	14829/14880	13330/13440	11598/14880	14216/14400	14820/14880	14324/14400
L1c	Availability	99.7 %	99.2 %	77.9 % (1,2)	98.7 %	99.6 %	99.5 %
O3M-80	NRT IASI CO	99.0 %	99.7 %	77.6 % (1,2)	98.6 %	99.3 %	99.2 %
O3M-57	NRT IASI SO2	99.0 %	99.7 %	77.6 % (1,2)	98.6 %	99.3 %	99.2 %
O3M-81	NRT IASI HNO3	99.0 %	99.7 %	77.6 % (1,2)	98.6 %	99.3 %	99.2 %
O3M-49	NRT IASI ozone profile	99.0 %	99.7 %	77.6 % (1,2)	98.6 %	99.3 %	99.2 %

Table 6.2. Availability of Metop-C L1c PDUs and IASI NRT products during the reporting period

Product Identifier	Product Name	1/2022	2/2022	3/2022	4/2022	5/2022	6/2022
L1c	PDUs available / PDUs expected	14817/14880	13348/13440	14778/14880	14324/14400	148331/4880	14320/14400
L1c	Availability	99.6 %	99.3 %	99.3 %	99.5 %	99.7 %	99.4 %
O3M-352	NRT IASI CO	99.7 %	99.3 %	98.9 %	99.3 %	99.3 %	99.2 %
O3M-377	NRT IASI SO2	99.7 %	99.3 %	98.9 %	99.3 %	99.3 %	99.2 %
O3M-336	NRT IASI HNO3	99.7 %	99.3 %	98.9 %	99.3 %	99.3 %	99.2 %
O3M-315	NRT IASI ozone profile	99.7 %	99.3 %	98.9 %	99.3 %	99.3 %	99.2 %

6.1.2. Timeliness

Timeliness indicates the elapsed time between sensing and product dissemination. Timeliness requirement is 3 hours for NRT products. If the requirements have been violated, those values are marked with red colour. In addition, the violations are identified by numbers and reported in Table 6.8 if they have caused the availability values to drop below the allowed limits.

Note: timeliness violations are not listed as anomalies if the availability is above the limit.

The values in Table 6.3 and Table 6.4 indicate elapsed times (hours and minutes in the format hh:mm) from sensing to EUMETCast Reference Receiving Station, i.e., end-to-end timeliness. In each cell, the values from top to bottom represent observed monthly average, minimum and maximum times.

Table 6.3. Timeliness of Metop-B IASI NRT products during the reporting period

Product Identifier	Product Name	1/2022	2/2022	3/2022	4/2022	5/2022	6/2022
O3M-80	NRT IASI CO	avg: 01:04 min: 00:29 max: 02:46	avg: 01:04 min: 00:43 max: 02:24	avg: 01:08 min: 00:32 max: 02:13	avg: 01:08 min: 00:44 max: 02:16	avg: 01:08 min: 00:41 max: 01:54	avg: 01:09 min: 00:44 max: 02:27
O3M-57	NRT IASI SO2	avg: 01:04 min: 00:29 max: 02:46	avg: 01:04 min: 00:43 max: 02:24	avg: 01:08 min: 00:32 max: 02:13	avg: 01:08 min: 00:44 max: 02:21	avg: 01:08 min: 00:41 max: 01:54	avg: 01:09 min: 00:44 max: 02:24
O3M-81	NRT IASI HNO3	avg: 01:04 min: 00:29 max: 02:46	avg: 01:04 min: 00:43 max: 02:24	avg: 01:08 min: 00:32 max: 02:13	avg: 01:08 min: 00:44 max: 02:21	avg: 01:09 min: 00:41 max: 01:54	avg: 01:09 min: 00:44 max: 02:21
O3M-49	NRT IASI ozone profile	avg: 01:04 min: 00:29 max: 02:46	avg: 01:04 min: 00:43 max: 02:24	avg: 01:08 min: 00:32 max: 02:13	avg: 01:08 min: 00:44 max: 02:21	avg: 01:09 min: 00:41 max: 01:54	avg: 01:09 min: 00:44 max: 02:24

Table 6.4. Timeliness of Metop-C IASI NRT products during the reporting period

Product Identifier	Product Name	1/2022	2/2022	3/2022	4/2022	5/2022	6/2022
O3M-352	NRT IASI CO	avg: 01:37 min: 00:53 max: 02:41	avg: 01:37 min: 00:49 max: 03:00	avg: 01:36 min: 00:55 max: 02:25	avg: 01:37 min: 00:54 max: 02:20	avg: 01:39 min: 00:57 max: 02:21	avg: 01:40 min: 00:57 max: 02:27
O3M-377	NRT IASI SO2	avg: 01:37 min: 00:53 max: 02:44	avg: 01:38 min: 00:49 max: 03:00	avg: 01:37 min: 00:55 max: 02:23	avg: 01:37 min: 00:54 max: 02:20	avg: 01:40 min: 00:57 max: 02:22	avg: 01:40 min: 00:57 max: 02:27
O3M-336	NRT IASI HNO3	avg: 01:37 min: 00:53 max: 02:44	avg: 01:38 min: 00:49 max: 03:00	avg: 01:37 min: 00:56 max: 02:23	avg: 01:37 min: 00:54 max: 02:20	avg: 01:40 min: 00:57 max: 02:22	avg: 01:40 min: 00:57 max: 02:27
O3M-315	NRT IASI ozone profile	avg: 01:37 min: 00:53 max: 02:44	avg: 01:38 min: 00:49 max: 03:00	avg: 01:37 min: 00:56 max: 02:23	avg: 01:37 min: 00:54 max: 02:20	avg: 01:40 min: 00:57 max: 02:22	avg: 01:40 min: 00:57 max: 02:27

6.2. Services, main events and anomalies

Table 6.5. Number of products stored locally at EUMETSAT[1]

Product Identifier	Product Name	Metop satellite	1/2022	2/2022	3/2022	4/2022	5/2022	6/2022
O3M-80	NRT IASI CO	B	14765	13285	11547	14215	14802	14315
O3M-352		C	14838	13233	14722	14325	14793	14325
O3M-57	NRT IASI SO2	B	14764	13285	11547	14215	14802	14307
O3M-377		C	14838	13233	14723	14325	14793	14323
O3M-81	NRT IASI HNO3	B	14764	13285	11547	14215	14802	14307
O3M-336		C	14838	13233	14723	14325	14793	14323
O3M-49	NRT IASI ozone profile	B	14764	13285	11547	14215	14802	14307
O3M-315		C	14838	13233	14723	14325	14793	14323

[1] PDUs are concatenated back to orbit-based products before being stored

Table 6.6. EUMETCast uploads[1]

Product Identifier	Product Name	Metop satellite	1/2022	2/2022	3/2022	4/2022	5/2022	6/2022
O3M-80	NRT IASI CO	B	14736	13399	11551	14202	14779	14290
O3M-352		C	14829	13351	14716	14299	14774	14287
O3M-57	NRT IASI SO2	B	14734	13399	11551	14202	14779	14291
O3M-377		C	14829	13351	14716	14299	14774	14287
O3M-81	NRT IASI HNO3	B	14735	13399	11551	14202	14779	14289
O3M-336		C	14829	13351	14716	14299	14774	14287
O3M-49	NRT IASI ozone profile	B	14735	13399	11551	14202	14779	14290
O3M-315		C	14829	13351	14716	14299	14774	14287

[1] NRT IASI products are disseminated via EUMETCast (in BUFR format)

Table 6.7 lists the main events (product/service/hardware/software updates etc.) at EUMETSAT during the reporting period.

Table 6.7. Main planned activities at EUMETSAT during the reporting period

ID	Date	Description
1	8-14 March	200K IASI decontamination
2	29 March	External calibration

Table 6.8 lists the main local and external anomalies at EUMETSAT during the reporting period. Corrective and preventive actions should be provided also when applicable.

Table 6.8. Main local and external anomalies affecting EUMETSAT systems and performance during the reporting period

ID	Time period	Description
		Nothing to report.

7. Validation and quality monitoring

This section describes the validation status and validation/quality monitoring activities of NRT and offline data products during the reporting period. Validation reports for data records are found from https://acsaf.org/valreps.html

Reference documents are listed in Section 1.3 and accuracy requirements in Section 1.5.

7.1. Total ozone column products

Table 7.1. Validation status of total ozone column products

Product Identifier	Product Name	Accuracy	Reference	Validating Institute	Correlative data sources
O3M-41.1	NRT total O3	Fulfils threshold accuracy requirement	RD5	AUTH	World Ozone Mapping Centre
O3M-300			RD27		
O3M-06.1	Offline total O3	Fulfils threshold accuracy requirement	RD5	AUTH	World Ozone and Ultraviolet Radiation Data Center (WOUDC), of the World Meteorological Organization, (WMO), Global Atmosphere Watch, (GAW)
O3M-42.1					
O3M-301			RD27		

Validation results can be found in more detail on the AC SAF validation & quality assessment website at http://acsaf.physics.auth.gr/eumetsat/validation/near_real and http://acsaf.physics.auth.gr/eumetsat/validation/offline

7.1.1. GOME-2A, GOME-2B and GOME-2C total ozone column validation

This summary presents the validation activities for total ozone column products (TOCs), reported by the GOME-2/Metop-A, GOME-2/Metop-B and GOME-2/Metop-C instruments. Members of the Laboratory of Atmospheric Physics of the Aristotle University of Thessaloniki (LAP/AUTH), Thessaloniki, Greece, involved in the validation activities include Professor, Dr. Dimitris Balis, Special Teaching Fellow & Researcher, Dr. Katerina Garane and Research Associate, Dr. MariLiza Koukouli.

During the reporting period, the operational validation of offline total ozone and NRT total ozone products continued as per previous periods.

The GOME-2A sensor was decommissioned in November 2021, but the total ozone validation results are still included herein due to the fact that the ground-based dataset has been updated during the past six months.

7.1.1.1 Update of database for reference ground-based data

For the nominal validation, the ground-based TOCs from Brewer, Dobson and M-124 instruments reported to the World Ozone and Ultraviolet Radiation Data Centre (WOUDC), are employed. WOUDC is one of the World Data Centres which are part of the Global Atmosphere Watch (GAW) programme of the World Meteorological Organization (WMO). For the quality of the reference ground-based data used for the validation of the total ozone products, updated information were extracted from recent inter-comparisons and calibration records. This continuously updated selection of ground-based measurements has already been used numerous times in the validation and analysis of global total ozone records such as the inter-comparison between the OMI/Aura

TOMS and OMI/Aura DOAS algorithms [Balis *et al.*, 2007a], the validation of ten years of GOME/ERS-2 ozone record [Balis *et al.*, 2007b], the validation of the updated version of the OMI/Aura TOMS algorithm [Antón *et al.*, 2009], the GOME-2/Metop-A validation [Loyola *et al.*, 2011; Koukouli *et al.*, 2012], the GOME-2/Metop-B validation [Hao et al., 2014] and the evaluation of the European Space Agency's Ozone Climate Change Initiative project [O_3-CCI] TOCs [Koukouli *et al.*, 2015, Garane *et al.*, 2018], as well as in TROPOMI/S5P TOCs validation [Garane et al., 2019]. In all the aforementioned works, LAP/AUTH assumes the leading role in the validation efforts. The number of WOUDC ground-based stations used in the full operational periods of the two instruments, alongside the mean difference between ground- and space-based TOC estimates is given in Table 7.2.

7.1.1.2 GOME-2A, GOME-2B and GOME-2C TOC validation | The Dobson comparisons

GOME-2A, GOME-2B and GOME-2C OTO data for the period January 2007 to June 2022 have been downloaded, quality assured and pre-processed in order to perform the validation strategies. The GDP-4.8 algorithm is the latest version of the GDP-4.x suite of algorithms that have been used for the operational processing of GOME-2A and GOME-2B total ozone columns. GOME-2C is processed with GDP-4.9. The main differences between GDP-4.8 and GDP-4.9 concern the SO_2 vertical column retrieval. For ozone only minor updates have been performed, such as the optimization of the slit function, the introduction of a pseudo absorber for possible orbital variations of the resolution etc. Therefore, the ozone columns from GOME-2C can be assumed to be similar to the respective data from GOME-2 on Metop-B and Metop-A, analyzed with the previous version of the algorithm.

This period's satellite-to-ground-based measurements comparisons were performed and were added to the existing time series. The majority of the quality-assured ground-based Brewer and Dobson TOCs are reported to the WOUDC repository between 3 and 6 months after measurement, which accounts for the last couple of months missing from the comparative plots shown below. This is a common reporting feature, quite unavoidable.

The plots shown in Figure 7.1 panels a and b, show the status of the GOME-2A and GOME-2B since the beginning of each individual mission in the form of a monthly mean time-series of the percentage differences between each sensor and the Dobson stations (Northern Hemisphere stations to the left and Southern Hemisphere stations to the right). The monthly mean time series, both for the Northern (NH-left) as well as the Southern Hemisphere (SH -right), the differences appear well-stable in time and within -1 to +2.5 % to the ground network, depending on the season.

This seasonality in the differences between satellite and ground-based Dobson observations is a well-known feature which appears in most operational and scientific satellite TOC comparisons, see for e.g. the validation of the OMI/Aura products [Balis *et al.*, 2007a], the GOME/ERS-2 product [Balis *et al.*, 2007b] and even the recent GOME/ERS-2, SCIAMACHY/Envisat and GOME-2/Metop-A ESA products [Koukouli *et al.*, 2015, Garane *et al.*, 2018]. The reasons have to do with the treatment of the variability of the stratospheric temperature and how that affects the ozone absorption coefficients used in the different algorithms [Fragkos *et al.*, 2013; Serdyuchenko *et al.*, 2014]. Hence, when the stratospheric temperature deviates strongly from what is assumed by the algorithms, which is usually the case during the winter months, the differences between ground and satellite increase. See the work of Koukouli *et al.*, 2016, and discussion therein, on this topic.

The plots shown in panels c and d of Figure 7.1, show the common time period of operation of the GOME-2A and GOME-2B sensors, hence since the beginning of year 2013 onwards. There appear to be periods where the two instruments deviate in both the NH (panel c) and the SH (panel d); for the NH, a difference of ~ 1 % is seen for year 2013 as well as from mid-2015 onwards which manifests as a GOME-2A over-estimation in the former and under-estimation in the latter period. For the SH, the 2013 differences are observed again at the ~1 % difference level, extending up until mid-2014. The very good agreement between the two sensors is only interrupted between January and mid-March 2019, between mid-November 2019 and mid-April 2020, and since July 2020 due to the loss of solar visibility for GOME-2A. During these periods, a switch to the empirical solar model took place to substitute the sensor's normal measurements.

- For the period **January – March 2019**, the solar model deviated from GOME-2B by about -2 to -3 % in both Hemispheres
- For the period **November 2019 – April 2020** the deviation was about -2 % for the NH and -0.5 % for the SH
- GOME-2A was switched to the solar model again in **mid-July 2020** until its end of operation in November 2021. Its performance was almost the same as it was for in 2019, since the observed deviations between the two sensors go up to -3 %. The same feature is shown in Brewer comparisons.

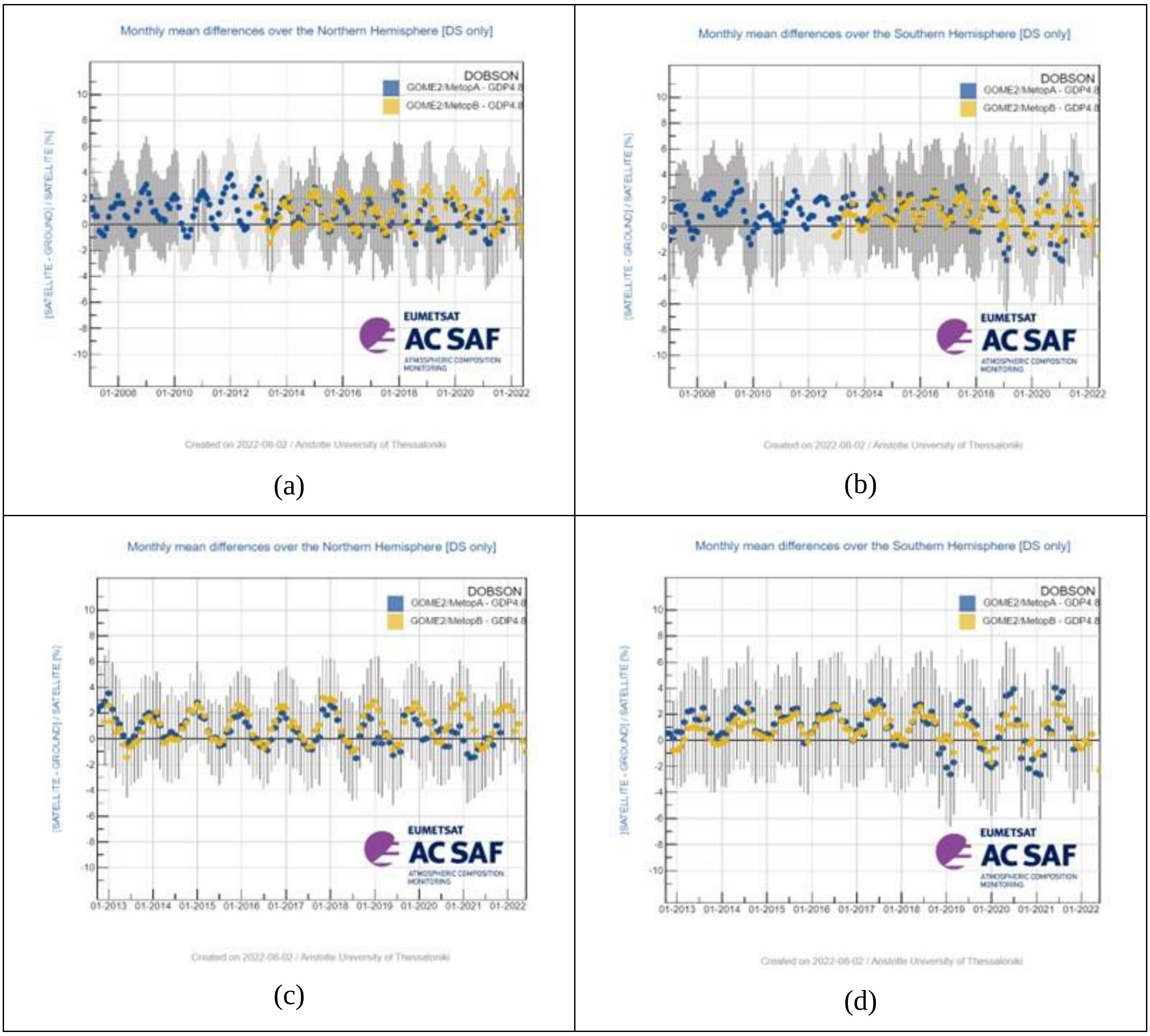

Figure 7.1. Time-series of the monthly mean percentage differences between GOME-2A GDP-4.8 (blue symbols) and GOME-2B GDP-4.8 (orange symbols) against the Dobson Northern Hemisphere stations

(left panels) and the Dobson Southern Hemisphere stations (right panels). Panels a and b show the full time period of operation of the two sensors, while the common time period of operation is shown in panels c and d.

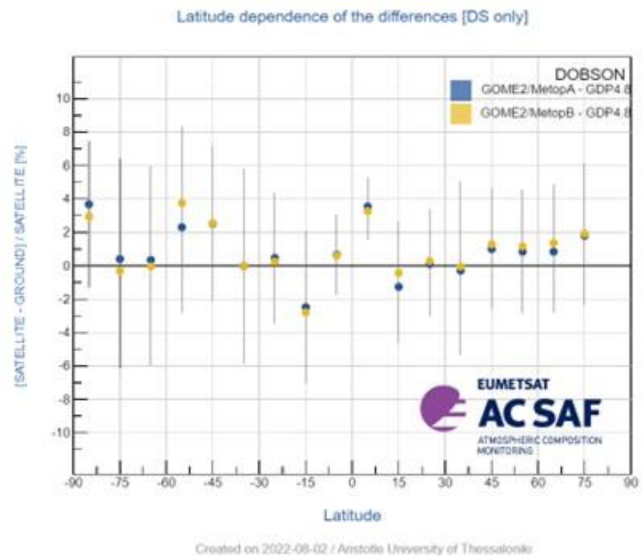

Figure 7.2. The latitudinal dependency of the differences for the Dobson network.

From the latitudinal variability plot shown in Figure 7.2, it can be seen that in the high southern latitudes, GOME-2A slightly (<1 %) over-estimates TOCs compared to GOME-2B, whereas in the NH their correlation is inverted. It must be stressed, though, that the periods of the switch to the solar model are included in these comparisons, increasing the deviation between the two sensors.

In Figure 7.3, the time-series of the monthly mean percentage differences for both hemispheres (panels a and b) and the pole-to-pole graph of the GOME-2B and GOME-2C comparisons are shown (panel c), for their common time period of operation (since January 2019). The agreement between the two sensors in the NH is different before and after spring of 2020:

- Before that point, the deviation of the two sensors was ~ 0 – 1 %, with GOME-2C reporting higher TOCs during summer months by up to ~0.8%.
- Since April 2020, their deviation gradually increases up to 2.2 % with GOME-2C reporting continuously higher TOCs than GOME-2B. The increased difference between the two sensors has a seasonal dependence, being lower during winter months (~0.5% for January 2020, ~0.9% for January 2021) and higher during summer months (~1.7% for June 2020, ~2.2% for June 2021). There is already a strong indication that their difference continues to increase during summer 2022: based on the limited number of co-locations for the most recent months, GOME-2C has a mean relative bias higher than GOME-2B by ~ 3 % for June 2022. In the SH, for the spring-summer months, an increased difference is also seen, going up to 2 – 2.5 %, with GOME-2C reporting higher O_3 values than GOME-2B. For the first 4-6 months of 2022, the number of ground-based measurements is still limited, especially for the SH, so these results are expected to be confirmed when more data are available.

In the latitudinal plot (Figure 7.3, panel c), it is shown that the TOC overestimation of GOME-2C with respect to GOME-2B is global and up to now it is more evident for the mid-latitudes and the tropics, where GOME-2C reports higher TOCs by about 1 – 2 % with respect to GOME-2B. The overall agreement of both sensors to the ground-based measurements is within 0 – 2 % in the tropics and the mid-latitudes. Additionally, it is noticeable that the comparisons of GOME-2C with respect to ground-based measurements have almost no dependency on latitude, having a very stable relative mean bias of ~2 % for the NH stations and for co-locations northwards 70°S.

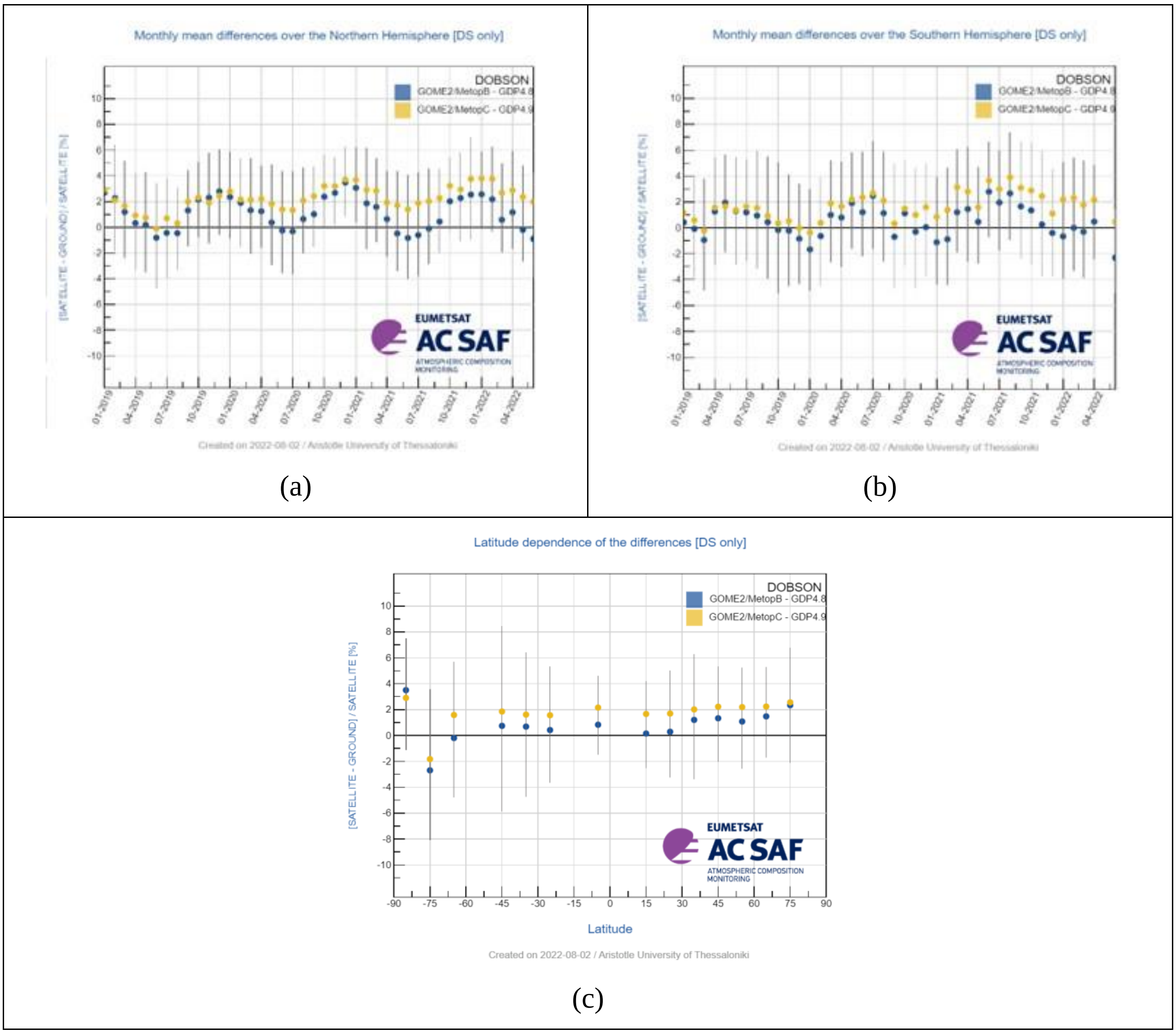

Figure 7.3. Panels (a) and (b) show the time-series of the monthly mean percentage differences between GOME-2B GDP-4.8 (blue symbols) and GOME-2C GDP-4.9 (orange symbols) against the Dobson Northern Hemisphere stations (panel a) and the Dobson Southern Hemisphere stations (panel b). Panel c shows the latitudinal dependency of the differences for the Dobson network.

7.1.1.3 GOME-2A, GOME-2B and GOME-2C TOC validation | The Brewer comparisons

In Figure 7.4, the time-series of the comparisons between GOME-2A and GOME-2B and Brewer TOCs are shown for the Northern Hemisphere (upper plots). In panel (a) the whole time series for each sensor is shown and in panel (b) only the common period of operation, between 2013 and June 2022, is used. A very similar behaviour is observed in the latter plot (panel b), as per Figure 7.1 panel c, for the Dobson comparisons. The respective deviations by ~ 2 – 3 % between the two sensors during the switches to the empirical solar model are also seen here. In the panel c of Figure 7.4, the latitudinal variability of the differences is presented, which shows a very good agreement between the two sensors for the years of common operation.

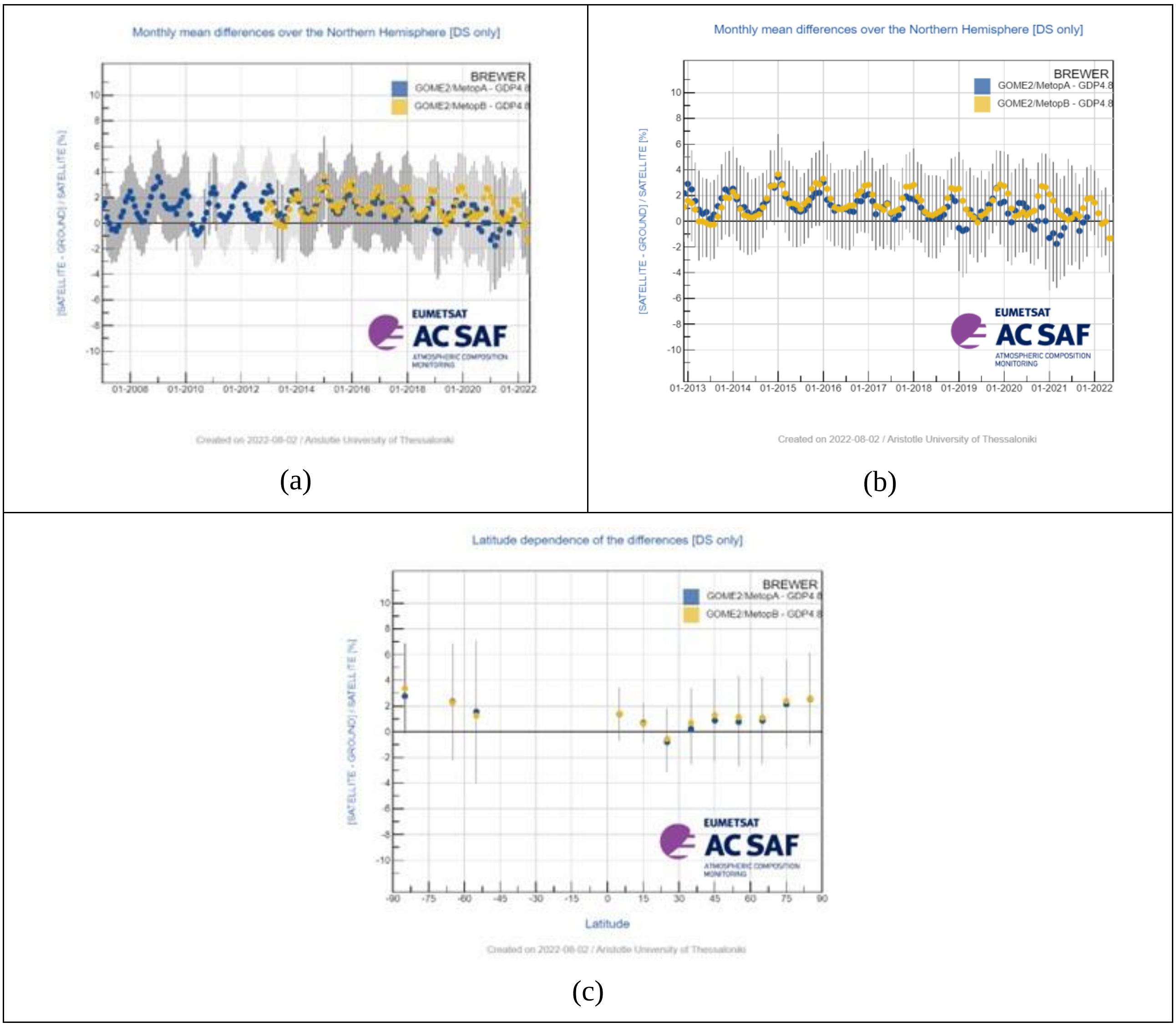

Figure 7.4. Panels (a) and (b) show the time-series of the monthly mean percentage differences between GOME-2A GDP-4.8 (blue symbols) and GOME-2B GDP-4.8 (orange symbols) against the Brewer reported TOCs. Panel a shows the full time series of operation for the two sensors and panel b shows the common time period of operation, since 2013. Panel (c) shows the latitudinal dependency of the differences for the Brewer network.

Figure 7.5 shows the same time series and latitudinal plots as in Figure 7.4, for the GOME-2B and GOME-2C common time period of operation, thus since January 2019. The higher deviation between the two sensors for the spring-summer months is also seen here, and is again increasingly enhanced during 2020, 2021 and early 2022. In the latitudinal plot, it is seen that for the Northern high latitude Brewer comparisons GOME-2C has an almost constant positive bias with respect to GOME-2B of about 0.5 %, which is increased to 1 % for the co-locations within the tropics.

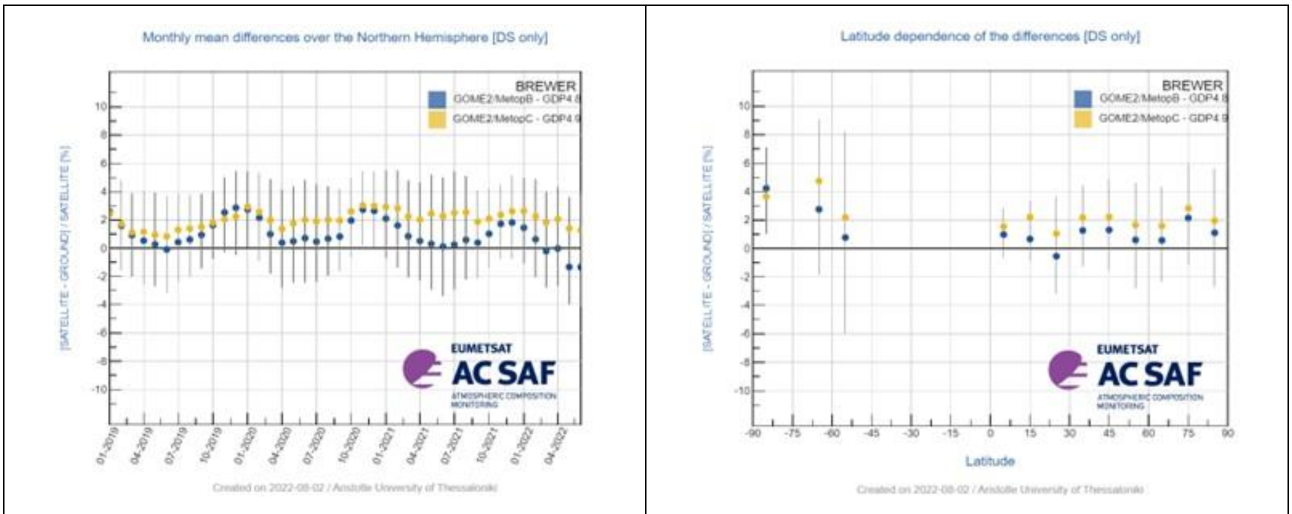

(a) (b)

Figure 7.5. Panel (a) shows the time-series of the monthly mean percentage differences between GOME-2B GDP-4.8 (blue symbols) and GOME-2C GDP-4.9 (orange symbols) against the Brewer reported TOCs. Panel (b) shows the latitudinal dependency of the differences for the Brewer network.

7.1.1.4 GOME-2A, GOME-2B and GOME-2C TOC validation | Tables of statistics

In Table 7.2, the summary statistics for the comparisons presented in Sections 7.1.1.2 and 7.1.1.3, for the Dobson and the Brewer stations, are enumerated. The number of individual daily common observations for the Dobsons apply to the entire globe, whereas the Brewer comparisons depict only the NH. As can be noted, the relative differences between GOME-2A and GOME-2B against Brewer and Dobson stations are very stable, with an average mean difference of less than +1 ± 4.5 %. GOME-2C has a higher mean relative bias with respect to ground-based measurements, of +1.5 ± 4.0 %.

Table 7.2. Summary statistics for the respective time period of operation of each sensor, based on GOME-2A, GOME-2B & GOME-2C OTO data compared to WOUDC Brewer & Dobson observations

		Brewer	**Dobson**
GOME-2/Metop-A 01/2007 – 11/2021	# stations:	76	68
	# obs:	211353	147057
	Mean Rel. Bias (%):	**0.76 ± 4.41**	**0.74 ± 4.74**
GOME-2/Metop-B 01/2013 – 06/2022	# stations:	66	64
	# obs:	150611	99683
	Mean Rel. Bias (%):	**0.90 ± 4.17**	**0.76 ± 4.52**
GOME-2/Metop-C 01/2019 – 06/2022	# stations:	50	46
	# obs:	48391	25913
	Mean Rel. Bias (%):	**1.52 ± 3.79**	**1.70 ± 4.31**

7.1.2. Validation website update

The AC SAF Ozone Validation & Quality Assessment was launched on the initiation of the project's CDOP 2 phase in 2013. The validation webpages host the validation results of GOME-2A GDP-4.8, GOME-2B GDP4.8 and GOME-2C GDP4.9 near real-time and offline total ozone data. Currently, the validation results are available until June 2022.

The website and the processing algorithms that run behind it are routinely inspected and quality controlled. All the necessary actions, needed to keep it at its current good state, are taken by the LAP/AUTH team.

In Figure 7.6 and Figure 7.7 some example statistics about the website traffic are shown for the period 1 January – 30 June 2022, as extracted from Google Analytics.

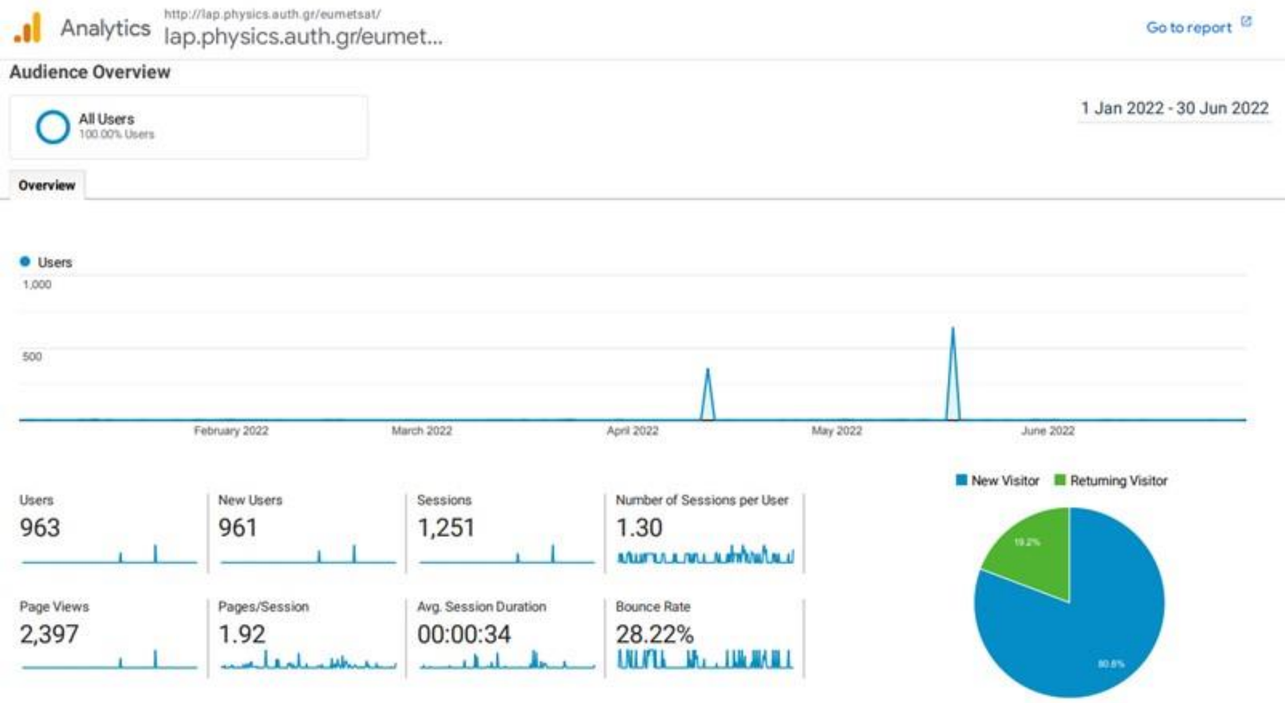

Figure 7.6. The activity of the users of the AC SAF validation web pages.

Country	Acquisition: Users	Acquisition: New Users	Acquisition: Sessions	Behaviour: Bounce Rate	Behaviour: Pages/Session	Behaviour: Avg. Session Duration	Conversions: Goal Conversion Rate	Conversions: Goal Completions	Conversions: Goal Value
	963 % of Total: 100.00% (963)	962 % of Total: 100.10% (961)	1,251 % of Total: 100.00% (1,251)	28.22% Avg for View: 28.22% (0.00%)	1.92 Avg for View: 1.92 (0.00%)	00:00:34 Avg for View: 00:00:34 (0.00%)	0.00% Avg for View: 0.00% (0.00%)	0 % of Total: 0.00% (0)	US$0.00 % of Total: 0.00% (US$0.00)
1. United States	79	79	102	29.41%	1.73	00:00:13	0.00%	0	US$0.00
2. China	47	47	60	30.00%	1.77	00:00:08	0.00%	0	US$0.00
3. Japan	40	40	52	30.77%	1.69	00:00:07	0.00%	0	US$0.00
4. India	37	37	52	28.85%	1.71	00:00:07	0.00%	0	US$0.00
5. Brazil	36	36	46	32.61%	1.67	00:00:07	0.00%	0	US$0.00
6. United Kingdom	27	27	30	26.67%	1.90	00:00:21	0.00%	0	US$0.00
7. Germany	26	26	38	18.42%	2.42	00:00:56	0.00%	0	US$0.00
8. France	26	26	33	39.39%	1.61	00:00:06	0.00%	0	US$0.00
9. Mexico	26	26	27	25.93%	1.74	00:00:07	0.00%	0	US$0.00
10. Russia	24	24	35	17.14%	1.83	00:00:08	0.00%	0	US$0.00

Rows 1 - 10 of 114

Figure 7.7. The location of the website visitors.

References:

Antón, M., Loyola, D., López, M., Vilaplana, J. M., Bañón, M., Zimmer, W., and Serrano, A.: Comparison of GOME-2/MetOpA total ozone data with Brewer spectroradiometer data over the Iberian Peninsula, Annales Geophysicae, 27, 1377–1386, 2009. https://doi.org/10.5194/angeo-27-1377-2009

Balis, D., Kroon M., Koukouli, M.E., Brinksma, E. J., Labow, G., Veefkind, J. P., and McPeters, R. D.: Validation of Ozone Monitoring Instrument total ozone column measurements using Brewer and Dobson spectrophotometer ground-based observations, J. Geophys. Res., 112, D24S46, 2007a. https://doi.org/10.1029/2007JD008796

Balis, D., Lambert, J-C., Van Roozendael, M., Spurr, R., Loyola, D., Livschitz, Y., Valks, P., Amiridis, V., Gerard, P., Granville, J., and Zehner, C.: Ten years of GOME/ERS-2 total ozone data – The new GOME data processor (GDP) version 4: 2. Ground-based validation and comparisons with TOMS V7/V8, J. Geophys. Res., vol. 112, D07307, 2007b. https://doi.org/10.1029/2005JD006376

Fragkos, K., Bais, A. F., Balis, D., Meleti, C., and Koukouli, M. E.: The effect of three different absorption cross-sections and their temperature dependence on total ozone measured by a mid-latitude Brewer spectrophotometer, Atmos. Ocean, 53, 2015. https://doi.org/10.1080/07055900.2013.847816

Hao, N., Koukouli, M. E., Inness, A., Valks, P., Loyola, D. G., Zimmer, W., Balis, D. S., Zyrichidou, I., Van Roozendael, M., Lerot, C., and Spurr, R. J. D.: GOME-2 total ozone columns from MetOp-A/MetOp-B and assimilation in the MACC system, Atmos. Meas. Tech., 7, 2937-2951, 2014. https://doi.org/10.5194/amt-7-2937-2014

Koukouli, M. E., Balis, D. S., Loyola, D., Valks, P., Zimmer, W., Hao, N., Lambert, J.-C., Van Roozendael, M., Lerot, C., and Spurr, R. J. D.: Geophysical validation and long-term consistency between GOME-2/MetOp-A total ozone column and measurements from the sensors GOME/ERS-2, SCIAMACHY/ENVISAT and OMI/Aura, Atmos. Meas. Tech., 5, 2169-2181, 2012. https://doi.org/10.5194/amt-5-2169-2012

Koukouli, M. E., Lerot, C., Granville, J., Goutail, F., Lambert, J.-C., Pommereau, J.-P., Balis, D., Zyrichidou, I., Van Roozendael, M., Coldewey-Egbers, M., Loyola, D., Labow, G., Frith, S., Spurr, S., and Zehner, C.: Evaluating a new homogeneous total ozone climate data record from GOME/ERS-2, SCIAMACHY/Envisat and GOME-2/MetOp-A, J. Geophys. Res. Atmos., 120, 12296-12312, 2015. https://doi.org/10.1002/2015JD023699

Koukouli, M. E., Zara, M., Lerot, C., Fragkos, K., Balis, D., van Roozendael, M., Allart, M. A. F., and van der A, R. J.: The impact of the ozone effective temperature on satellite validation using the Dobson spectrophotometer network, Atmos. Meas. Tech., 9, 2055-2065, 2016. https://doi.org/10.5194/amt-9-2055-2016

Loyola, D. G., Koukouli, M. E., Valks, P., Balis, D. S., Hao, N., Van Roozendael, M., Spurr, R. J. D., Zimmer, W., Kiemle, S., Lerot, C., and Lambert, J.-C.: The GOME-2 total column ozone product: Retrieval algorithm and ground-based validation, J. Geophys. Res., 116, 2011. https://doi.org/10.1029/2010JD014675

Serdyuchenko, A., Gorshelev, V., Weber, M., Chehade, W., and Burrows, J. P.: High spectral resolution ozone absorption cross-sections – Part 2: Temperature dependence, Atmos. Meas. Tech.,7, 625–636, 2014. https://doi.org/10.5194/amt-7-625-2014

Garane, K., Lerot, C., Coldewey-Egbers, M., Verhoelst, T., Koukouli, M. E., Zyrichidou, I., Balis, D. S., Danckaert, T., Goutail, F., Granville, J., Hubert, D., Keppens, A., Lambert, J.-C., Loyola, D., Pommereau, J.-P., Van Roozendael, M., and Zehner, C.: Quality assessment of the Ozone_cci

Climate Research Data Package (release 2017) – Part 1: Ground-based validation of total ozone column data products, Atmos. Meas. Tech., 11, 1385-1402, 2018.
https://doi.org/10.5194/amt-11-1385-2018

Garane, K., Koukouli, M.-E., Verhoelst, T., Lerot, C., Heue, K.-P., Fioletov, V., Balis, D., Bais, A., Bazureau, A., Dehn, A., Goutail, F., Granville, J., Griffin, D., Hubert, D., Keppens, A., Lambert, J.-C., Loyola, D., McLinden, C., Pazmino, A., Pommereau, J.-P., Redondas, A., Romahn, F., Valks, P., Van Roozendael, M., Xu, J., Zehner, C., Zerefos, C., and Zimmer, W.: TROPOMI/S5P total ozone column data: global ground-based validation and consistency with other satellite missions, Atmos. Meas. Tech., 12, 5263–5287, 2019.
https://doi.org/10.5194/amt-12-5263-2019

7.1.3. Online quality monitoring

The online quality monitoring tool is operational and consists of the continuous generation of plots showing the slant column density (SCD) distribution, the vertical column density (VCD) distribution as well as the root mean square (RMS) as histograms per sensing day as well as time series per sensing month. These plots are generated for three different geographic regions, the pacific ocean (25-15S, 210-250E), the Sahara desert (20-30N, 0-30E) and global, in order to represent typical extremes of ground reflectivity and atmospheric conditions as well as the global mean. The plots are generated per sensing instrument (GOME-2A, GOME-2B, GOME-2C) and per product (O3, NO2, BrO, HCHO, SO2, H2O).

The online quality monitoring plots are published in PDF format on the DLR AC SAF FTP server (acsaf.eoc.dlr.de) using the following directory schemes:

/oq/GOME-2[ABC]/[O3 NO2 BrO HCHO SO2 H2O]/daily/YYYY/MM/DD/[global sahara pacific]/*.[vcd scd rms]_hist.pdf
/oq/GOME-2[ABC]/[O3 NO2 BrO HCHO SO2 H2O]/monthly/YYYY/MM/[global sahara pacific]/*.[vcd scd rms]_series.pdf

More information about quality monitoring of the operational GOME-2 total ozone columns by other AC SAF and external partners is available at the following websites:
https://acsaf.org → Validation & QA → QM websites
http://acsaf.physics.auth.gr/eumetsat/validation/near_real
http://acsaf.physics.auth.gr/eumetsat/validation/offline
https://www.temis.nl/acsaf/vod.php
https://www.ecmwf.int/en/forecasts/charts/obstat/?facets=Parameter,Ozone;Instrument,GOME2

7.2. Tropospheric ozone products

Table 7.3. Validation status of tropospheric ozone products

Product Identifier	Product Name	Accuracy	Reference	Validating Institute	Correlative data sources
O3M-35	Offline tropical tropospheric ozone	Fulfils target accuracy requirement	RD18	KMI	Ozonesonde data from SHADOZ, NDACC, NILU and WOUDC
O3M-43					
O3M-302			RD24		
O3M-174	NRT global tropospheric ozone	Fulfils target accuracy requirement	RD19	KMI	Ozonesonde data from SHADOZ, NDACC, NILU and WOUDC
O3M-304			RD25		

Product Identifier	Product Name	Accuracy	Reference	Validating Institute	Correlative data sources
O3M-173	Offline global tropospheric ozone	Fulfils target accuracy requirement	RD19	KMI	Ozonesonde data from SHADOZ, NDACC, NILU and WOUDC
O3M-175					
O3M-305			RD25		

Validation activities summary for global tropospheric ozone:

This summary contains validation results of the GOME-2B and GOME-2C high resolution (HR) global tropospheric ozone column (TrOC) products, retrieved by the Ozone Profile Retrieval Algorithm (OPERA) at KNMI. It covers the time period July 2021 – June 2022. Validation results are shown from two TrOC products, i.e. the tropopause related product and a fixed altitude TrOC product. The TrOC products are derived from the daily operational ozone profile product.

Since these TrOC products are derived from the OPERA ozone profile product, OPERA averaging kernel smoothing has been applied to the ground-based reference profiles before calculating comparison statistics. This AVK smoothing is expected to reduce the vertical smoothing difference error between satellite and ground-based measurements. The outcome is summarized at the end of this section.

The global tropospheric ozone column (TrOC) product has the following user requirements:

- Threshold accuracy: within 50 %
- Target accuracy: within 20 %
- Optimal accuracy: within 15 %

This summary was made available by Dr. Andy Delcloo from KMI. More information on how these values are extracted is available in the validation report. The collocation data used are the same as for the ozone profiles (Figure 7.23).

The statistics on the accuracy of the GOME-2B and GOME-2C HR tropospheric ozone column products (tropopause related) for different latitude belts, validated against $X_{AVK\text{-}sonde}$, are shown in Table 7.4 and Table 7.5.

Table 7.4. Relative differences (RD) and standard deviation (STDEV) are shown (in percent) together with the absolute difference (DU) on the accuracy of the GOME-2B HR tropospheric ozone column products (tropopause related) for five different latitude belts, validated against $X_{AVK\text{-}sonde}$

July 2021 – June 2022	GOME-2B HR			
	RD (%)	STDEV (%)	AD (DU)	STDEV (DU)
Northern Polar Region	-8.00	12.6	-2.26	5.89
Northern Mid-Latitudes	-3.98	19.1	-1.30	5.39
Tropical region	2.15	25.55	0.44	5.64
Southern Mid-Latitudes	-0.06	20.7	0.26	4.89
Southern Polar Region	-14.0	41.5	-2.26	6.68

Table 7.5. Relative differences (RD) and standard deviation (STDEV) are shown (in percent) together with the absolute difference (DU) on the accuracy of the GOME-2C HR tropospheric ozone column products (tropopause related) for five different latitude belts, validated against $X_{AVK\text{-}sonde}$

July 2021 – June 2022	GOME-2C HR			
	RD (%)	**STDEV (%)**	**AD (DU)**	**STDEV (DU)**
Northern Polar Region	-12.8	12.6	-3.96	5.66
Northern Mid-Latitudes	13.2	22.2	3.82	6.46
Tropical region	**51.6**	33.9	11.8	6.59
Southern Mid-Latitudes	9.35	30.5	2.11	6.77
Southern Polar Region	-6.95	39.2	-0.82	4.97

The statistics on the accuracy of the GOME-2A, GOME-2B and GOME-2C HR tropospheric ozone column products (fixed altitude) for different latitude belts, validated against $X_{AVK\text{-}sonde}$, are shown in Table 7.6 and Table 7.7.

Table 7.6. Relative differences (RD) and standard deviation (STDEV) are shown (in percent) together with the absolute difference (DU) on the accuracy of the GOME-2B HR tropospheric ozone column products (fixed altitude) for five different latitude belts, validated against $X_{AVK\text{-}sonde}$

July 2021 – June 2022	GOME-2B HR			
	RD (%)	**STDEV (%)**	**AD (DU)**	**STDEV (DU)**
Northern Polar Region	-3.62	5.41	-0.63	0.93
Northern Mid-Latitudes	-2.84	10.2	-0.50	1.77
Tropical region	-1.88	26.9	-0.17	3.05
Southern Mid-Latitudes	-0.22	11.7	-0.01	1.33
Southern Polar Region	2.49	31.0	-0.29	1.16

Table 7.7. Relative differences (RD) and standard deviation (STDEV) are shown (in percent) together with the absolute difference (DU) on the accuracy of the GOME-2C HR tropospheric ozone column products (fixed altitude) for five different latitude belts, validated against $X_{AVK\text{-}sonde}$

July 2021 – June 2022	GOME-2C HR			
	RD (%)	**STDEV (%)**	**AD (DU)**	**STDEV (DU)**
Northern Polar Region	-3.47	6.13	-0.59	1.03
Northern Mid-Latitudes	6.66	11.7	1.13	2.01
Tropical region	**50.3**	35.3	5.93	3.46
Southern Mid-Latitudes	4.11	14.5	0.43	1.63
Southern Polar Region	7.47	43.8	-0.13	1.33

For the GOME-2B and GOME-2C TrOC products, most of these products comply with the target accuracy requirement. Only for the tropical region (GOME-2C), this is not the case. Between all sensors, there is a clear offset visible in the results. Also here, a degradation correction will be necessary to correct for this offset.

Validation activities summary for tropical tropospheric ozone:

This summary contains validation results of the GOME-2B and GOME-2C tropical tropospheric ozone column (TTrOC) products, using the cloud slicing method. The tropospheric ozone retrieval is based on the GOME-2 ozone columns as derived by the GOME Data Processor (GDP, version 4.8) and covers the tropical latitude belt (20S – 20N). This product is available on a monthly basis and has a resolution of 1.25° latitude x 2.5° longitude.

The tropical tropospheric ozone column product has the following user requirements:

- Threshold accuracy: within 50 %
- Target accuracy: within 25 %
- Optimal accuracy: within 15 %

This summary was made available by Dr. Andy Delcloo from KMI. More information on how these values are extracted is available in the validation report. The collocation data used are the same as for the ozone profiles (Figure 7.23).

The time period covered is January 2020 – December 2021 for the GOME-2B and GOME-2C offline TTrOC products.

In Table 7.8 and Table 7.9, the statistics on the accuracy of the GOME-2B/C tropical tropospheric ozone column products for different stations under consideration are shown, showing some general statistics for each dataset. It is shown that most of the stations are within the target accuracy (25 %). The correlation varies between 0.3 and 0.9 with a rmse between 2.6 and 4.7 DU. There is also an offset present between GOME-2B/GOME-2C as described in the validation report. These TTrOC products still fulfill the user requirements.

Table 7.8. Relative Differences (RD), standard deviation (STDEV), correlation, bias and RMSE are shown on the accuracy of the GOME-2B TTrOC product for the time period January 2020 – December 2021

Station	RD (%)	STDEV (%)	Correlation	Bias (DU)	RMSE (DU)
Paramaribu	14.5	25.9	0.33	2.55	5.21
Alajuela	30.2	22.4	0.59	4.69	5.71
Samoa	18.1	24.2	0.63	2.42	4.07
Ascension Island	2.10	9.92	0.87	0.67	2.92
Kuala Lumpur	-5.94	11.8	0.78	-1.43	3.08
Natal	5.65	16.3	0.81	1.38	3.72

Table 7.9. Relative Differences (RD), standard deviation (STDEV), correlation, bias and RMSE are shown on the accuracy of the GOME-2C TTrOC product for the time period January 2020 – December 2021

Station	RD (%)	STDEV (%)	Correlation	Bias (DU)	RMSE (DU)
Paramaribu	14.5	24.6	0.18	2.49	5.12
Alajuela	27.3	17.4	0.74	4.34	5.02
Samoa	20.8	22.3	0.82	3.21	5.07
Ascension Island	4.30	13.1	0.79	1.38	4.12
Kuala Lumpur	-6.23	14.8	0.81	-1.43	2.79
Natal	3.34	14.9	0.86	0.94	3.37

7.3. Trace gas products

Table 7.10. Validation status of trace gas products

Product Identifier	Product Name	Accuracy	Reference	Validating Institute	Correlative data sources
O3M-50.1	NRT total NO2	Fulfils threshold accuracy requirement	RD6	BIRA-IASB	NDACC zenithSky measurements
O3M-338			RD28		
O3M-52.1	NRT tropospheric NO2	Fulfils threshold accuracy requirement	RD6	BIRA-IASB	BIRA-IASB MAXDOAS stations
O3M-341			RD28		
O3M-55.1	NRT total SO2	Fulfils threshold accuracy requirement	RD10	BIRA-IASB	BIRA-IASB Xianghe MAXDOAS station
O3M-374			RD34		
O3M-177	NRT total HCHO	Fulfils threshold accuracy requirement	RD12	BIRA-IASB	BIRA-IASB MAXDOAS stations
O3M-344			RD29		
O3M-51.1	Offline total NO2	Fulfils threshold accuracy requirement	RD6	BIRA-IASB	NDACC zenithSky measurements
O3M-339			RD28		
O3M-37.1	Offline tropospheric NO2	Fulfils threshold accuracy requirement	RD6	BIRA-IASB	BIRA-IASB MAXDOAS stations
O3M-53.1					
O3M-342			RD28		
O3M-09.1	Offline total SO2	Fulfils threshold accuracy requirement	RD10	BIRA-IASB	BIRA-IASB Xianghe MAXDOAS station
O3M-56.1					
O3M-375					
O3M-08.1	Offline total BrO	Fulfils threshold accuracy requirement	RD11	BIRA-IASB	BIRA-IASB Harestua zenithSky station
O3M-82.1					
O3M-317			RD30		

Product Identifier	Product Name	Accuracy	Reference	Validating Institute	Correlative data sources
O3M-10.1	Offline total HCHO	Fulfils target accuracy requirement	RD12	BIRA-IASB	BIRA-IASB MAXDOAS stations
O3M-58.1					
O3M-345			RD29		
O3M-12.1	Offline total H2O	Fulfils threshold accuracy requirement	RD13	FMI, DLR	IGRA, COSMIC-SuomiNet, SSM/I
O3M-86.1					
O3M-386			RD31		Comparison against GOME-2B water vapour data

Validation activities summary:

This summary presents validation activities for offline total and tropospheric NO_2, total HCHO, total BrO and SO_2 data products of GOME-2B/C as performed at BIRA-IASB.

The authors of this summary are Gaia Pinardi (for tropospheric NO_2, HCHO and SO_2 validation), Jean-Christopher Lambert, José Granville and Tijl Verhoelst (for total/stratospheric NO_2 validation), François Hendrick (for BrO validation) and Jeroen van Gent (for quality assessment).

Validation exercises are performed following the protocols described in the original Metop-A, Metop-B and Metop-C validation reports and updated in Pinardi *et al*. (AMT 2020) and Verhoelst *et al*. (AMT 2021), and the results presented in this report are based on updates of the correlative datasets with the last available – and sometimes improved – versions. While illustrations at a few stations are included in this report, all the updated figures are reported on the BIRA-IASB trace gases validation server.

Update of database for reference data

The validation database was updated with ground-based BIRA-IASB MAXDOAS NO_2 and HCHO data, BIRA-IASB ZenithSky BrO data at Harestua, NDACC UVVIS ZenithSky NO_2 data and Xianghe MAXDOAS SO_2 data, in order to cover as much as possible of the period until mid-2022.

ZenithSky NO_2 total columns are collected from the NDACC Data Host Facility (to where the data have to be uploaded by instrument PIs within 1 year after data acquisition) and from the SAOZ rapid delivery operational facility operated by LATMOS. The ground-based data are then quality assessed and post-processed at BIRA-IASB in preparation for the data comparisons. This preparation includes calculation of the effective ground-based airmasses with which GOME-2 data co-locations will be sought.

Ground-based BrO columns are derived at Harestua from vertical profiles retrieved by applying an OEM (Optimal Estimation Method)-based profiling technique to zenith-sky measurements at sunrise (Hendrick *et al.*, 2007).

The BIRA-IASB MAXDOAS ground-based dataset are automatically retrieved with an improved version of the bePRO profiling algorithm (Clémer *et al.*, 2010; Hendrick *et al.*, 2014, Vlemmix *et al.*, 2015) developed within the EU FP7 NORS and QA4ECV projects (aiming at rapid delivery of improved NO_2 and HCHO profiles), and is progressively shifting to the FRM4DOAS analysis chain. The FRM4DOAS (Fiducial Reference Measurements for Ground-Based DOAS Air-Quality Observations) is an ESA activity aiming at the development of the first centralised NRT processing system for MAX-DOAS instruments operated within the international Network for the Detection of Atmospheric Composition Change (NDACC). It includes the launch of the NDACC MAX-DOAS

Processing Service in a demonstration mode, focusing on tropospheric and stratospheric NO2 vertical profiles, total O3 columns, and tropospheric HCHO profiles as target MAX-DOAS products for the first phase of the project (July 2016 - August 2021), see https://frm4doas.aeronomie.be/. The lower tropospheric profiles and vertical columns processing chain rely on parallel runs of optimal-estimation based MMF (Friedrich *et al.*, 2019) and parametrized approach MAPA (Beirle *et al.*, 2019) algorithms and testings of their results coherence. The service is running in a best-effort mode at the time of writing for a limited number of stations belonging to the project partners.

The NO_2 and HCHO datasets include the following ground-based stations:

- OHP (from June 2007 to July 2014 with the geometrical approximation, and since August 2014 to March 2017 with the bePRO profiling tool)
- Beijing (from June 2008 to April 2009)
- Uccle (from April 2011 to March 2016 with a miniMAXDOAS instrument (Uccle-miniDOAS) and from end of January 2017 to February 2020 with a scientific grade MAXDOAS: Uccle-SG)
- Bujumbura (from November 2013 to July 2017; since then the instrument had a power failure and only limited operations and data transfer was possible)
- LePort, on Reunion Island (from April 2016 to 10 January 2018). The instrument has been reinstalled in June 2018 on the Maido site, and data analysis from the FRM4DOAS analysis chain was tested, but it is not adapted for tropospheric (NO_2, HCHO) gases validation at this mountaneous site and is not used for this report.
- Xianghe (from March 2010 to July 2018 and since October 2019). Unfortunately, since November 2021 the retrievals in the UV are of bad quality and the UV channel broke down early 2022. SO_2 MAXDOAS profiles were also analysed for the whole time-series (2010 to Oct. 2021), although the SO_2 levels are very low now in China nowadays.

Xianghe MAX-DOAS is the only station measuring during this report period and only tropopsheric NO_2 could be updated for this station.

Status of GOME-2A, GOME-2B and GOME-2C tropospheric NO_2

Comparisons with ground-based MAXDOAS instruments is performed similarly as in previous validation report. In Pinardi *et al*. (2020) it is shown that best results are achieved by filtering out the largest pixels and selecting only pixels covering the stations. For GOME-2, the selection includes keeping only pixels with a size of less than 100 km, while selecting pixels over the station, only slightly changes the results, as generally pixels with their center within 50 km, are covering the station. This improvement of the biases comes at the expenses of a strongly reduced number of pixels (see AC SAF Operations Report 1/2020).

For this report only Xianghe has data until mid-2022, and Figure 7.8 shows example of results for GOME-2B and GOME-2C for Xianghe. Monthly mean differences are calculated for every year and for the whole time-series in order to see the evolution in time of the bias. Table 7.11 reports the median differences and the spread (half the percentile 68) at the stations, with and without the smoothing, and the figures for all the stations can be found on the BIRA-IASB validation web server.

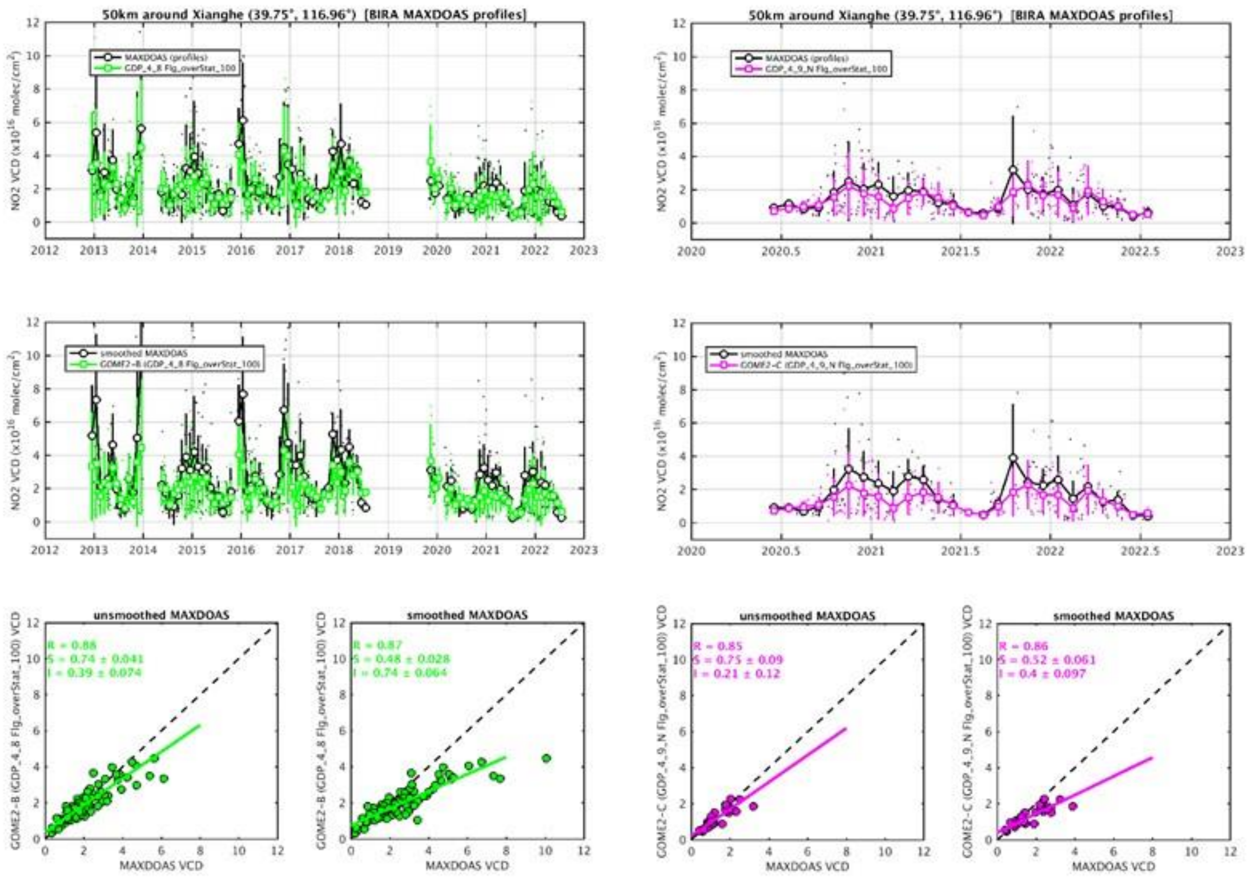

Figure 7.8. Illustration for the Xianghe MAXDOAS versus GOME-2B GDP-4.8 (left) and GOME-2C GDP-4.9 (right) tropospheric NO_2 comparisons, of the application of the satellite averaging kernels on MAXDOAS profiles.

Table 7.11. Median Absolute Differences (AD, in 10^{15} molec/cm²), Relative Differences (RD, in %) and spread (0.5*IP68) on the accuracy of GOME-2A, GOME-2B and GOME-2C tropospheric NO_2 products when comparing to MAXDOAS data (NOT cloud filtered). Values for the last 12 months are given, and the values for the whole time-series are reported in brackets for comparison. Results for both the original comparisons (pixels over the station, for pixels smaller than 100 km side) and for the smoothed comparisons are reported. <u>Only Xianghe data covers up to mid-2022. Note that GOME-2A mission ended 15 November 2021.</u>

	GOME-2A			GOME-2B			GOME-2C		
	AD ($\times 10^{15}$)	RD (%)	SPREAD (%)	AD ($\times 10^{15}$)	RD (%)	SPREAD (%)	AD ($\times 10^{15}$)	RD (%)	SPREAD (%)
Uccle SG last 12 months: 03/2019 – 02/2020 [whole period: 02/2017 – 02/2020]	-2.1 [-1.6]	-29 [-20]	40 [30]	-1.2 [-1.4]	-16 [-20]	33 [36]	-	-	-
Uccle SG smoothed	-3.7 [-2.3]	-51 [-24]	36 [28]	-2.5 [-2.7]	-26 [-29]	38 [36]	-	-	-

Reunion Maido (last 12 months: 12/2018 – 11/2019) [whole period: 06/2018 – 11/2019]	-0.09 [-0.01]	2 [37]	175 [201]	-0.02 [-0.02]	-4.2 [-4.3]	76 [93]	-	-	-
Reunion Maido smoothed	-0.08 [-0.03]	33 [13]	288 [237]	-0.03 [-0.01]	-1.4 [-9]	85 [115]	-	-	-
Xianghe (last 12 months: 12/2020 – 07/2022) [whole period: 03/2010 – 07/2022]	-7.2 [-2.21]	-51 [-13]	45 [23]	0.9 [-0.8]	-4.9 [-4.4]	26 [25]	-0.3 [-0.8]	-1.2 [-9]	23 [21]
Xianghe smoothed	-15 [-6.2]	-59 [-24]	28 [32]	-2.2 [-3.8]	-17 [-18]	28 [36]	-2.1 [-2.4]	-13 [-21]	29 [36]
Beijing [whole period: 06/2008 – 04/2009]	[-17]	[-47]	[21]	-	-	-	-	-	-
Beijing smoothed	[-15]	[-47]	[32]	-	-	-	-	-	-
Bujumbura (last 12 months: 07/2016 – 07/2017) [whole period: 11/2013 – 07/2017]	-3.2 [-3.4]	-80 [-77]	32 [35]	-3.4 [-3.2]	-83 [-81]	42 [28]	-	-	-
Bujumbura smoothed	-2.5 [-2]	-68 [-71]	31 [45]	-2 [-1.8]	-70 [-74]	21 [35]	-	-	-
OHP (last 12months: 03/2016 – 03/2017) [whole period: 08/2014 – 03/2017]	-0.9 [-0.8]	-51 [-42]	66 [44]	-0.7 [-0.6]	-37 [-28]	34 [36]	-	-	-
OHP smoothed	-1.1 [-0.8]	-51 [-42]	60 [51]	-0.5 [-0.4]	-36 [-24]	41 [39]	-	-	-
Reunion LePort Last 12 months: 12/2016 – 12/2017) [whole period: 04/2016 – 12/2017]	-1.5 [-1.6]	-84 [-86]	29 [28]	-1.4 [-1.4]	-83 [-84]	25 [25]	-	-	-
Reunion LePort smoothed	-0.5 [-0.5]	-62 [-67]	29 [31]	-0.41 [-0.42]	-59 [-60]	22 [25]	-	-	-
Uccle minDOAS (last 12 months: 03/2015 – 03/2016) [whole period: 04/2011 – 03/2016]	-3.2 [-3.9]	-27 [-37]	29 [30]	-2.6 [-3]	-26 [-31]	25 [24]	-	-	-
Uccle minDOAS smoothed	-4.5 [-5]	-36 [-44]	31 [34]	-3.6 [-3.3]	-29 [-33]	20 [30]	-	-	-

For GOME-2C, scatter plot results are similar to what obtained with GOME-2B in Xianghe (slopes around 0.75 and 0.74, respectively), probably due to the absence of large NO_2 columns (>4×10^{15} molec/cm²) that strongly influence the regression analysis (Pinardi *et al*., 2020). The absolute and relative differences are similar/slightly smaller to what obtained with GOME-2B in the last year.

The GOME-2C results for Xianghe are within the requirements (target accuracy requirement of 30 % in polluted conditions and optimal accuracy of 20 %), as it was the case for the other sesonsors for Xianghe and Uccle. Beijing and OHP report about 50 % biases, while larger values are found for Bujumbura and Reunion, as previously (Pinardi *et al.*, 2014; NO_2 Validation Report 2015; Pinardi *et al*., 2020). As before, smoothing the MAXDOAS profiles with the satellite averaging kernels is not always reducing the mean comparison differences, with an impact of ~10-20 % depending on the station (AC SAF Operations Report 1/2018, PT meeting of May 2018). In term of stability most of the stations report differences over time up to 10 %, which is also about the level of difference between GOME-2A and GOME-2B (10 to 15 %). These biases could be reduced in the future with GDP-4.9 GOME-2 data (Liu *et al.*, 2019) showing improved validation results e.g for Xianghe.

Status of GOME-2A, GOME-2B and GOME-2C total (stratospheric) NO2

Quality monitoring of the GOME-2 NO_2 total (stratospheric) column data is regularly carried out using correlative ground-based measurements collected from about 20 Zenith-Scattered-Light DOAS UV-visible (ZSL-DOAS) instruments affiliated with the Network for the Detection of Atmospheric Composition Change (NDACC). The NO_2 column validation protocol has already been described in previous AC SAF validation reports with its latest updates published in Verhoelst *et al*. (AMT 2021). This protocol includes the selection of GOME-2/NDACC co-located data pairs based on the air-mass matching technique, a model-based photochemical correction compensating for significant solar local time differences between GOME-2 mid-morning and NDACC twilight observations in polar summer, and a cloud-based filtering of NO_2 data over polluted stations aiming at the removal of pollution-affected pixels. At some stations, real-time processing of the ground-based observations still uses NO_2 absorption cross-sections at room temperature instead of stratospheric temperature. As a result, the retrieved total NO_2 column is affected by a negative systematic bias of 15 – 20 % with a seasonal component. Such data are removed. Thanks to this strict protocol, data comparisons can be carried out within a residual uncertainty of maximum $2 - 3\times10^{14}$ molec/cm^2 combining both the ground-based data uncertainty and comparison errors. This uncertainty is indicated by the shaded area on the pole-to-pole graphs.

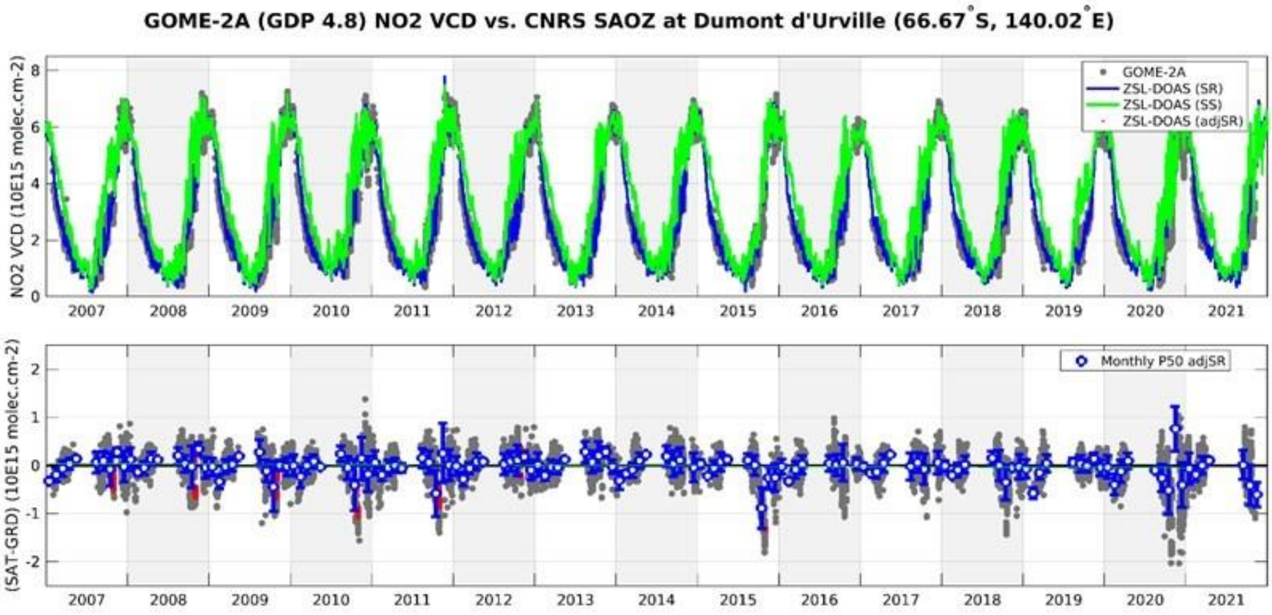

GOME2 NRT_OFL GDP 4.8 NO2 vertical column
33034 pixels in 2951 days (27/01/2007 - 14/11/2021)

Dumont d'Urville (66.67°S,140.02°E)
CNRS SAOZ (CP200_NMOS1024), source: NDACC_COMPLETED_BY_RT
11025 meas. in 5618 days (01/07/2006 - 14/03/2022)

Method: zovp pixels (all CF) vs. Twilights
Global agreement: -0.0 ± 0.3 (10^{15} molec.cm^{-2})
Linear drift: -0.01*t + 0.05 (10^{15} molec.cm^{-2}/year), σ = 0.007

	January	February	March	April	May	June	July	August	September	October	November	December
2007	-0.3 ± 0.0	-0.2 ± 0.1	-0.1 ± 0.2	0.0 ± 0.1	0.1 ± 0.1	-	-	0.1 ± 0.2	0.1 ± 0.2	-0.1 ± 0.3	0.3 ± 0.1	-0.0 ± 0.3
2008	0.1 ± 0.2	-0.1 ± 0.1	-0.0 ± 0.1	0.1 ± 0.1	0.1 ± 0.0	-	-	0.2 ± 0.2	0.0 ± 0.2	-0.0 ± 0.4	0.3 ± 0.1	-0.0 ± 0.2
2009	-0.0 ± 0.2	-0.3 ± 0.1	-0.0 ± 0.1	0.0 ± 0.1	0.2 ± 0.0	-	-	0.3 ± 0.3	-0.1 ± 0.2	-0.4 ± 0.5	0.0 ± 0.1	-0.0 ± 0.2
2010	0.0 ± 0.2	-0.2 ± 0.2	0.0 ± 0.2	0.1 ± 0.1	-0.0 ± 0.0	-	-	0.2 ± 0.2	-0.1 ± 0.2	-0.4 ± 0.5	0.1 ± 0.4	-0.2 ± 0.4
2011	0.1 ± 0.2	-0.2 ± 0.1	-0.0 ± 0.2	0.0 ± 0.2	-0.1 ± 0.1	-	-	0.2 ± 0.2	0.1 ± 0.2	-0.6 ± 0.5	0.3 ± 0.6	0.0 ± 0.3
2012	-0.0 ± 0.2	-0.3 ± 0.1	-0.1 ± 0.1	0.1 ± 0.2	0.1 ± 0.1	-	-	0.0 ± 0.2	0.1 ± 0.2	0.1 ± 0.3	0.2 ± 0.1	-0.1 ± 0.2
2013	0.0 ± 0.2	-0.2 ± 0.1	-0.0 ± 0.1	-0.0 ± 0.1	0.1 ± 0.0	-	-	0.3 ± 0.2	0.1 ± 0.2	0.2 ± 0.3	0.3 ± 0.1	-0.0 ± 0.1
2014	-0.3 ± 0.2	-0.2 ± 0.1	-0.1 ± 0.2	0.1 ± 0.2	0.2 ± 0.0	-	-	0.2 ± 0.2	0.0 ± 0.3	0.1 ± 0.3	-	-0.0 ± 0.3
2015	0.0 ± 0.1	-0.2 ± 0.0	-0.1 ± 0.2	0.1 ± 0.2	0.1 ± 0.1	-	-	0.1 ± 0.1	0.0 ± 0.2	-0.9 ± 0.4	-0.3 ± 0.2	-0.3 ± 0.3
2016	-0.0 ± 0.2	-0.3 ± 0.0	-0.1 ± 0.2	0.0 ± 0.2	-	-	-	0.0 ± 0.2	0.0 ± 0.2	0.1 ± 0.4	-	0.0 ± 0.1
2017	-0.0 ± 0.1	-0.2 ± 0.0	-0.1 ± 0.1	0.1 ± 0.2	0.2 ± 0.0	-	-	-0.0 ± 0.3	0.1 ± 0.2	-0.1 ± 0.3	-	0.1 ± 0.2
2018	-0.0 ± 0.1	-0.2 ± 0.0	-0.1 ± 0.1	0.0 ± 0.2	-	-	-	0.2 ± 0.1	0.0 ± 0.3	-0.3 ± 0.4	-0.0 ± 0.0	-0.0 ± 0.3
2019	-0.1 ± 0.2	-0.6 ± 0.1	-0.2 ± 0.1	0.0 ± 0.2	-	-	-	0.1 ± 0.1	0.0 ± 0.2	-0.0 ± 0.1	0.1 ± 0.1	-0.0 ± 0.2
2020	-0.0 ± 0.2	-0.4 ± 0.2	-0.1 ± 0.2	0.1 ± 0.2	-	-	-	-0.1 ± 0.0	-0.3 ± 0.3	-0.5 ± 0.5	0.8 ± 0.5	-0.4 ± 0.5
2021	-0.1 ± 0.3	-0.2 ± 0.1	0.0 ± 0.2	0.1 ± 0.1	-	-	-	-	0.0 ± 0.3	-0.4 ± 0.4	-0.6 ± 0.3	-
2022	-	-	-	-	-	-	-	-	-	-	-	-

Figure 7.9. Comparison of NO_2 column data measured at the NDACC Antarctic station of Dumont d'Urville by GOME-2A (GDP-4.8) and by the CNRS/LATMOS ZSL-DOAS spectrometer. Top: time series of NO_2 column data; centre: time series of NO_2 column difference; bottom (table): monthly median value (and its ±1σ scatter) of the difference between GOME-2A GDP-4.8 and the NDACC ZSL-DOAS NO_2 column data.

Figure 7.9 (for GOME-2A), Figure 7.10 (for GOME-2B) and Figure 7.11 (for GOME-2C) show the comparison of NO_2 column data at the NDACC Antarctic station of Dumont d'Urville, a station located on the polar circle, in a pristine environment without any known source of tropospheric NO_2. Comparison results at this station are representative of the validation of purely stratospheric data series, at moderate and large solar zenith angle, and over the full range of NO_2 stratospheric column values from winter lows of about 10^{14} molec/cm^2 (wintertime denoxification episodes) up to summer highs of 7×10^{15} molec/cm^2 (complete depletion of N_2O_5 into NO_2 due to polar midnight Sun). On a monthly median basis, and over the 14 years of GOME-2A operation and 9 years of GOME-2B operation, the target bias of 3 – 5×10^{14} molec/cm^2 has never been exceeded, except occasionally in October when the station is overpassed frequently by the border of the polar vortex, thus when atmospheric variability contributes significant co-location mismatch noise and bias to the difference in stratospheric NO_2. The ground dataset shown in this figure is a composite dataset consisting of the NDACC reprocessed dataset extended through the last year by the near-real-time dataset (latmos_rt).

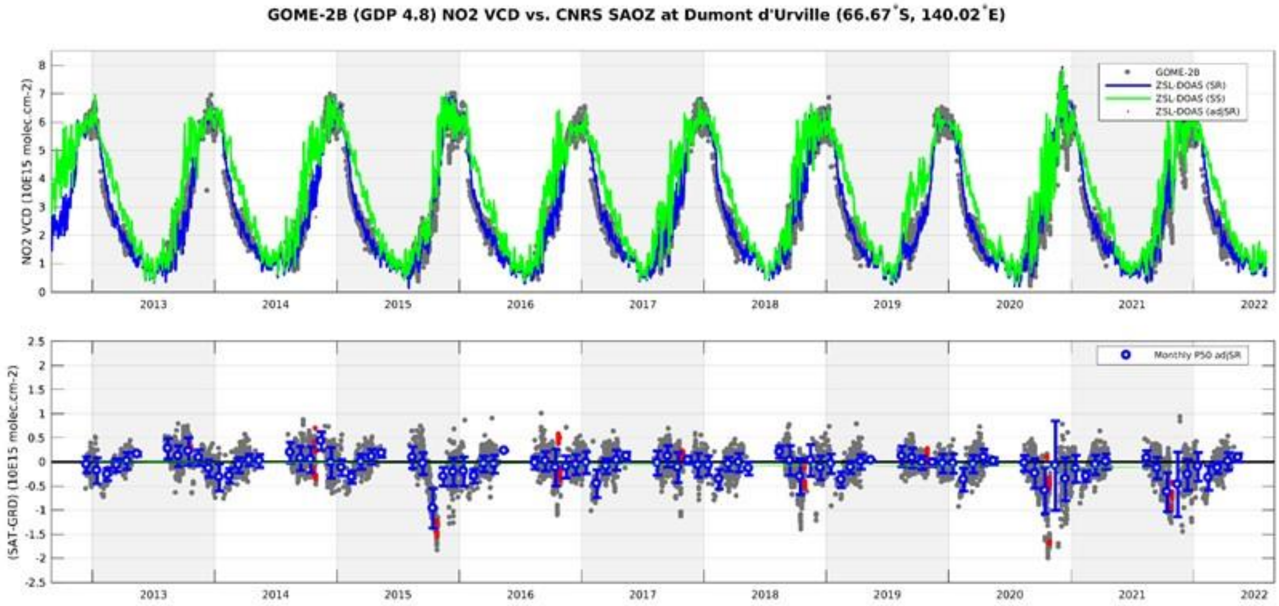

GOME2 NRT_OFL GDP 4.8 NO2 vertical column

22423 pixels in 2163 days (13/12/2012 - 06/05/2022)

Dumont d'Urville (66.67˚S,140.02˚E)

CNRS SAOZ (CP200_NM0S1024), source: NDACC_COMPLETED_BY_RT

6973 meas. in 3554 days (01/09/2012 - 06/08/2022)

Method: zsvp pixels (all CF) vs. Twilights

Global agreement: -0.1 ± 0.3 (10^{15} mol.cm^{-2})

Linear drift: 0.019 ± 0.01 (10^{15} mol.cm^{-2}/year) , ρ = 0.323

	January	February	March	April	May	June	July	August	September	October	November	December
2012	-	-	-	-	-	-	-	-	-	-	-	-0.1 ± 0.2
2013	-0.2 ± 0.3	-0.3 ± 0.1	-0.1 ± 0.1	0.0 ± 0.2	0.2 ± 0.0	-	-	0.3 ± 0.2	0.1 ± 0.2	0.2 ± 0.3	0.1 ± 0.2	-0.1 ± 0.2
2014	-0.3 ± 0.3	-0.3 ± 0.1	-0.1 ± 0.2	0.0 ± 0.1	0.0 ± 0.1	-	-	0.2 ± 0.2	0.1 ± 0.3	0.0 ± 0.3	0.4 ± 0.2	0.0 ± 0.3
2015	-0.1 ± 0.2	-0.3 ± 0.1	0.0 ± 0.1	0.1 ± 0.2	0.2 ± 0.1	-	-	0.1 ± 0.2	-0.0 ± 0.2	-1.0 ± 0.4	-0.3 ± 0.2	-0.2 ± 0.3
2016	-0.2 ± 0.3	-0.3 ± 0.1	-0.0 ± 0.2	-0.1 ± 0.2	0.2 ± 0.0	-	-	-0.0 ± 0.1	0.0 ± 0.2	-0.1 ± 0.4	-0.1 ± 0.2	-0.1 ± 0.2
2017	-0.0 ± 0.2	-0.5 ± 0.3	-0.1 ± 0.2	0.0 ± 0.2	0.1 ± 0.1	-	-	-0.0 ± 0.2	0.1 ± 0.2	-0.1 ± 0.3	0.0 ± 0.1	-0.1 ± 0.3
2018	-0.1 ± 0.2	-0.4 ± 0.2	-0.0 ± 0.1	-0.0 ± 0.2	-0.1 ± 0.1	-	-	0.2 ± 0.1	0.0 ± 0.3	-0.3 ± 0.4	0.0 ± 0.3	-0.1 ± 0.3
2019	-0.0 ± 0.2	-0.4 ± 0.2	-0.1 ± 0.1	0.0 ± 0.1	0.0 ± 0.0	-	-	0.1 ± 0.2	0.1 ± 0.2	-0.0 ± 0.1	-0.0 ± 0.1	-0.0 ± 0.2
2020	-0.0 ± 0.2	-0.4 ± 0.2	-0.0 ± 0.2	0.1 ± 0.2	0.0 ± 0.1	-	-	0.0 ± 0.2	-0.2 ± 0.3	-0.6 ± 0.5	-0.1 ± 0.9	-0.4 ± 0.4
2021	-0.1 ± 0.3	-0.3 ± 0.1	-0.1 ± 0.2	0.0 ± 0.2	-	-	-	0.1 ± 0.2	-0.1 ± 0.2	-0.6 ± 0.4	-0.5 ± 0.7	-0.3 ± 0.3
2022	-0.1 ± 0.3	-0.3 ± 0.3	-0.1 ± 0.1	0.0 ± 0.2	0.1 ± 0.1	-	-	-	-	-	-	-

Figure 7.10. Same as Figure 7.9 but with GOME-2 on Metop-B (GDP4.8), from December 2012 to May 2022.

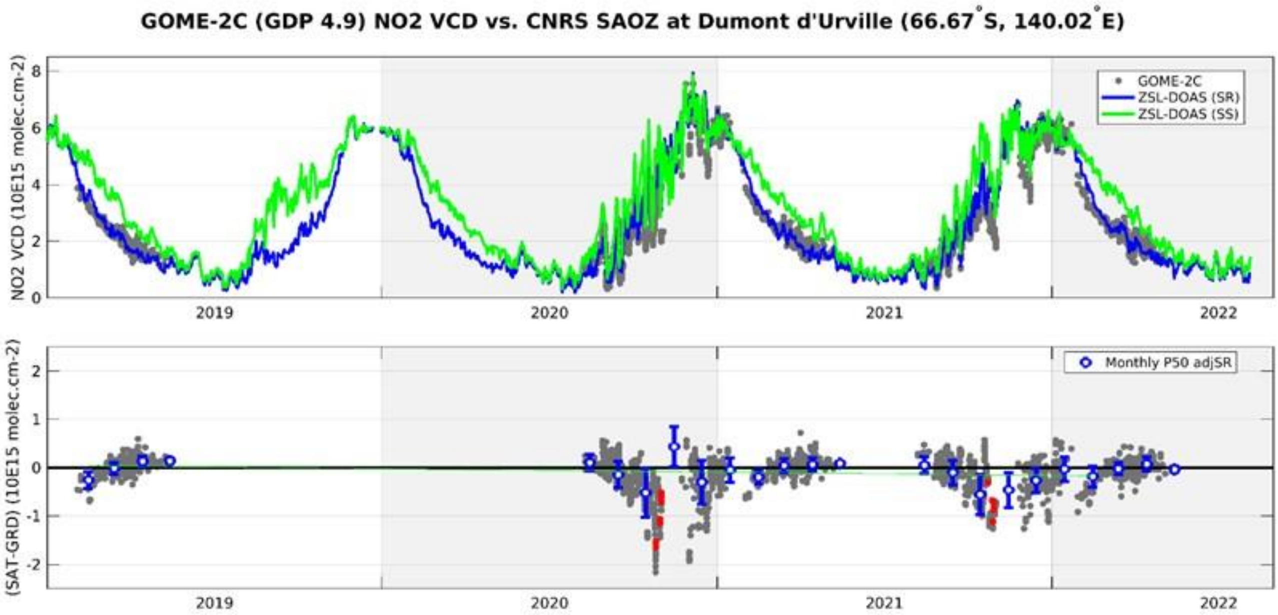

GOME2 NRT_OFL GDP 4.9 NO2 vertical column

5668 pixels in 540 days (02/02/2019 - 13/05/2022)

Dumont d'Urville (66.67°S,140.02°E)

CNRS SAOZ (CP200_NMOS1024), source: NDACC_COMPLETED_BY_RT

2621 meas. in 1341 days (01/11/2018 - 06/08/2022)

Method: zovp pixels (all CF) vs. Twilights

Global agreement: -0.1 ± 0.3 (10^{15}mol.cm^{-2})

Linear drift: -0.07*t + 0.06 (10^{15}mol.cm^{-2}/year) , ρ = -0.061

	January	February	March	April	May	June	July	August	September	October	November	December
2019	-	-0.3 ± 0.2	-0.0 ± 0.1	0.1 ± 0.1	0.2 ± 0.1	-	-	-	-	-	-	-
2020	-	-	-	-	-	-	-	0.1 ± 0.2	-0.1 ± 0.3	-0.5 ± 0.5	0.4 ± 0.4	-0.3 ± 0.4
2021	-0.0 ± 0.3	-0.2 ± 0.1	0.0 ± 0.1	0.1 ± 0.1	0.1 ± 0.0	-	-	0.1 ± 0.2	-0.1 ± 0.3	-0.6 ± 0.4	-0.5 ± 0.4	-0.3 ± 0.3
2022	-0.0 ± 0.3	-0.2 ± 0.2	-0.0 ± 0.1	0.1 ± 0.1	-0.0 ± 0.1	-	-	-	-	-	-	-

Figure 7.11. Same as Figure 7.9 but with GOME-2 on Metop-C (GDP4.9), from February 2019 to May 2022.

Figure 7.12 and Figure 7.13 display similar results obtained at the NDACC Alpine station of Observatoire de Haute Provence in Southern France and the NDACC Southern Tropic station of Saint-Denis de la Réunion, thus in occasional presence of pollution and over a wider range of solar zenith angle. Again, the target bias of 3 – 5×10^{14} molec/cm^2 has rarely been exceeded, except in very few cases.

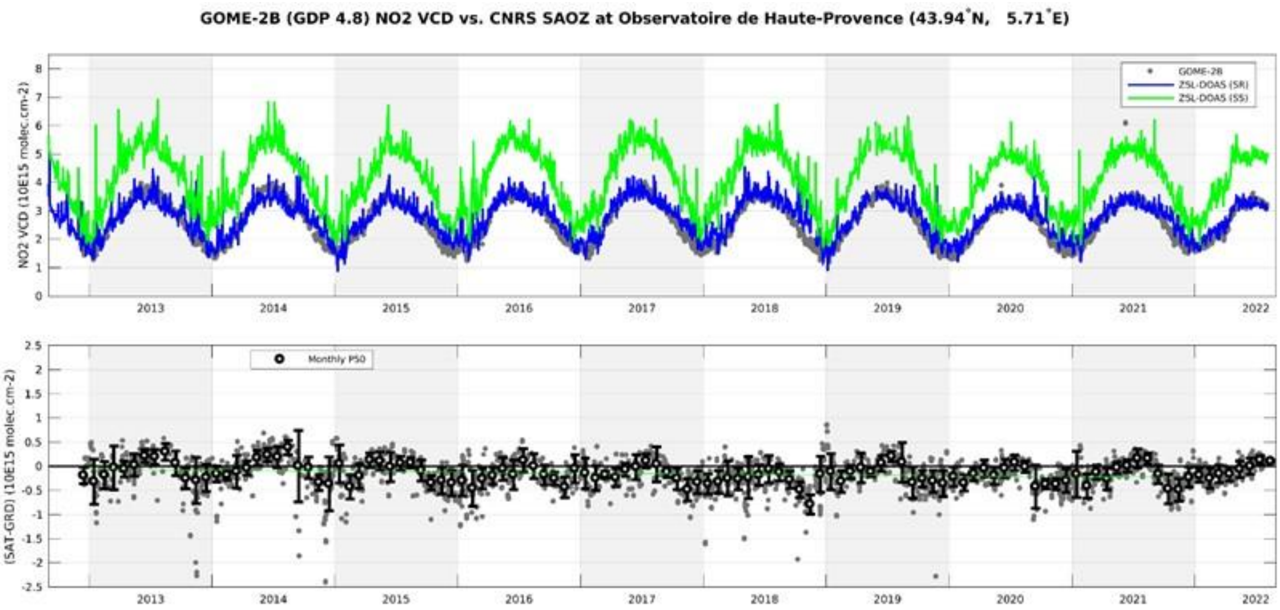

GOME2 NRT_OFL GDP 4.8 NO2 vertical column 8098 pixels in 2945 days (15/12/2012 - 06/08/2022)				Observatoire de Haute-Provence (43.94°N, 5.71°E) CNRS SAOZ (CP200_NHOS1024), source: NDACC_COMPLETED_BY_RT 6881 meas. in 3554 days (01/09/2012 - 06/08/2022)				Method: zovp pixels (CF≤25%) vs. Twilights Global agreement: -0.2 ± 0.2 (10^{15} mol cm^{-2}) Linear drift: -0.02*t - 0.06 (10^{15} mol cm^{-2}/year), ρ = 0.553				
	January	February	March	April	May	June	July	August	September	October	November	December
2012	-	-	-	-	-	-	-	-	-	-	-	-0.2 ± 0.2
2013	-0.3 ± 0.5	-0.2 ± 0.3	-0.0 ± 0.5	-0.1 ± 0.2	0.0 ± 0.2	0.2 ± 0.1	0.2 ± 0.1	0.3 ± 0.2	0.1 ± 0.3	-0.3 ± 0.2	-0.3 ± 0.5	-0.2 ± 0.3
2014	-0.2 ± 0.2	0.2 ± 0.1	-0.1 ± 0.3	-0.0 ± 0.1	0.2 ± 0.2	0.2 ± 0.1	0.2 ± 0.2	0.4 ± 0.1	0.0 ± 0.7	-0.0 ± 0.2	-0.3 ± 0.2	-0.4 ± 0.6
2015	0.0 ± 0.4	-0.4 ± 0.2	-0.2 ± 0.3	0.1 ± 0.2	0.1 ± 0.2	-0.0 ± 0.3	0.1 ± 0.1	0.1 ± 0.1	-0.1 ± 0.2	-0.3 ± 0.1	-0.3 ± 0.3	-0.4 ± 0.3
2016	-0.3 ± 0.3	-0.5 ± 0.4	-0.3 ± 0.2	-0.2 ± 0.2	-0.1 ± 0.2	-0.2 ± 0.3	0.1 ± 0.2	-0.0 ± 0.3	-0.2 ± 0.2	-0.3 ± 0.1	-0.4 ± 0.2	-0.1 ± 0.3
2017	-0.1 ± 0.3	0.2 ± 0.3	0.2 ± 0.3	-0.2 ± 0.2	0.1 ± 0.1	-0.0 ± 0.3	0.1 ± 0.1	0.0 ± 0.4	0.1 ± 0.1	0.3 ± 0.2	-0.5 ± 0.2	0.1 ± 0.2
2018	0.4 ± 0.2	0.3 ± 0.2	0.3 ± 0.4	0.3 ± 0.2	0.2 ± 0.4	0.2 ± 0.2	0.1 ± 0.3	0.1 ± 0.2	0.3 ± 0.2	0.5 ± 0.2	0.8 ± 0.2	0.2 ± 0.4
2019	-0.1 ± 0.4	-0.3 ± 0.2	-0.1 ± 0.1	-0.0 ± 0.3	-0.1 ± 0.1	0.1 ± 0.2	0.2 ± 0.1	0.1 ± 0.4	-0.3 ± 0.3	-0.3 ± 0.2	-0.3 ± 0.2	-0.4 ± 0.3
2020	-0.2 ± 0.2	-0.4 ± 0.2	-0.2 ± 0.1	-0.0 ± 0.2	-0.2 ± 0.2	-0.0 ± 0.2	0.1 ± 0.2	-0.0 ± 0.1	-0.4 ± 0.4	-0.4 ± 0.1	-0.4 ± 0.1	-0.3 ± 0.2
2021	-0.2 ± 0.5	-0.4 ± 0.3	-0.1 ± 0.1	-0.3 ± 0.2	-0.0 ± 0.1	0.0 ± 0.1	0.2 ± 0.2	0.2 ± 0.1	-0.2 ± 0.2	-0.5 ± 0.3	-0.5 ± 0.2	-0.2 ± 0.2
2022	-0.2 ± 0.1	-0.3 ± 0.2	-0.2 ± 0.2	-0.2 ± 0.2	-0.1 ± 0.2	-0.0 ± 0.2	0.1 ± 0.1	0.1 ± 0.0	-	-	-	-

Figure 7.12. Same as Figure 7.9 but at the NDACC Alpine station of Observatoire de Haute Provence by GOME-2B (GDP-4.8) and by the LATMOS ZSL-DOAS spectrometer (NDACC and latmos_rt). Top: time series of NO_2 column data; centre: time series of NO_2 column difference; bottom (table): monthly median value (and its ±1σ scatter) of the difference between GOME-2B GDP-4.8 and the NDACC NO_2 column data.

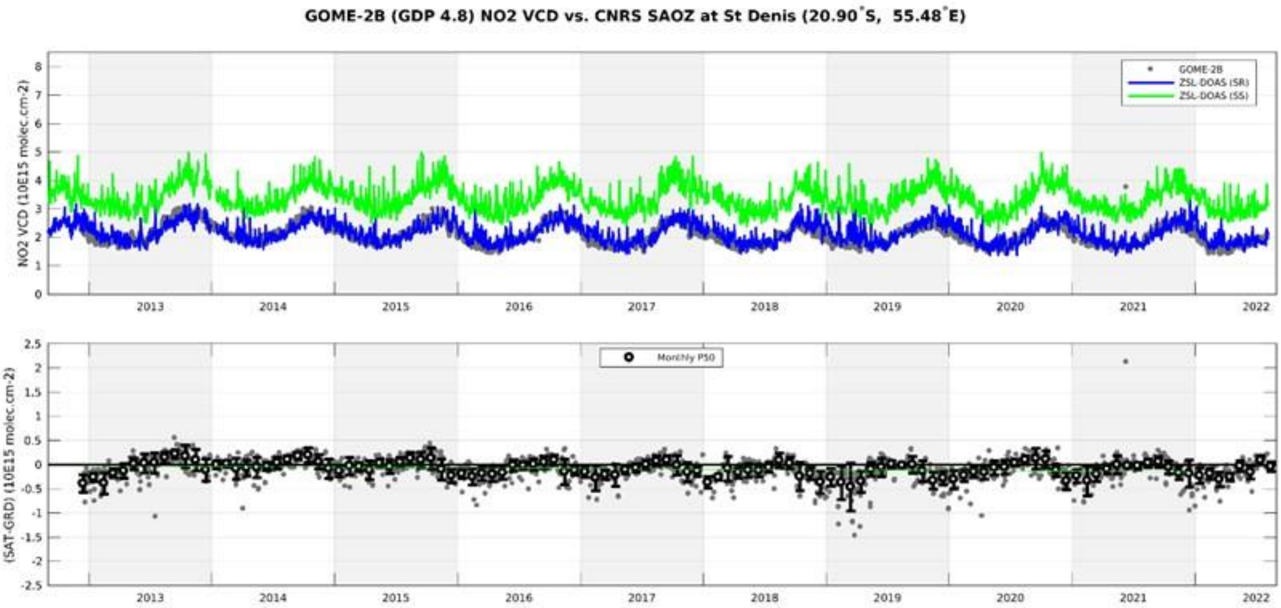

GOME2 NRT_OFL GDP 4.8 NO2 vertical column — 3987 pixels in 2474 days (17/12/2012 - 06/08/2022)

St Denis (20.90˚S, 55.48˚E) — CNRS SAOZ (CP200_NMOS1024), source: NDACC_COMPLETED_BY_RT — 6757 meas. in 3520 days (01/09/2012 - 06/08/2022)

Method: rovp pixels (all CF) vs. Twilights — Global agreement: -0.1 ± 0.2 (10¹⁵ mol.cm⁻²) — Linear drift: -0.01 ± 0.02 (10¹⁵ mol.cm⁻²/year), r = 0.729

	January	February	March	April	May	June	July	August	September	October	November	December
2012	-	-	-	-	-	-	-	-	-	-	-	-0.4 ± 0.2
2013	-0.3 ± 0.1	-0.4 ± 0.2	-0.2 ± 0.1	-0.1 ± 0.2	0.0 ± 0.1	0.0 ± 0.2	0.0 ± 0.2	0.1 ± 0.1	0.2 ± 0.1	0.2 ± 0.2	0.1 ± 0.2	-0.1 ± 0.2
2014	-0.0 ± 0.1	0.0 ± 0.1	-0.1 ± 0.2	-0.1 ± 0.2	-0.1 ± 0.2	-0.0 ± 0.1	0.0 ± 0.1	0.1 ± 0.1	0.2 ± 0.1	0.2 ± 0.1	0.1 ± 0.1	-0.1 ± 0.2
2015	-0.1 ± 0.1	-0.0 ± 0.2	-0.0 ± 0.1	-0.1 ± 0.2	0.0 ± 0.1	-0.0 ± 0.1	0.0 ± 0.1	0.1 ± 0.1	0.1 ± 0.2	0.1 ± 0.2	-0.1 ± 0.2	-0.2 ± 0.1
2016	-0.2 ± 0.1	-0.1 ± 0.2	-0.2 ± 0.1	-0.2 ± 0.1	-0.2 ± 0.1	-0.0 ± 0.1	-0.0 ± 0.1	0.0 ± 0.1	0.0 ± 0.1	0.1 ± 0.1	-0.1 ± 0.1	-0.1 ± 0.1
2017	0.2 ± 0.1	0.1 ± 0.1	0.2 ± 0.1	-0.2 ± 0.2	-0.1 ± 0.1	-0.1 ± 0.1	-0.0 ± 0.1	0.1 ± 0.1	0.1 ± 0.1	-0.0 ± 0.2	-0.2 ± 0.2	-0.1 ± 0.1
2018	0.4 ± 0.1	0.3 ± 0.1	0.1 ± 0.3	-0.2 ± 0.1	-0.1 ± 0.1	0.1 ± 0.1	-0.1 ± 0.1	0.1 ± 0.2	0.0 ± 0.1	-0.2 ± 0.3	-0.2 ± 0.1	0.4 ± 0.2
2019	-0.3 ± 0.2	-0.4 ± 0.3	-0.5 ± 0.5	-0.4 ± 0.2	-0.1 ± 0.1	-0.1 ± 0.2	0.0 ± 0.1	-0.0 ± 0.0	-0.0 ± 0.2	-0.1 ± 0.2	-0.3 ± 0.2	-0.3 ± 0.1
2020	-0.3 ± 0.2	-0.2 ± 0.1	-0.2 ± 0.1	-0.2 ± 0.1	-0.1 ± 0.1	-0.1 ± 0.1	0.0 ± 0.1	0.1 ± 0.1	0.1 ± 0.2	0.1 ± 0.2	-0.1 ± 0.1	-0.3 ± 0.2
2021	-0.2 ± 0.1	-0.3 ± 0.3	-0.2 ± 0.1	-0.1 ± 0.1	-0.0 ± 0.2	-0.0 ± 0.0	-0.0 ± 0.1	0.0 ± 0.1	0.1 ± 0.1	-0.1 ± 0.1	-0.2 ± 0.1	-0.2 ± 0.3
2022	-0.2 ± 0.2	-0.2 ± 0.1	-0.3 ± 0.1	-0.3 ± 0.1	-0.0 ± 0.1	-0.2 ± 0.1	0.1 ± 0.1	-0.0 ± 0.1	-	-	-	-

Figure 7.13. Same as Figure 7.9 and Figure 7.10, but at the NDACC Southern Tropic station of Saint-Denis de la Réunion by GOME-2B (GDP-4.8) and by LATMOS ZSL-DOAS spectrometer (NDACC and latmos_rt). Top: time series of NO_2 column data; centre: time series of NO_2 column difference; bottom (table): monthly median value (and its ±1σ scatter) of the difference between GOME-2B GDP-4.8 and the NDACC NO_2 column data.

Figure 7.14 reports from pole to pole the median value of the systematic bias between GOME-2 and NDACC ZSL-DOAS data, assessed on the basis of all co-located data pairs available so far with the entire GOME-2A/B/C time-series until August 2022, while Figure 7.15 displays, again from pole to pole, the linear drift between GOME-2A/B/C and NDACC data.Those graphs show the good long-term stability of the satellite NO_2 column data with respect to NDACC ZSL-DOAS data at all stations.

They also show that the target bias of 3 – 5×10^{14} molec/cm^2 in unpolluted conditions is achieved for all three satellites. Figure 7.13 also confirms the slight difference already noticed in previous validation reports between the biases observed respectively in the Southern and Northern hemispheres. Averaging median differences separately over the Northern and Southern Hemispheres concludes to an inter-hemispheric bias of about 2 – 3×10^{14} molec/cm^2. GOME-2C NO_2 column data present a slightly more positive bias across all latitudes.

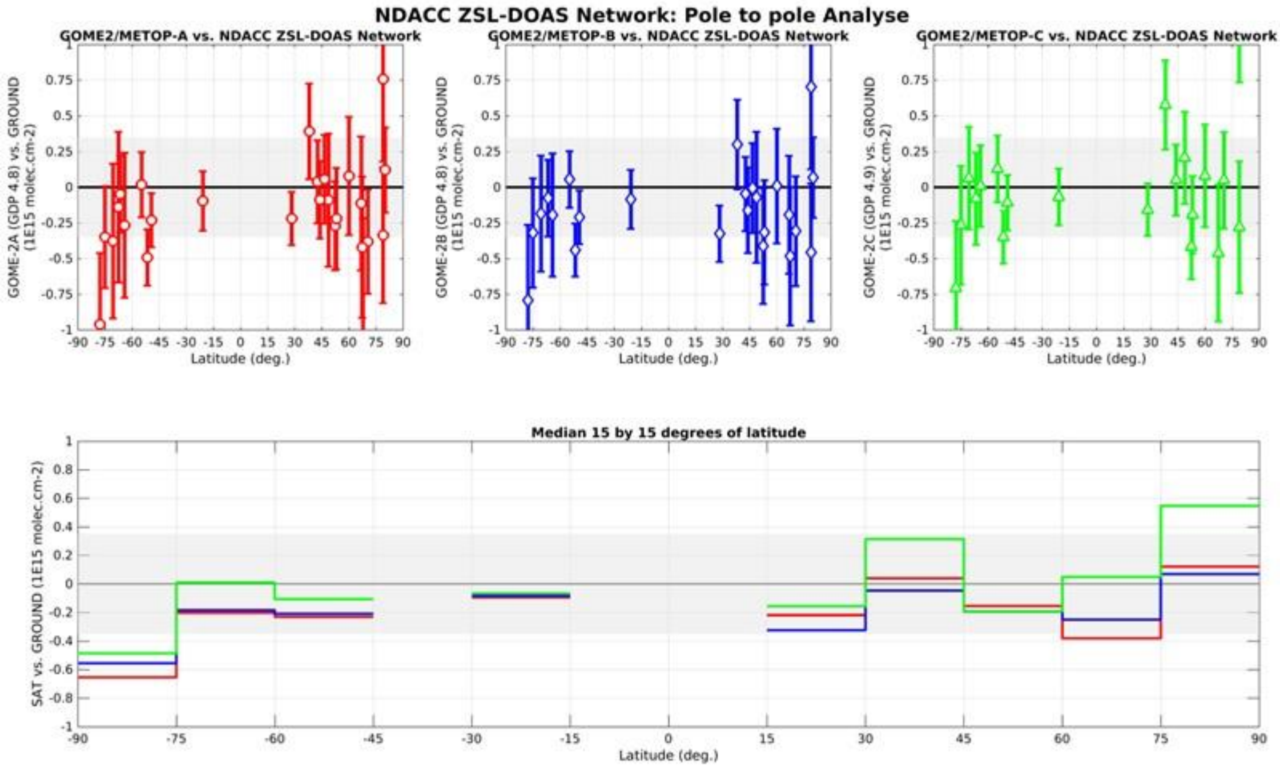

Figure 7.14. From pole to pole, median difference between the NO_2 column data reported by GOME-2A/B/C (red/ blue/ green) GDP-4.8 (GDP 4.9 for GOME-2C) and by ground-based ZSL-DOAS spectrometers at about 20 NDACC stations, calculated over 2007 – November 2021 for GOME-2A, 2012 – August 2022 for GOME-2B and 2019 – August 2022 for GOME-2C. Top: median difference at individual stations. Bottom: median difference averaged over 15° latitude bins.

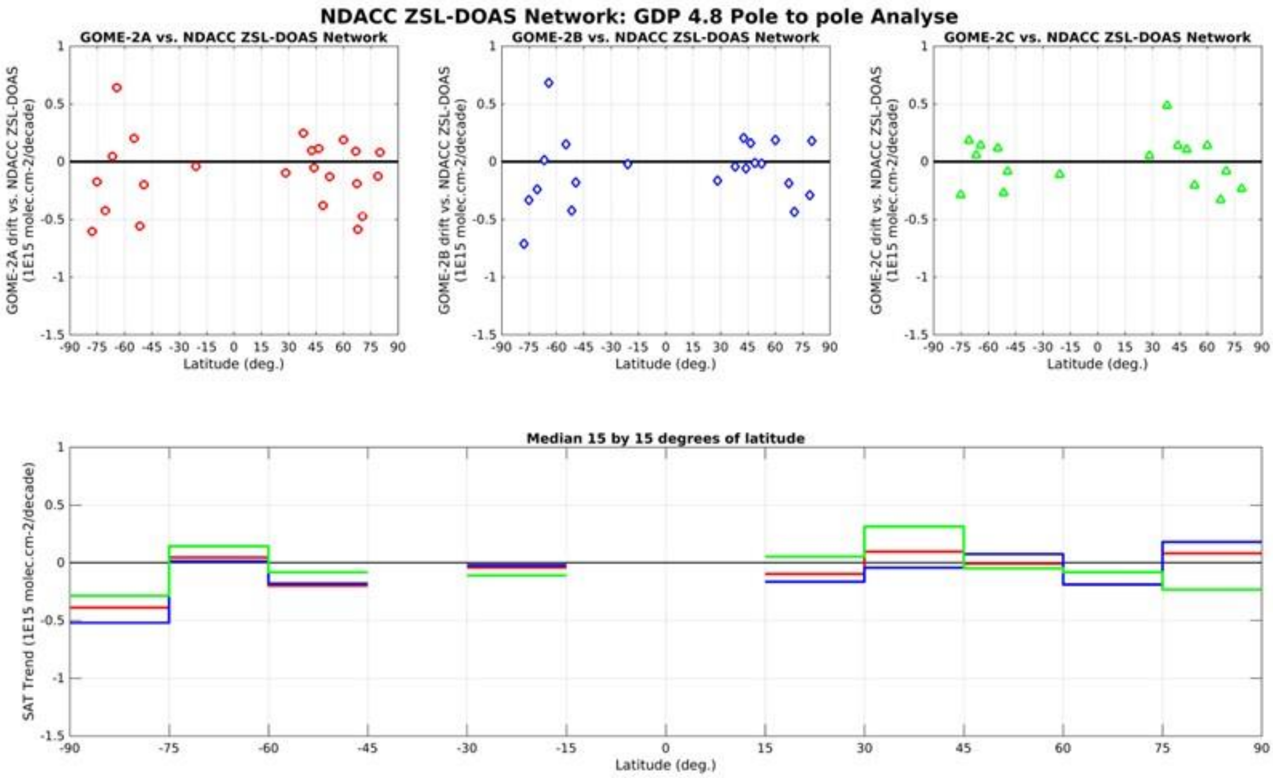

Figure 7.15. From pole to pole, linear drift (in percent by decade) of the difference between the NO_2 column data reported by GOME 2A/B/C (red/ blue/ green) GDP 4.8 (GDP 4.9 for GOME-2C) and by ground-based ZSL-DOAS spectrometers at about 20 NDACC stations, calculated over 2007 – November 2021 for GOME-2A, 2012 – August 2022 for GOME-2B and 2019 – August 2022 for GOME-2C. Top: linear drift estimates at individual stations. Bottom: same linear drift estimates but averaged over 15° latitude bins.

Status of GOME-2A, GOME-2B and GOME-2C total HCHO

This validation exercise is an extension of what is presented in the HCHO GDP-4.8 validation report, relying on correlative observations from MAX-DOAS instruments operated by BIRA-IASB at Xianghe, Bujumbura, Uccle (miniDOAS and SG), OHP and Reunion (Le Port and Maido). Unfortunately, due to an instrumental problem in the UV channel at Xianghe, no updates are possible for this report. Past figures can be found on the BIRA validation web server and a summary is presented in Table 7.12.

Table 7.12. Summary of the mean biases (in 10^{15} molec/cm^2) between GOME-2A/B/C and MAX-DOAS HCHO VCDs. The values in parentheses correspond to the mean relative biases and R is the correlation coefficients and S the slope of the linear regression of the monthly mean points. No update was possible for the first half of 2022.

	GOME-2A	GOME-2B	GOME-2C
UCCLE-SG (50.8°N, 4.3°E) (whole period: 02/2017 – 12/2019)	1.3 ± 2.0 (29 ± 56) R = 0.33, S = 0.29	0.3 ± 1.6 (7 ± 52) R = 0.75, S = 0.96	-
With smoothing	2.5 ± 1.8 (74 ± 81) R = 0.32, S = 0.38	1.6 ± 1.7 (49 ± 75) R = 0.76, S = 1.34	-

REUNION MAIDO (20.9°S, 55.3°E) (whole period: 06/2018 – 11/2019)	0.3 ± 1.6 (15 ± 78) R = 0.71, S = 2.32	2.1 ± 0.8 (94 ± 54) R = 0.84, S = 1.17	-
With smoothing	0.0 ± 1.5 (-0.04 ± 68) R = 0.77, S = 2.36	1.7 ± 0.8 (68 ± 43) R = 0.69, S = 1.29	-
XIANGHE (39.7°N, 117.0°E) (whole period: 03/2010 – 12/2021)	-5.3 ± 3.2 (-43 ± 18) R = 0.84, S = 0.51	-6.4 ± 2.7 (-48 ± 16) R = 0.88, S = 0.67	-8.9 ± 2.6 (-60 ± 21) R = 0.82, S = 0.76
With smoothing	-0.20 ± 2.0 (-2.7 ± 31) R = 0.85, S = 0.85	0.59 ± 2.2 (-8 ± 31) R = 0.88, S = 1.19	-2.4 ± 2.7 (-29 ± 37) R = 0.79, S = 1.40
BUJUMBURA (3.0°S, 29.0°E) (whole period: 11/2013 – 07/2017)	-6.3 ± 2.4 (-44 ± 10) R = 0.83, S = 0.46	-4.4 ± 2.2 (-32 ± 10) R = 0.88, S = 0.52	-
With smoothing	-1.6 ± 2.4 (-17 ± 24) R = 0.50, S = 0.43	0.3 ± 2.0 (3.2 ± 25) R = 0.72, S = 0.65	-
OHP (whole period: 08/2014 – 03/2017)	-0.1 ± 2.5 (1.7 ± 40) R = 0.42, S = 0.29	0.3 ± 1.1 (4.2 ± 21) R = 0.90, S = 0.75	-
With smoothing	0.9 ± 2.3 (16 ± 42) R = 0.39, S = 0.32	103.51 ± 1.0 (17 ± 22) R = 0.86, S = 1.01	-
REUNION LEPORT (20.9°S, 55.3°E) (whole period: 04/2016 – 12/2017)	-0.3 ± 1.0 (-10 ± 43) R = 0.66, S = 1.23	103.51 ± 0.8 (39 ± 26) R = 0.80, S = 1.56	-
With smoothing	103.51 ± 1.1 (71 ± 99) R = 0.59, S = 1.56	2.6 ± 0.1 (180 ± 56) R = 0.78, S = 2.83	-
UCCLE-miniDOAS (50.8°N, 4.3°E) (whole period: 04/2011 – 05/2015)	-0.5 ± 2.6 (-8.3 ± 49) R = 0.21, S = 0.25	-0.6 ± 1.6 (-9.4 ± 29) R = 0.76, S = 0.89	-
With smoothing	0.8 ± 2.7 (14 ± 81) R = 0.11, S = 0.13	-0.4 ± 1.7 (7.1 ± 34) R = 0.73, S = 0.88	-

In general, the results confirm that both satellite instruments capture well the HCHO VCD seasonality. In Reunion the signal is very small (less than ~0.5×10^{16} molec/cm²) and is more difficult to have firm conclusions. Differences with the newly installed Reunion Maido station need to be further investigated. In Uccle and OHP, the signal from GOME-2A is quite noisy, and the results are better with GOME-2B, which is probably related to GOME-2A degradation. A significant bias exists between GOME-2A/B and MAX-DOAS observations at the four stations (up to 50 %), but as already shown in the GDP-4.8 validation report, for some stations this bias can be significantly reduced when smoothing the MAX-DOAS profiles with the satellite column averaging kernels (see also values with smoothing in Table 7.12). The different figures for each stations can also be found on the BIRA validation web server.

For GOME-2C, scatter plot results are similar to what obtained with GOME-2B in Xianghe (slopes around 0.67/0.79 before smoothing). The absolute and relative differences are slightly larger than GOME-2B.

Status of GOME-2A, GOME-2B and GOME-2C total BrO

GOME-2A/B/C total columns of BrO from GDP-4.8 (4.9 in the case of GOME-2C) operational product are compared to ground-based UV-visible zenith-sky measurements at Harestua, Norway (60°N, 11°E). As done in previous validation report, the ground-based columns are derived from the vertical profiles retrieved by applying an OEM (Optimal Estimation Method) –based profiling technique to zenith-sky measurements at sunrise (Hendrick *et al.*, 2007).

The sensitivity of these measurements to the troposphere is increased by using a fixed reference spectrum corresponding to clear-sky noon summer conditions for the spectral analysis. In order to ensure the photochemical matching between satellite and ground-based observations, sunrise ground-based columns have been photochemically converted to the satellite overpass SZAs using a stacked box photochemical model (Hendrick *et al.*, 2007 and 2008).

Comparison results (150 km overpasses) for GOME-2A (until Dec 2021), GOME-2B and GOME-2C are shown in Figure 7.16, Figure 7.17 and Figure 7.18, respectively.

Mean biases values between GOME-2A/B/C and ground-based data are of -10 ± 12 %, -15 ± 11 % and -9 ± 10 %. GOME-2A/B/C BrO columns are thus all within the target accuracy of 30 % and also within the optimal accuracy of 15 %, except GOME-2B which is slightly above the required optimal accuracy threshold. Between 2013 and 2017, there is also an overall positive slope in the relative difference between GOME-2A and ground-based data. Given the fact that this slope is significantly less marked in GOME-2B comparisons, this indicates a possible drift in GOME-2A data likely related to the known degradation of the instrument. However, one cannot exclude that ground-based observations also partly contribute to this drift, due to the large uncertainty in the determination of the residual amount of BrO in the yearly selected reference spectra.

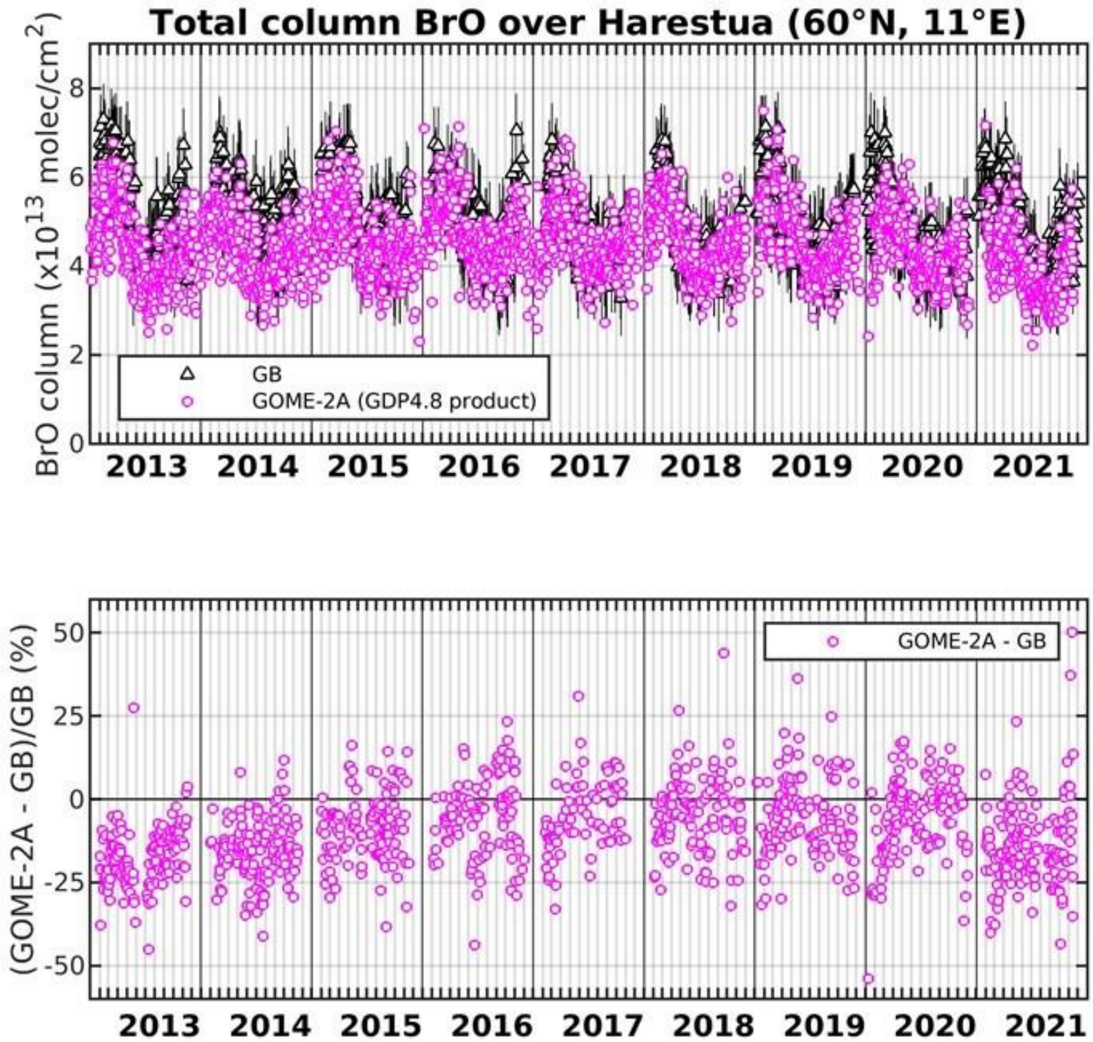

Figure 7.16. Comparison between GOME-2A GDP-4.8 and ground-based total BrO columns at Harestua (60°N, 11°E). The relative differences appear in the lower plot.

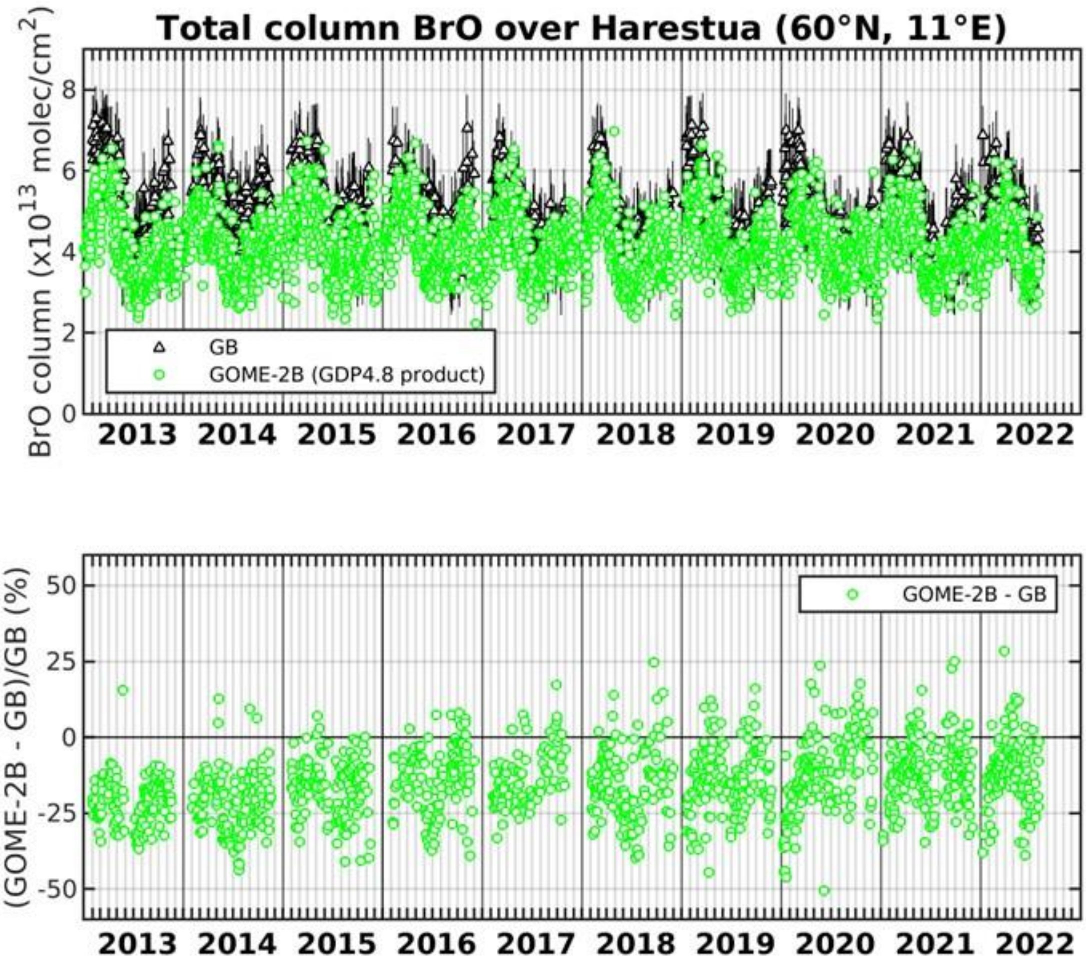

Figure 7.17. Comparison between GOME-2B GDP-4.8 and ground-based total BrO columns at Harestua (60°N, 11°E). The relative differences appear in the lower plot.

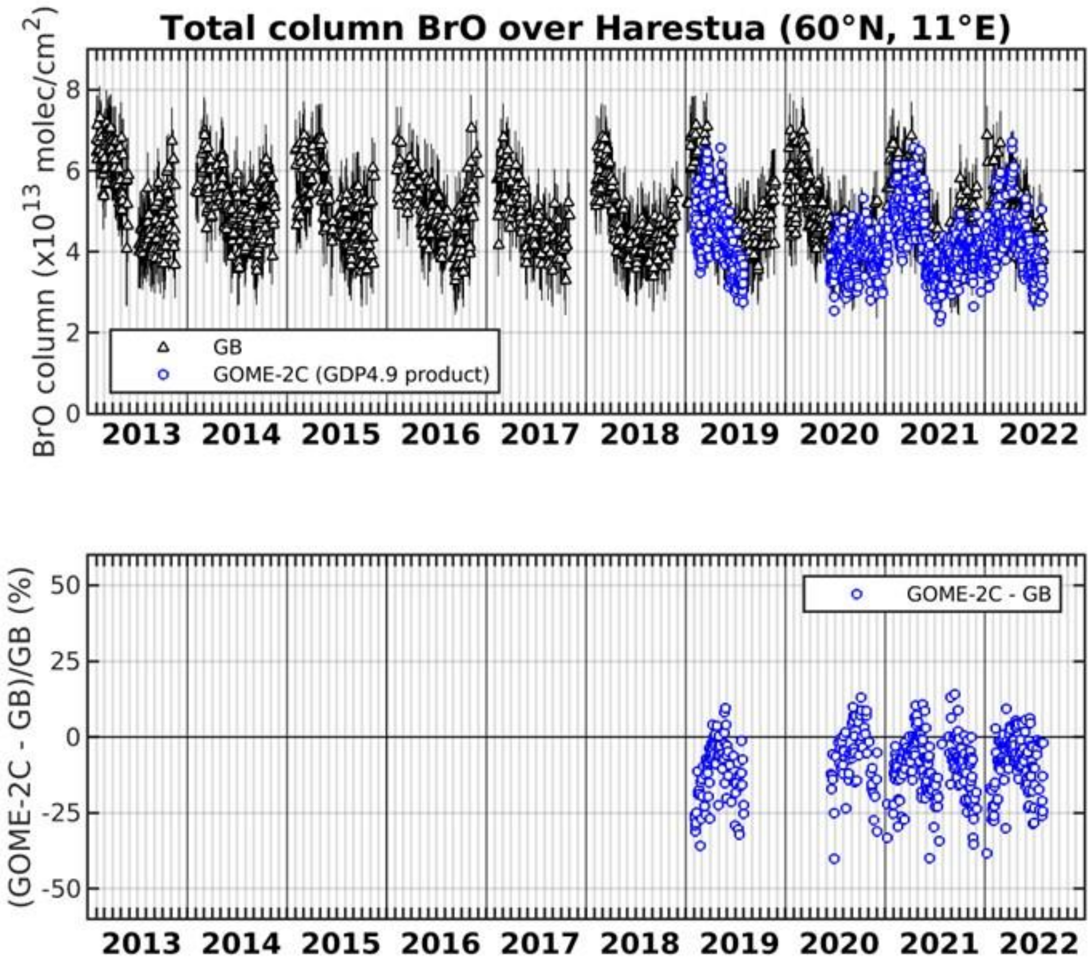

Figure 7.18. Comparison between GOME-2C GDP-4.9 and ground-based total BrO columns at Harestua (60°N, 11°E). The relative differences appear in the lower plot.

Status of GOME-2A, GOME-2B and GOME-2C SO_2

GOME-2 SO_2 GDP-4.8 continues to be used for the near-real-time observation of volcanic activity within the SACS service. The Support to Aviation Control Service (SACS) hosted by the Royal Belgian Institute for Space Aeronomy (BIRA-IASB) aims at supporting the Volcanic Ash Advisory Centers, like Toulouse VAAC and London VAAC. This is achieved by delivering near real-time data of SO_2 and aerosols derived from satellite measurements regarding volcanic emissions by UV-VIS (OMI, GOME-2A and GOME-2B composite until 31 March 2021 and GOME-2B and GOME-2C composite since then, OMPS, TROPOMI) and infrared (AIRS, IASI-A, IASI-B) instruments. In case of volcanic eruptions, notifications are sent out by email to interested parties. The SACS notification archive service gathers all the notifications; the results can be found here.

In the first half of 2022, SACS reported several clusters of cases where the maximum SO_2 detected by GOME-2 instruments was larger than 6 DU, as shown in Figure 7.19. These cover the Hunga-Tunga eruption in January 2022 (regions 310-311 and 410-412), Etna in February 2022 (regions 207 and 208) and Mutnovsky (Southern Kamchatka, Russia) in region 111. Similar SO_2 levels and alerts are seen by GOME-2B and GOME-2C, with some small differences due to differences of the maximum SO_2 levels.

An example is shown in Figure 7.20 for the 15 January 2022 Hunga-Tunga eruption (SACS region 412) and all the cases can be visualized on the SACS website by following the links found here.

The coherence of the GOME-2B/C measurements with the other morning instruments (first line) is clear, as the temporal evolution with the afternoon platform instruments (second and third line).

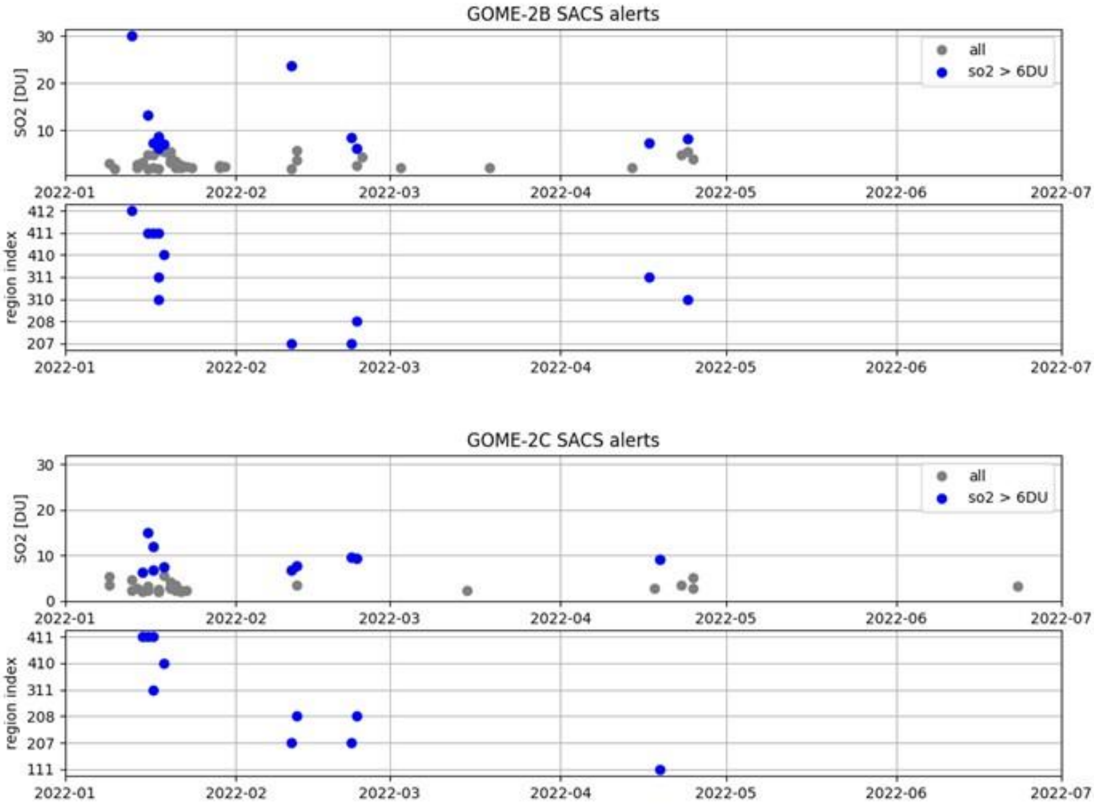

Figure 7.19. Illustration of the SACS alerts (with focus on alerts with SO2 VCD > 6 DU) for GOME-2B (top) and GOME-2C (bottom), for first half of 2022. SO_2 amount and region numbers are indicated as a function of time.

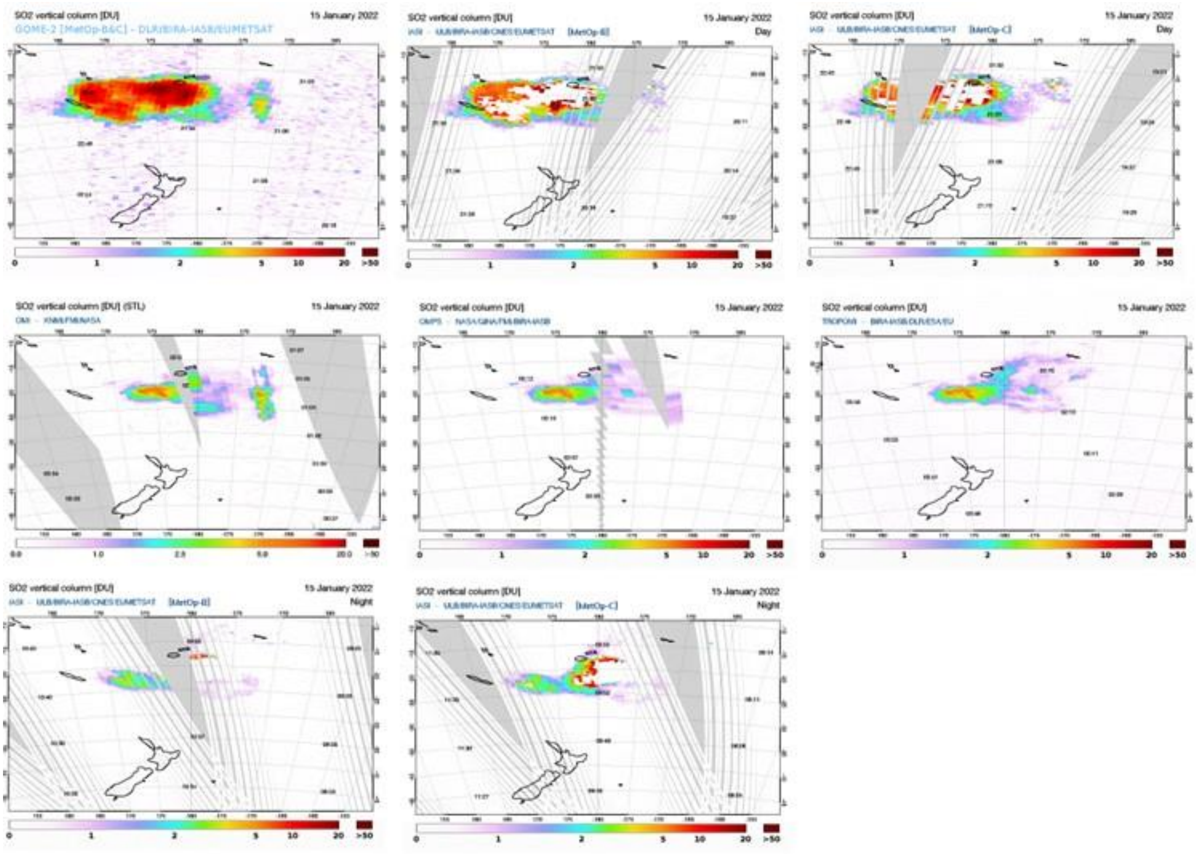

Figure 7.20. Illustration of the eruption of Hunga-Tunga eruption in 15 January 2022 (SACS region 412) as seen by GOME-2B and GOME-2C (composite), IASI-A and IASI-B, OMI, AIRS, OMPS and TROPOMI instruments.

GDP-4.8 also contains an anthropogenic SO_2 product that can be compared with ground-based MAXDOAS/DirectSun data from the Xianghe station, similarly to what is done in the SO_2 report. For this Operations Report however, between the instrumental problem in the UV for the Xianghe MAXDOAS and the SO_2 levels in China dropping from year to year, a proper comparison could not be performed and the (noisy) PBL product time-series are shown (see Figure 7.21). Test validation were also performed with respect to Mexico City (unam) Pandora data received from PGN team (A. Cede, M. Tiefengraben), but without much success (see AC SAF Operations Report 2/2020).

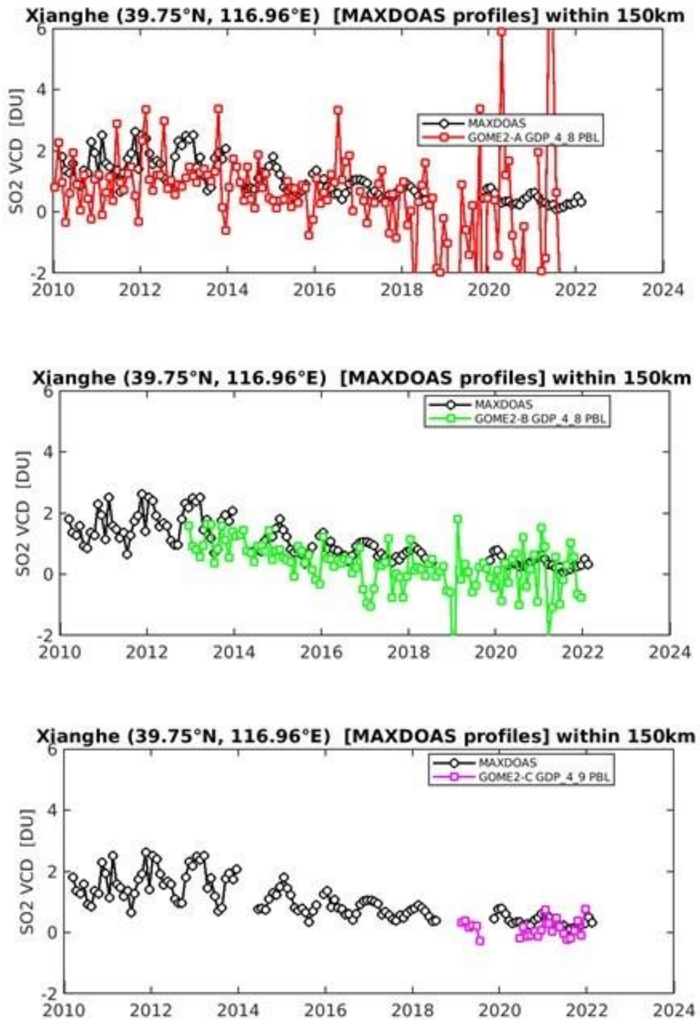

Figure 7.21. Time-series of the SO2 PBL around Xianghe for GOME-2A, GOME-2B, GOME-2C and MAXDOAS data. Left: daily points, right: monthly means.

As discussed in previous Operations Reports, the plan for the improvement of the SO_2 GOME-2 products is to follow BIRA-IASB recommendations and bring the GDP SO_2 algorithm consistent to the TROPOMI product (Theys *et al.*, 2017). This has been tested for the GOME-2C validation, with change of the DOAS wavelength fit region, but has been found not appropriate for GOME-2A and GOME-2B, due to issues with L1 data.

References:

Clémer, K., Van Roozendael, M., Fayt, C., Hendrick, F., Hermans, C., Pinardi, G., Spurr, R., Wang, P., and De Mazière, M.: Multiple wavelength retrieval of tropospheric aerosol optical properties from MAXDOAS measurements in Beijing, Atmos. Meas. Tech., 3, 863-878, 2010. https://doi.org/10.5194/amt-3-863-2010

De Smedt, I., Stavrakou, T., Hendrick, F., Danckaert, T., Vlemmix, T., Pinardi, G., Theys, N., Lerot, C., Gielen, C., Vigouroux, C., Hermans, C., Fayt, C., Veefkind, P., Müller, J.-F., and Van Roozendael, M.: Diurnal, seasonal and long-term variations of global formaldehyde columns

inferred from combined OMI and GOME-2 observations, Atmos. Chem. Phys., 15, 12519-12545, 2015.
https://doi.org/10.5194/acp-15-12519-2015

Gielen, C., Van Roozendael, M., Hendrick, F., Pinardi, G., Vlemmix, T., De Bock, V., De Backer, H., Fayt, C., Hermans, C., Gillotay, D., and Wang, P.: A simple and versatile cloud-screening method for MAX-DOAS retrievals, Atmos. Meas. Tech., 7, 3509–3527, 2014.
https://doi.org/10.5194/amt-7-3509-2014

Hendrick, F.M., Van Roozendael, M., Chipperfield, M.P., Dorf, M., Goutail, F., Yang, X., Fayt, C., Hermans, C., Pfeilsticker, K., Pommereau, J.-P., Pyle, J.A., Theys, N., and De Maziere, M.: Retrieval of stratospheric and tropospheric BrO profiles and columns using ground-based zenith-sky DOAS observations at Harestua, 60° N., Atmos. Chem. Phys., 7, 4869-4885, 2007.
https://doi.org/10.5194/acp-7-4869-2007

Hendrick, F., Johnston, P.V., De Mazière, M., Fayt, C., Hermans, C., Kreher, K., Theys, N., Thomas, A., and Van Roozendael, M.: One-decade trend analysis of stratospheric BrO over Harestua (60°N) and Lauder (45°S) reveals a decline, Geophys. Res. Letters, 35, L14801, 2008.
https://doi.org/10.1029/2008gl034154

Hendrick, F., Müller, J.-F., Clémer, K., Wang, P., De Mazière, M., Fayt, C., Gielen, C., Hermans, C., Ma, J.Z., Pinardi, G., Stavrakou, T., Vlemmix, T., and Van Roozendael, M.: Four years of ground-based MAX-DOAS observations of HONO and NO2 in the Beijing area, Atmos. Chem. Phys., 14, 765–781, 2014.
https://doi.org/10.5194/acp-14-765-2014

Pinardi, G., Van Roozendael, M., Lambert, J.-C., Granville, J., Hendrick, F., Tack, F., Yu, H., Cede, A., Kanaya, Y., Irie, I., Goutail, F., Pommereau, J.-P., Pazmino, A., Wittrock, F., Richter, A., Wagner, T., Gu, M., Remmers, J., Friess, U., Vlemmix, T., Piters, A., Hao, N., Tiefengraber, M., Herman, J., Abuhassan, N., Bais, A., Kouremeti, N., Hovila, J., Holla, R., Chong, J., Postylyakov, O., Ma, J.: GOME-2 total and tropospheric NO_2 validation based on zenith-sky, direct-sun and multi-axis DOAS network observations, Proceeding of the EUMETSAT conference, 22-26 September 2014, Geneva, Switzerland.

Pinardi, G., Van Roozendael, M., Hendrick, F., Theys, N., Abuhassan, N., Bais, A., Boersma, F., Cede, A., Chong, J., Donner, S., Drosoglou, T., Frieß, U., Granville, J., Herman, J. R., Eskes, H., Holla, R., Hovila, J., Irie, H., Kanaya, Y., Karagkiozidis, D., Kouremeti, N., Lambert, J.-C., Ma, J., Peters, E., Piters, A., Postylyakov, O., Richter, A., Remmers, J., Takashima, H., Tiefengraber, M., Valks, P., Vlemmix, T., Wagner, T., and Wittrock, F.: Validation of tropospheric NO2 column measurements of GOME-2A and OMI using MAX-DOAS and direct sun network observations, Atmos. Meas. Tech., 13, 6141-6174, 2020.
https://doi.org/10.5194/amt-13-6141-2020

Richter, A., Behrens, L., Hilboll, A., Munassar, S., Burrows, J.P., Pinardi, G., and Van Roozendael, M.: Cloud effects on satellite retrievals of tropospheric NO2 over China, oral presentation at the DOAS workshop, September 2017, Yokohama, Japan.

Theys, N., De Smedt, I., Yu, H., Danckaert, T., van Gent, J., Hörmann, C., Wagner, T., Hedelt, P., Bauer, H., Romahn, F., Pedergnana, M., Loyola, D., and Van Roozendael, M.: Sulfur dioxide retrievals from TROPOMI onboard Sentinel-5 Precursor: algorithm theoretical basis, Atmos. Meas. Tech., 10, 119-153, 2017.
https://doi.org/10.5194/amt-10-119-2017

Verhoelst, T., Compernolle, S., Pinardi, G., Lambert, J.-C., Eskes, H. J., Eichmann, K.-U., Fjæraa, A. M., Granville, J., Niemeijer, S., Cede, A., Tiefengraber, M., Hendrick, F., Pazmiño, A., Bais, A., Bazureau, A., Boersma, K. F., Bognar, K., Dehn, A., Donner, S., Elokhov, A., Gebetsberger, M., Goutail, F., Grutter de la Mora, M., Gruzdev, A., Gratsea, M., Hansen, G. H., Irie, H., Jepsen, N., Kanaya, Y., Karagkiozidis, D., Kivi, R., Kreher, K., Levelt, P. F., Liu, C., Müller, M., Navarro Comas, M., Piters, A. J. M., Pommereau, J.-P., Portafaix, T., Prados-Roman, C., Puentedura, O., Querel, R., Remmers, J., Richter, A., Rimmer, J., Rivera Cárdenas, C., Saavedra de Miguel, L., Sinyakov, V. P., Stremme, W., Strong, K., Van Roozendael, M., Veefkind, J. P., Wagner, T., Wittrock, F., Yela González, M., and Zehner, C.: Ground-based validation of the Copernicus Sentinel-5P TROPOMI NO2 measurements with the NDACC ZSL-DOAS, MAX-DOAS and Pandonia global networks, Atmos. Meas. Tech., 14, 481–510, 2021.
https://doi.org/10.5194/amt-14-481-2021

Vlemmix, T., Hendrick, F., Pinardi, G., Smedt, I., Fayt, C., Hermans, C., Piters, A., Wang, P., Levelt, P, and Van Roozendael, M.: MAX-DOAS observations of aerosols, formaldehyde and nitrogen dioxide in the Beijing area: comparison of two profile retrieval approaches, Atmos. Meas. Tech., 2, 941–963, 2015.
https://doi.org/10.5194/amt-8-941-2015

Wang, T., Hendrick, F., Wang, P., Tang, G., Clémer, K., Yu, H., Fayt, C., Hermans, C., Gielen, C., Müller, J.-F., Pinardi, G., Theys, N., Brenot, H., and Van Roozendael, M.: Evaluation of tropospheric SO2 retrieved from MAX-DOAS measurements in Xianghe, China, Atmos. Chem. Phys., 14(20), 11149-11164, 2014.
https://doi.org/10.5194/acp-14-11149-2014

7.3.1. Online quality monitoring

Online quality monitoring plots are continuously generated at DLR and published for O_3, NO_2, BrO, HCHO, SO_2, H2O products as described in Section 7.1.3.

BIRA-IASB provides quality assessment (QA) pages for vertical column amounts of NO_2, HCHO, BrO and SO_2, derived from GOME-2B and GOME-2C, as well as IASI SO_2. These pages are available under https://cdop.aeronomie.be/quality-assessment/.

System developments:

- As mentioned in the previous reports, the GOME-2 monitoring page now shows time-series for Metop-B and Metop-C. Metop-A was monitored internally by the team until its end-of-life in November 2021 and the data is maintained internally.
- As indicated in the previous report, the current monitoring system, based on data storage in an SQL database, remains slow in use. A solution for a new system is currently being drafted and is expected to perform much more responsive. This system will be based on gridded data stored in NetCDF file format behind an OpenDAP request mechanism. Since the last report, general tests have taken place by initiating a dedicated test server and using the OpenDAP mechanism to obtain data from netCDF files. This has proved successful and over the next month the NetCDF data structure will be further defined and a permanent server will be installed. More details can be expected in future reports.

Monitoring status:

See example images for NO_2 and SO_2 below.

- GOME-2B: No anomalies. Increase in fit residuals can be observed, in line with nominal instrument degradation progressing with age.

- GOME-2C: No anomalies for NO_2, HCHO, and BrO. For SO_2, it is noticed that retrieved columns from GOME-2C are lower than those from GOME-2B.
- IASI SO_2: The offline phase of the IASI SO_2 monitoring, announced in previous reports, unfortunately continues to this date. This is related to the system being based on alerts for enhanced SO_2 amounts from the SACS system (sacs.aeronomie.be) that saw an interruption in the generation scheme. We now know that those alerts will not return in their previous form. In CDOP 4, monitoring of SO_2 time-series will be taken over by AUTH. The IASI SO_2 page at cdop.aeronomie.be will be taken offline soon.

NO_2 tropospheric column and fitting root-mean-square over India

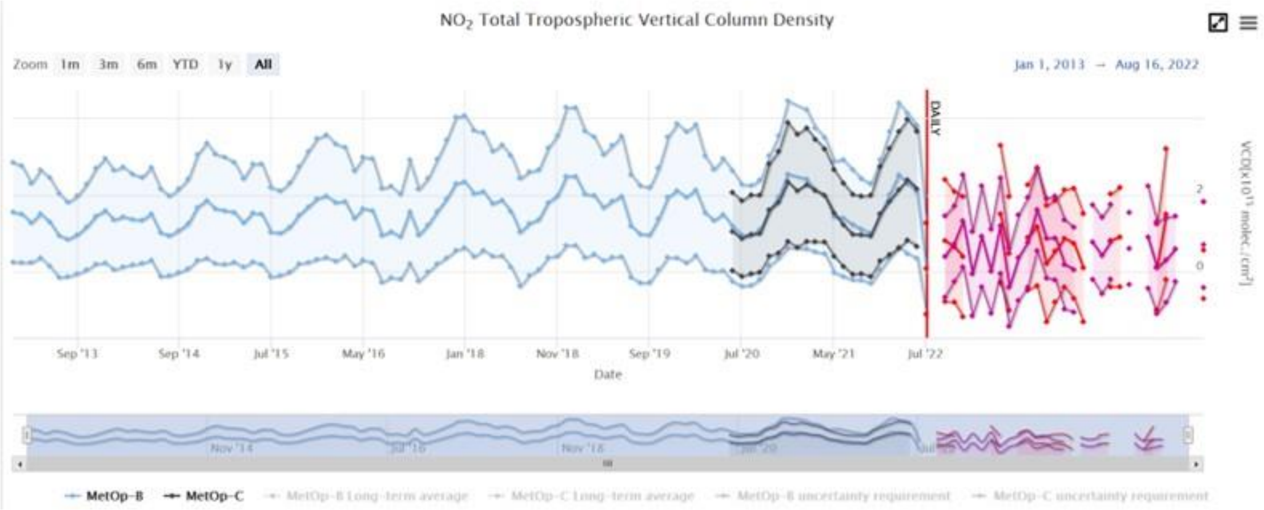

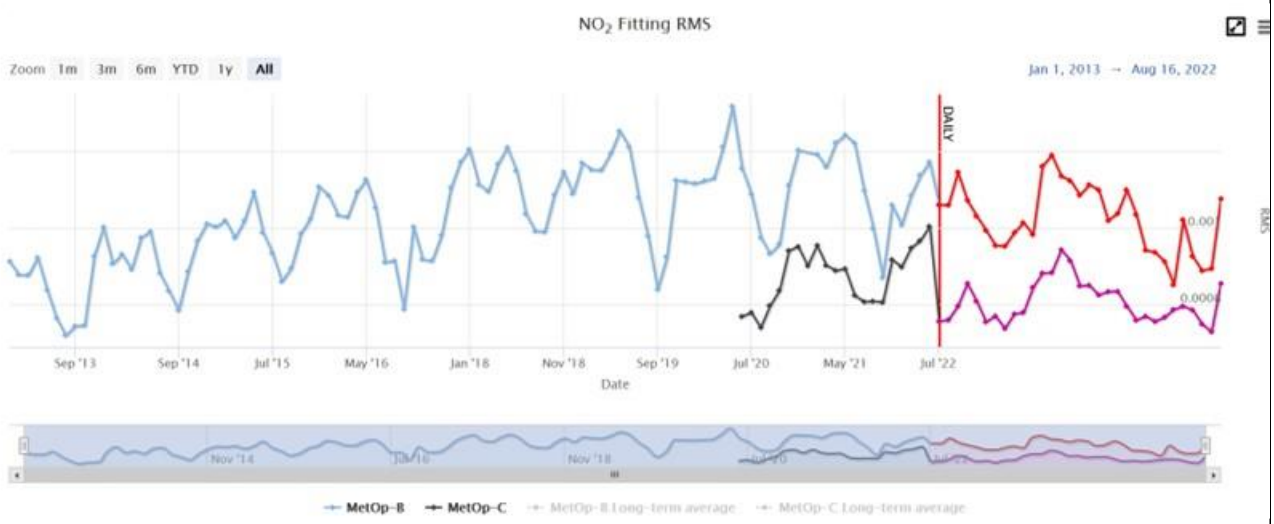

SO2 total vertical column over Northern China

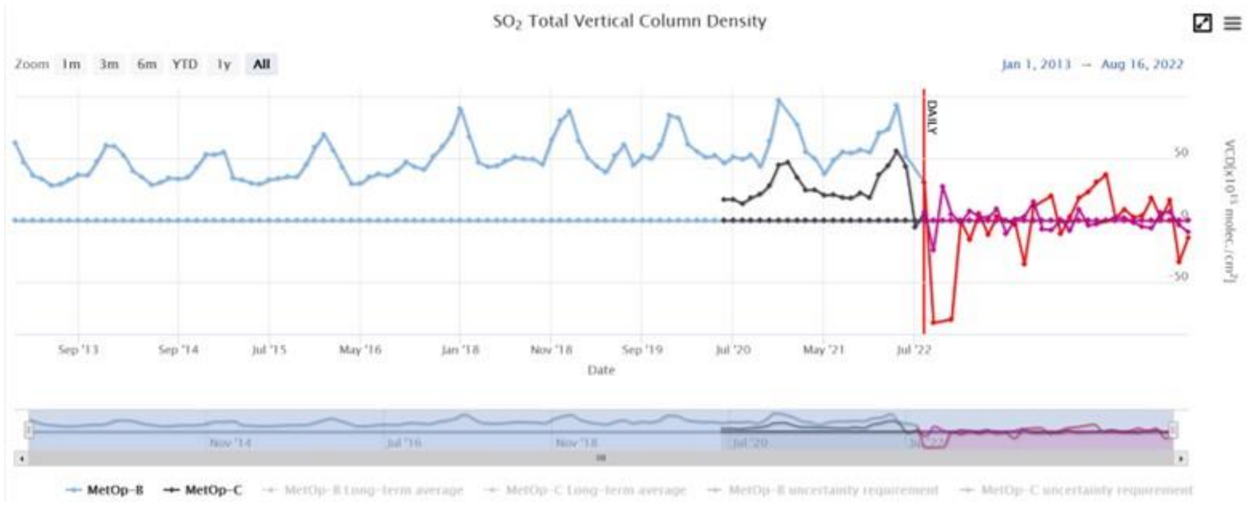

Figure 7.22. Time-series example for NO_2 and SO_2, comparing results from GOME-2B and GOME-2C. For GOME-2B, the blue curve shows monthly averaged values, red shows recent daily averages. The black and magenta curves are for GOME-2C.

7.4. Ozone profile products

Table 7.13. Validation status of ozone profile products

Product Identifier	Product Name	Accuracy	Reference	Validating Institute	Correlative data sources
O3M-47.1	NRT high-resolution ozone profile	Fulfils threshold accuracy requirements	RD8	KMI DWD	Ozonesonde data from SHADOZ, NDACC, NILU and WOUDC Lidar/microwave data from NDACC
O3M-311			RD26		
O3M-39	Offline high-resolution ozone profile	Fulfils threshold accuracy requirements	RD7	KMI DWD	Ozonesonde data from SHADOZ, NDACC, NILU and WOUDC Lidar/microwave data from NDACC
O3M-48			RD8		
O3M-312			RD26		

Validation results can be found in more detail on the at AC SAF validation & quality assessment website.

Validation activities summary:

This summary contains validation results for the GOME-2A, GOME-2B and GOME-2C high-resolution (HR) ozone profile products, retrieved by the Ozone Profile Retrieval Algorithm (OPERA) at KNMI. This validation section focuses on the time period July 2021 – June 2022.

The authors of this summary are Dr. Andy Delcloo from KMI and Dr. Peggy Achtert from DWD. More information on how these values are extracted is available in the validation report.

To report the skill scores of GOME-2 ozone profile products in a more condensed way, the statistics for the different output levels of GOME-2 are reduced to two layers: Lower Stratosphere (until an altitude of 30 km) and Upper Stratosphere (up to an altitude of 50 km). Table 7.14 gives an overview on how we define the ranges in height for the different belts for lower stratosphere and upper stratosphere.

The collocation data used for the validation using ozonesonde data are shown in Figure 7.23. The validation for the lower stratosphere is made with ozonesonde data, for the upper stratosphere with lidar and/or microwave data. The stations used in this validation for the lidar/microwave data are the Network for the Detection of Atmospheric Composition Change (NDACC) stations of Bern (microwave), Ny Ålesund (microwave), Payerne (microwave), Hohenpeissenberg (lidar), Table Mountain (lidar), Mauna Loa (microwave/lidar), Eureka (lidar), and Lauder (lidar).

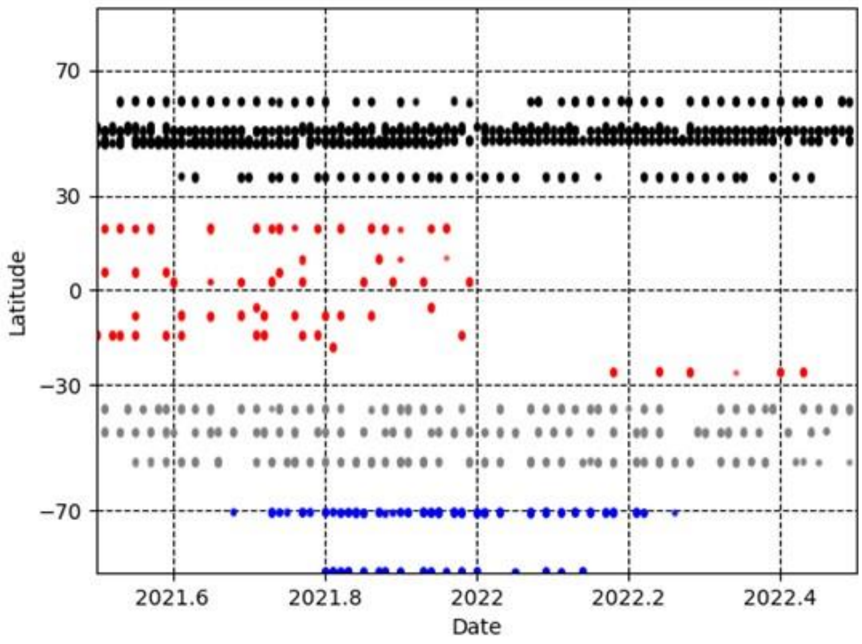

Figure 7.23. Collocation data for the validation with ozonesonde data for the time period July 2021 – June 2022.

Table 7.14. Definition of the ranges in km for lower and higher stratosphere for the different latitude belts

	Lower Stratosphere	Upper Stratosphere
Polar Region	12 km – 30 km	30 km – 50 km
Mid-Latitudes	14 km – 30 km	30 km – 50 km
Tropical Region	18 km – 30 km	30 km – 50 km

Relative differences (Eq. 1) are calculated against sounding data, which is convolved with the averaging kernels (Smoothed Sounding):

$$\frac{\text{(GOME-2 – Smoothed Sounding)} * 100}{\text{Smoothed Sounding}} \quad (1)$$

Table 7.15 shows an overview of the obtained results for the time period July 2021 – June 2022 only for the lower and the higher stratosphere, not taking into account the tropospheric ozone column products since a dedicated product is discussed earlier in this report. The statistics for the lower stratosphere are obtained by KMI, the statistics for the higher stratosphere by DWD.

Table 7.15. Absolute Differences (AD), Relative Differences (RD) and standard deviation (STDEV) are shown on the accuracy of GOME-2A/B/C HR ozone profile products for the lower and the higher stratosphere for five different latitude belts for the time period July 2021 – June 2022.

	GOME-2B HR					
	Lower Stratosphere			Upper Stratosphere		
	AD	RD	STDEV	AD	RD	STDEV
	(DU)	(%)	(%)	(DU)	(%)	(%)
Northern Polar Region	-12.9	-4.1	13.9	-5.6	-11.0	4.7
Northern Mid-Latitudes	2.0	1.0	8.4	-5.9	-9.9	3.8
Tropical Region	5.0	3.6	5.0	-8.8	-10.1	1.7
Southern Mid-Latitudes	9.0	5.5	10.1	0.3	0.5	1.2
Southern Polar Region	12.9	21.1	74.2	-	-	-
	GOME-2C HR					
	Lower Stratosphere			Upper Stratosphere		
	AD	RD	STDEV	AD	RD	STDEV
	(DU)	(%)	(%)	(DU)	(%)	(%)
Northern Polar Region	-7.9	-3.3	15.2	-4.5	-8.2	4.3
Northern Mid-Latitudes	-1.5	-0.2	7.6	-4.7	-9.3	3.9
Tropical Region	-0.8	0.1	4.9	-5.8	-8.6	2.7
Southern Mid-Latitudes	8.3	5.7	11.4	-0.6	-2.6	1.9
Southern Polar Region	4.1	25.8	71.1	-	-	-

The target value (15% accuracy) is met in both lower and upper stratosphere for all belts under consideration for Metop B and Metop-C. The discrepency is highest at high-latitude. The optimal values are met for GOME-2C (10 % accuracy).

More detailed ozone profile validation results can also be found on the AC SAF ozone profile validation website.

7.4.1. Online quality monitoring

Timeline of the vertically integrated Metop-B ozone profile with respect to time is presented in Figure 7.24.

More information and images at the following web addresses
https://www.temis.nl/acsaf/timeseries.php?sat=metopa
https://www.temis.nl/acsaf/timeseries.php?sat=metopb
https://www.temis.nl/acsaf/timeseries.php?sat=metopc

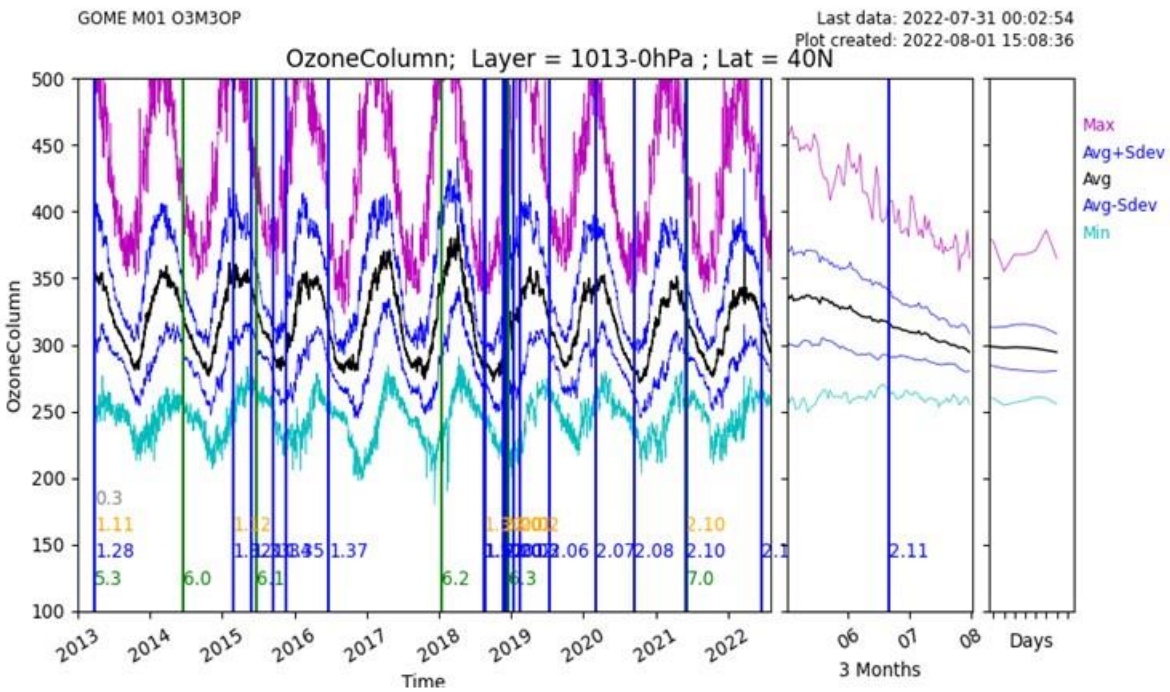

Figure 7.24. Timeline of vertically integrated Metop-B ozone profiles (=total ozone columns) and changes in data processor (vertical lines). The changes in late 2018 / early 2019, including the improved degradation correction, have resulted in much better ozone profiles and have also affected the total ozone columns shown here.

Legend of the coloured vertical lines:

- Green: PPF version
- Blue: Software version (PGE)
- Orange: Algorithm version
- Grey: Config version

7.5. Aerosol products

Table 7.16. Validation status of aerosol products

<table>
<tr><th>Product Identifier</th><th>Product Name</th><th>Accuracy</th><th>Reference</th><th>Validating Institute</th><th>Correlative data sources</th></tr>
<tr><td>O3M-78</td><td rowspan="2">NRT absorbing aerosol height</td><td rowspan="2">Fulfils threshold accuracy requirement</td><td rowspan="2">RD32</td><td rowspan="2">KMI, AUTH</td><td rowspan="2">CALIOP, EARLINET</td></tr>
<tr><td>O3M-364</td></tr>
<tr><td>O3M-72.1</td><td rowspan="2">NRT absorbing aerosol index from PMDs</td><td rowspan="2">Fulfils threshold accuracy requirement</td><td>RD14</td><td rowspan="2">KNMI</td><td>Comparisons with other satellite instruments: SCIAMACHY, OMI, and intercomparison of GOME-2A with GOME-2B</td></tr>
<tr><td>O3M-362</td><td>RD33</td><td>Comparisons with the AAI products from GOME-2A and GOME-2B</td></tr>
<tr><td>O3M-69</td><td rowspan="3">Offline absorbing aerosol height</td><td rowspan="3">Fulfils threshold accuracy requirements</td><td rowspan="3">RD32</td><td rowspan="3">KMI, AUTH</td><td rowspan="3">CALIOP, EARLINET</td></tr>
<tr><td>O3M-79</td></tr>
<tr><td>O3M-365</td></tr>
<tr><td>O3M-63.1</td><td rowspan="3">Offline absorbing aerosol index from PMDs</td><td rowspan="3">Fulfils threshold accuracy requirements</td><td rowspan="2">RD14</td><td rowspan="3">KNMI</td><td rowspan="2">Comparisons with other satellite instruments: SCIAMACHY, OMI, and intercomparison of GOME-2A with GOME-2B</td></tr>
<tr><td>O3M-73.1</td></tr>
<tr><td>O3M-363</td><td>RD33</td><td>Comparisons with the AAI products from GOME-2A and GOME-2B</td></tr>
</table>

Validation activities summary:

This summary contains validation results for the GOME-2A, GOME-2B and GOME-2C Absorbing Aerosol Height (AAH) products and is made available by the validation teams of AUTH and KMI. More information on how these values are extracted is available in the validation report validation report.

AAH is a new operational AC SAF product for aerosol layer height detection, developed by KNMI within the AC SAF. It uses the AAI as an indicator to derive the actual height of the absorbing aerosol layer in the O_2-A band using the Fast Retrieval Scheme for Clouds from the Oxygen A band (FRESCO) algorithm (Wang *et al*., 2012; Tilstra *et al*., 2020). The AAH reported by GOME-2 onboard Metop-A, Metop-B and Metop-C, between 2007 and 2019, has been validated by AUTH against ground-based lidar data from the European Aerosol Research Lidar Network (EARLINET) database and by KMI against CALIOP aerosol layer height (De Bock, *et al*. 2020; Michailidis *et al*., 2021).

AUTH results:

A wide choice of lidar stations around Europe was made in order to examine the behaviour of the comparisons for different common aerosol loads over the locations (see the first column of

Table 7.17). The total number of carefully screened collocations with the EARLINET lidar measurements was 232 for the three GOME-2 instruments. On average, the mean absolute bias (GOME-2 minus lidar height) was found to be -0.25 ± 1.86 km, with a near-Gaussian distribution and minimum and maximum differences of ~ ±5 km. On a station basis, and with a couple of exceptions, their mean biases fall in the ±1 km range, with an associated standard deviation between 0.6 – 2.4 km.

Table 7.17. Summary of statistics for the comparisons between GOME-2 AAH and LIDAR ALH for all stations

EARLINET Station	N	Statistical parameters (in km)			
		Mean absolute bias	**Std**	**Min**	**Max**
Athens, Greece	3	-2.00	1.38	-3.6	-1.06
Barcelona, Spain	36	-0.44	1.86	-4.66	2.86
Belsk, Poland	28	0.11	1.5	-3.11	3.24
Bucharest, Romania	17	-0.07	2.08	-4.81	3.37
Évora, Portugal	5	-0.07	1.95	-1.64	3.31
Granada, Spain	51	-0.6	1.86	-3.73	4.42
Lecce, Italy	18	-0.24	1.14	-3.47	2.05
Limassol, Cyprus	22	0.06	2.4	-4.08	4.43
Minsk, Belarus	5	0.56	0.61	-0.05	1.51
Potenza, Italy	12	-1.57	1.32	-3.49	1.17
Thessaloniki, Greece	27	0.02	1.87	-4.71	3.24
Warsaw, Poland	8	0.8	1.5	1.08	2.15
Summary	**232**	**-0.25**	**1.86**	**-4.91**	**5.14**

In Figure 7.25, the histogram of absolute differences between GOME-2 and EARLINET aerosol layer heights, calculated for all collocated cases is shown, with the associated statistics. The associated Absorbing Aerosol Index (AAI) value is color-coded. In the right panel, the scatter plot between GOME-2 AAH and aerosol layer height from EARLINET stations, for the totality of collocated cases is presented.

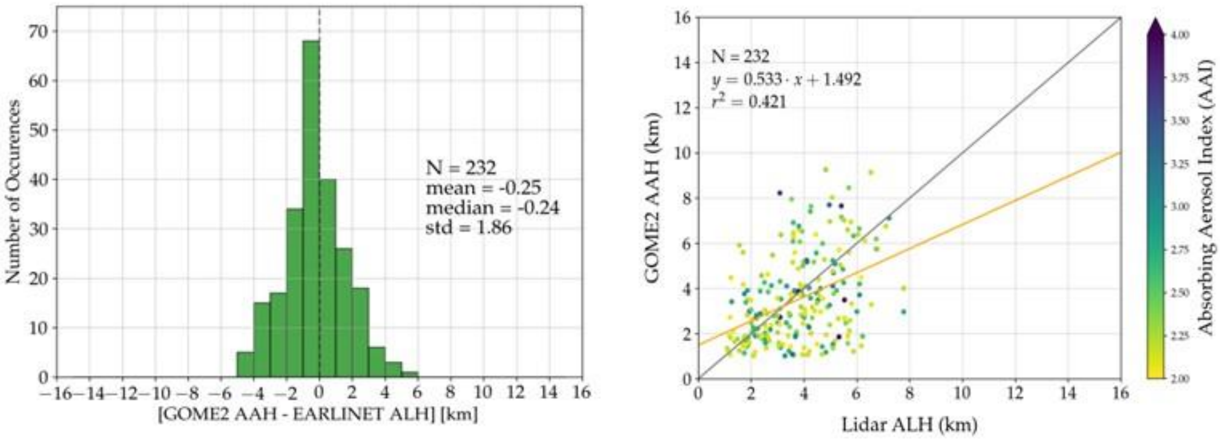

Figure 7.25. Histogram of absolute differences between GOME-2 AAH and aerosol layer height obtained from EARLINET backscatter profiles (using the WCT method), calculated for all collocated cases. The associated AAI value is color-coded. Right: Scatter plot between GOME-2 AAH and aerosol layer height from EARLINET stations, for the total of collocated cases.

Taking into account the possible temporal collocation mismatch and the spatial difference between the satellite pixel size and the point view of the ground-based observations, these results are quite promising and demonstrate that stable aerosol layers are well captured by the satellite sensors. The official AC SAF requirements for the accuracy of the GOME-2 AAH product state that, for heights <10 km, the threshold accuracy is 3 km, the target accuracy is 2 km, and the optimal accuracy is 1 km. This validation effort shows that for all cases the target accuracy is met, see Table 7.18. For the different regimes, which relate to the degree of cloud cover, please refer to the validation report and Michailidis *et al.*, 2021.

Table 7.18. Percentage of collocated lidar & GOME-2 AAH cases that fulfill the optimal accuracy criteria (first row), the target criteria (second row), the threshold criteria (third row) for Regime A in the first column, Regime B in the second, Regime C in the third and the totality of the collocations in the final column. The regimes are related to the degree of cloud cover.

	Regime A (108 cases)	Regime B (113 cases)	Regime C (11 cases)	Total (232 cases)
Optimal (1 km)	31.2 %	54.4 %	36.3 %	42.5 %
Target (2 km)	58.7 %	80.3 %	54.5 %	68.6 %
Threshold (3 km)	74.3 %	93.8 %	90.9 %	84.5 %

KMI results:

At the time of writing this report (rev. 1), there was no updated AAH reference data available. Therefore, all the results are as in AC SAF Operations Report 1/2021.

KMI validated the AAH only for specific case studies related to volcanic eruptions. AAH values are only included in the analysis if the corresponding AAI is higher than 4. CALIOP and GOME data are compared when the distance between both overpasses is maximum 100 km. There is currently no constraint on the time difference between both overpasses.

Compared to the results shown in the validation report, new data has been added to the study (i.e. Fournaise de la Piton 11-12 February 2020, Karymsky 1-2 April 2020, Kavachi 16 March 2020 and Kikai 29-30 April 2020) in this report. The updated results are summarized in Table 7.19.

Overall, just about 50-60 % of the AAH pixels from GOME-2A, GOME-2B and GOME-2C reach the threshold requirements (see Table 7.19 and Figure 7.26). The optimal requirement threshold is reached for GOME-2A, GOME-2B and GOME-2C in 18 %, 25 % and 24 % of the cases, respectively (when comparing the AAH with the minimum CALIOP layer height). If only the tropospheric aerosol species (as defined by CALIOP) are studied, the results improve. This can also be seen in Table 7.19 (values in brackets).

Table 7.19. Percentage of data for each GOME-2 instrument that reached the threshold, target and optimal accuracy requirements. Values obtained when only considering the tropospheric aerosol species are shown in brackets

GOME-2A				
		Layer height <10 km	**Layer height >10 km**	**Total**
Threshold	**AAH-minC**	56.0 % (69.6 %)	53.1 % (26.4 %)	55.9 % (68.9 %)
	AAH-maxC	56.4 % (69.5 %)	46.8 % (23.6 %)	56.2 % (68.7 %)
Target	**AAH-minC**	39.0 % (48.5 %)	43.5 % (19.1 %)	39.1 % (48.0 %)
	AAH-maxC	38.0 % (46.9 %)	32.4 % (23.6 %)	37.9 % (46.3 %)
Optimal	**AAH-minC**	17.3 % (21.5 %)	29.9 % (10.0 %)	17.6 % (21.3 %)
	AAH-maxC	18.1 % (22.3 %)	15.6 % (10.0 %)	18.1 % (22.1 %)
GOME-2B				
		Layer height <10 km	**Layer height >10 km**	**Total**
Threshold	**AAH-minC**	51.8 % (53.6 %)	22.9 % (11.7 %)	50.9 % (51.6 %)
	AAH-maxC	52.6 % (54.4 %)	20.6 % (10.2 %)	51.6 % (52.2 %)
Target	**AAH-minC**	42.9 % (44.5 %)	20.6 % (5.60 %)	42.2 % (42.6 %)
	AAH-maxC	37.0 % (38.3 %)	17.1 % (7.90 %)	36.4 % (36.8 %)
Optimal	**AAH-minC**	25.1 % (26.0 %)	17.1 % (3.40 %)	24.8 % (24.9 %)
	AAH-maxC	20.5 % (33.1 %)	16.5 % (3.00 %)	20.4 % (31.6 %)
GOME-2C				
		Layer height <10 km	**Layer height >10 km**	**Total**
Threshold	**AAH-minC**	50.8 % (50.8 %)	0.0 % (0.0 %)	46.8 % (46.8 %)
	AAH-maxC	57.1 % (57.1 %)	0.0 % (0.0 %)	52.9 % (52.9 %)
Target	**AAH-minC**	42.2 % (42.2 %)	0.0 % (0.0 %)	38.8 % (38.8 %)
	AAH-maxC	49.1 % (49.1 %)	0.0 % (0.0 %)	45.2 % (45.2 %)
Optimal	**AAH-minC**	26.3 % (26.3 %)	0.0 % (0.0 %)	24.1 % (24.1 %)
	AAH-maxC	34.5 % (34.5 %)	0.0 % (0.0 %)	31.6 % (31.6 %)

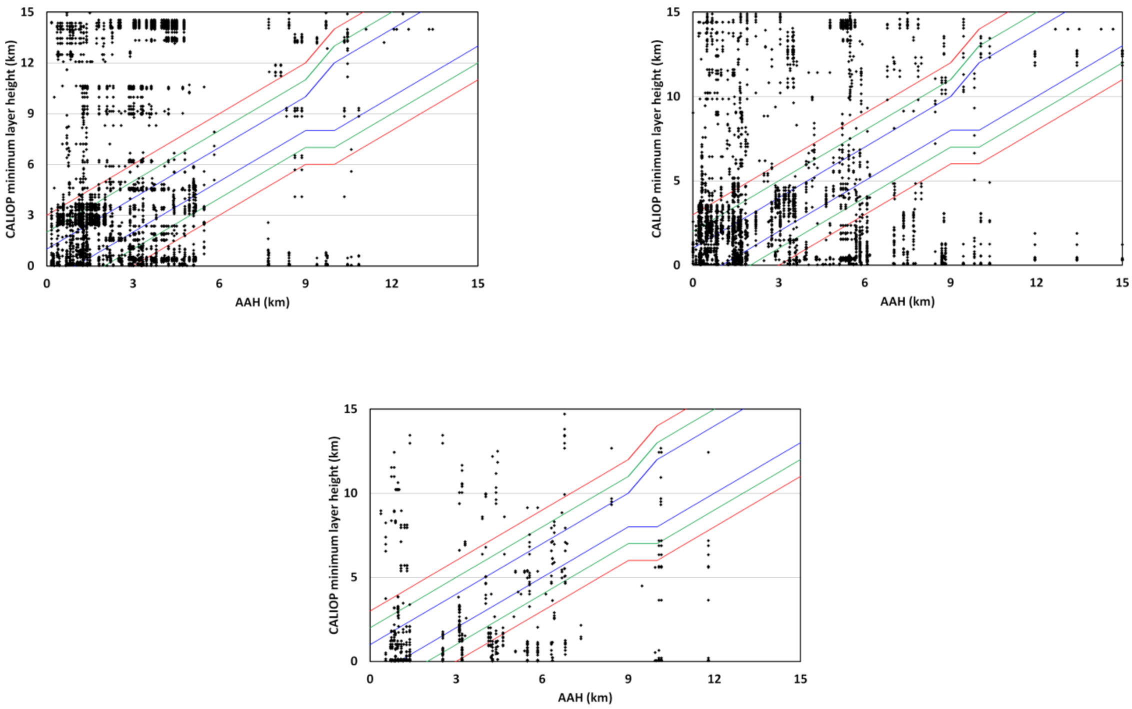

Figure 7.26. Requirement plots for GOME-2A (upper left), GOME-2B (upper right) and GOME-2C (lower middle).The red, green and blue lines represent the threshold, target and optimal requirements. CALIOP pixels are only shown up to a height of 15 km, which is the detection limit of GOME-2.

References:

Michailidis, K., Koukouli, M.-E., Siomos, N., Balis, D., Tuinder, O., Tilstra, L. G., Mona, L., Pappalardo, G. and Bortoli, D.: First validation of GOME-2/MetOp absorbing aerosol height using EARLINET lidar observations, Atmos. Chem. Phys., 21, 3193–3213, 2021. https://doi.org/10.5194/acp-21-3193-2021

Tilstra, L. G., Tuinder, O., Wang, P. and Stammes, P.: ALGORITHM THEORETICAL BASIS DOCUMENT GOME-2 Absorbing Aerosol Height, SAF/AC//KNMI/ATBD/005, 1.4, Royal Netherlands Meteorological Institute, de Bilt, 2019. https://acsaf.org/docs/atbd/Algorithm_Theoretical_Basis_Document_AAH_Apr_2019.pdf, last access: 31 March 2021.

Wang, P., Tuinder, O. N. E., Tilstra, L. G., De Graaf, M. and Stammes, P.: Interpretation of FRESCO cloud retrievals in case of absorbing aerosol events, Atmos. Chem. Phys., 12(19), 9057–9077, 2021. https://doi.org/10.5194/acp-12-9057-2012

De Bock, V., A. Delcloo, K. Michailidis, M. Koukouli and D. Balis, ACSAF Absorbing Aerosol Height products validation report, SAF/AC/AUTH-RMI/VR/001, 1/2020, 3 July 2020. https://acsaf.org/docs/vr/Validation_Report_AAH_Jul_2020.pdf, last access: 31 March 2021.

7.5.1. Online quality monitoring

The online quality monitoring of the AAI in this section show (left duo-plot) the radiance corrections for the PMD-AAI at 340 and 380 nm, and (right duo-plot) the uncorrected residue, and the corrected residue. The rightmost plot is the result of all the corrections and should stay more or less flat when seasonal cycles and differences are removed.

The break in the curves of the latter plot in August 2018 is caused by the introduction of a combination of the 'End-of-Orbit' corrections and a flattening of the AAI across the swath.

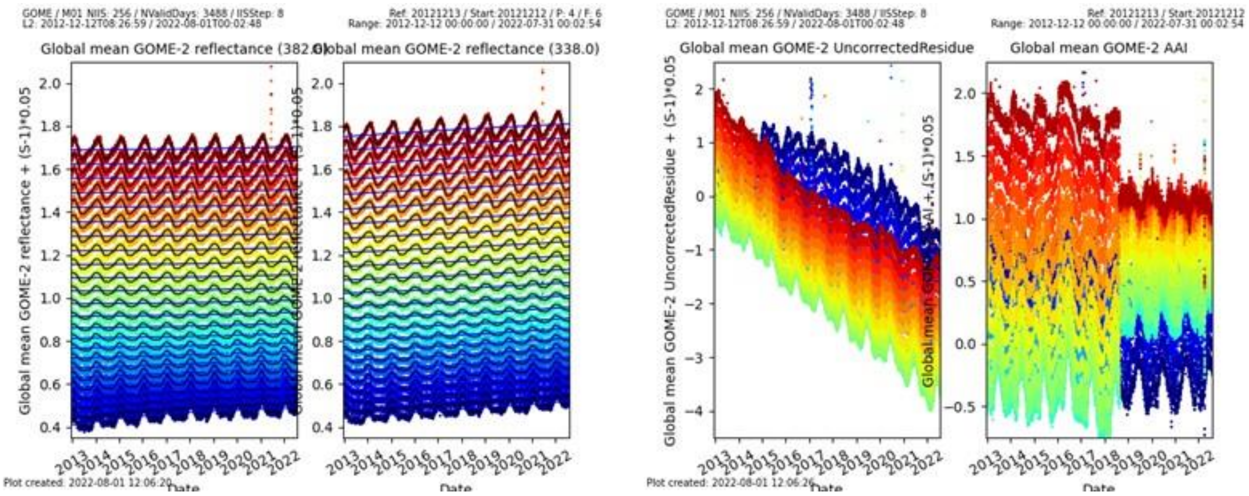

Figure 7.27. Timeline of global mean reflectances at 340 and 380 nm (left) and the uncorrected and corrected AAI from the PMDs of Metop-B.

7.6. UV products

Table 7.20. Validation status of UV products

Product Identifier	Product Name	Accuracy	Reference	Validating Institute	Correlative data sources
O3M-409	NRT UV index, clear-sky	Fulfils threshold accuracy requirements	RD9	DMI	WOUDC, NEUBrew, NSF
O3M-410	NRT UV index, cloud-corrected				
O3M-450 – O3M-464	Offline surface UV	Fulfils target accuracy requirements	RD15	FMI	Brewers and SUV-spectroradiometers from WOUDC, NEUBrew, NSF, NOAA, AUTH and FMI

7.6.1. Online quality monitoring

NUV:

Online quality monitoring of the NRT UV index is found on NUV web page. It can be traced that the quality of the NUV products is stable since the last validation. No problems with the data quality was found in the reporting period.

OUV:

Online quality monitoring of offline surface UV has not shown any unexpected, permanent changes in the monitoring value after the latest validation, indicating that the product accuracy has remained within requirements also during the reporting period. The latest OUV validation reports were published in February 2009 covering June 2007 – May 2008 (Metop-A data) and in February 2015 covering June 2012 – May 2013 (Metop-B data).

Figure 7.28 presents the long-term monitoring graph of OUV, which illustrates seasonal variation of **global average of erythemal daily dose** (yellow markers). Any sudden changes would indicate problems with data quality. Additionally, six-month average values (January – June and July – December) are represented by red markers.

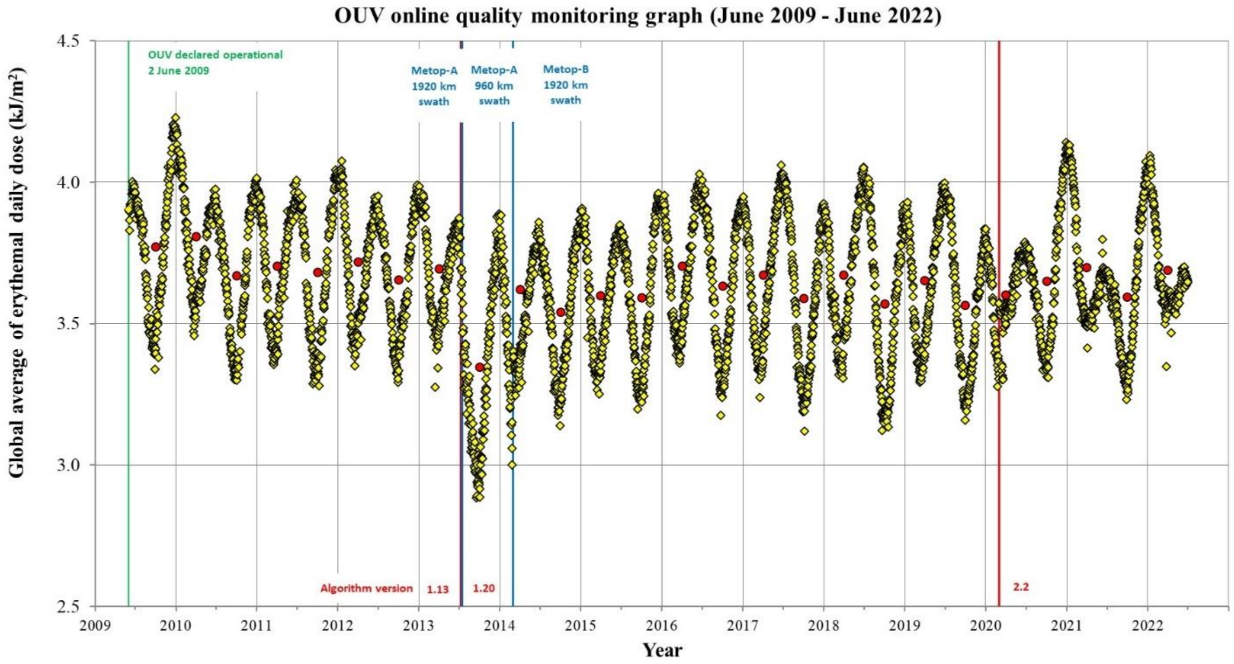

Figure 7.28. OUV long-term monitoring graph.

NOTES:

- GOME-2A was switched from nominal swath width (1920 km) to reduced swath width (960 km) 15 July 2013. The effect to OUV monitoring values can be clearly seen as more wide-spread global average values of erythemal daily dose. This is due to the dominance of lower EDD values in high latitudes when the satellite coverage near the equator is poor due to narrower swath width.
- OUV data processing was switched to use Metop-B data having nominal swath width of 1920 km 1 March 2014
- OUV data processing was switched to use Metop-B+C data 1 March 2020

7.7. IASI NRT products

Table 7.21. Validation status of the IASI CO, SO2, O3 and HNO3 products

Product Identifier	Product Name	Accuracy	Reference	Validating Institute	Correlative data sources
O3M-80	IASI NRT CO	Fulfils threshold accuracy requirement	RD20	LATMOS	FTIR NDACC, MOPITT
O3M-57	IASI NRT SO2	Fulfils threshold accuracy requirement	RD22	AUTH, BIRA-IASB, LATMOS, ULB	MAXDOAS
O3M-44 O3M-49	IASI NRT O3	Fulfils threshold accuracy requirement	RD35	AUTH, KMI, DWD	GOME-2, balloon sonde, lidar and microwave radiometer, Brewer and Dobson
O3M-81	IASI NRT HNO3	Fulfils threshold accuracy requirement	RD36	BIRA-IASB	FTIR NDACC (only available in 2021)

IASI NRT O3 and IASI NRT HNO3 products have been released by EUMETSAT as ‘operational’ on 18 May 2022.

IASI benchmark validation is performed at ULB and LATMOS.

Dissemination monitoring activities summary:

IASI CO:

The IASI NRT CO product (v6.3) has been declared operational on 2 March 2017. Here we present statistical results when comparing the EUMETSAT product disseminated by EUMETCast in BUFR format (COX) with the native product produced at ULB (FORLI-CO v20191122) for 6 days representative of 6 months: January 15th, February 15th, March 15th, April 15th, May 15th and June 15th, 2022, for Metop-B and Metop-C. This allows monitoring if any discrepancy occurs between the two, EUMETSAT and native, products. So far, the discrepancies are found within the numerical errors inherent to the use of different IT infrastructure.

CO total column and profiles are investigated. Statistics between COX data and FORLI-CO data (v20191122) are presented in Table 7.22. Profiles correlation (“Correlation”) score is computed using the discreet cross correlation integral between two profiles, normalized by the square root of the product of their auto-correlation integral. Score of 1 is expected for perfectly matching profiles, 0 for unrelated ones. Absolute and relative differences are calculated for the total columns. These tables are extracted from the Daily Reports prepared by Daniel Hurtmans at ULB.

Table 7.22. Statistics between COX data and FORLI-CO data for 6 days: January 15th, February 15th, March 15th, April 15th, May 15th and June 15th, 2022.

15/01/2022:

		IASI-c		IASI-b	
		Native	COX	Native	COX
Individual Pixels		544868	544370	559283	558798
Common Pixels		543942 (99.83%)		558372 (99.84%)	
Correlation	Mean	0.9997±0.0006		0.9997±0.0010	
	Max	1.0000		1.0000	
	Min	0.9417		0.8146	
Total Column Differences	Mean (10^{19} mol/cm^2)	0.0044±0.0036		0.0043±0.0042	
	Max (10^{19} mol/cm^2)	0.1548		1.2382	
	Min (10^{19} mol/cm^2)	-0.3397		-0.1706	
Total Column Relative Differences	Mean (%)	2.4342±1.3755		2.4216±1.4450	
	Max (%)	26.6855		77.2018	
	Min (%)	-60.8765		-30.9167	

15/02/2022:

		IASI-b		IASI-c	
		Native	COX	Native	COX
Individual Pixels		572473	572580	574257	573850
Common Pixels		571090 (99.74%)		573436 (99.86%)	
Correlation	Mean	0.9997±0.0006		0.9997±0.0006	
	Max	1.0000		1.0000	
	Min	0.8571		0.8749	
Total Column Differences	Mean (10^{19} mol/cm^2)	0.0046±0.0052		0.0045±0.0051	
	Max (10^{19} mol/cm^2)	0.9276		0.9323	
	Min (10^{19} mol/cm^2)	-0.1030		-1.0636	
Total Column Relative Differences	Mean (%)	2.4482±1.3119		2.4454±1.3199	
	Max (%)	53.2650		53.4354	
	Min (%)	-33.5298		-103.5717	

15/03/2022:

		IASI-b		IASI-c	
		Native	COX	Native	COX
Individual Pixels		570328	569738	561440	560890
Common Pixels		569309 (99.82%)		560463 (99.83%)	
Correlation	Mean	0.9997±0.0006		0.9997±0.0006	
	Max	1.0000		1.0000	
	Min	0.8185		0.8998	
Total Column Differences	Mean (10^{19} mol/cm^2)	0.0049±0.0043		0.0048±0.0037	
	Max (10^{19} mol/cm^2)	0.8326		0.6966	
	Min (10^{19} mol/cm^2)	-1.0244		-0.5912	
Total Column Relative Differences	Mean (%)	2.5537±1.2822		2.5391±1.2669	
	Max (%)	71.5087		52.5968	
	Min (%)	-47.2467		-46.4068	

15/04/2022:

		IASI-b		IASI-c	
		Native	COX	Native	COX
Individual Pixels		571485	570907	566297	565900
Common Pixels		570471 (99.82%)		565454 (99.85%)	
Correlation	Mean	0.9997±0.0009		0.9997±0.0009	
	Max	1.0000		1.0000	
	Min	0.8624		0.8420	
Total Column Differences	Mean (10^{19} mol/cm^2)	0.0047±0.0045		0.0048±0.0048	
	Max (10^{19} mol/cm^2)	0.6185		1.8205	
	Min (10^{19} mol/cm^2)	-1.3099		-0.8724	
Total Column Relative Differences	Mean (%)	2.5436±1.3081		2.5378±1.6237	
	Max (%)	44.9689		68.8290	
	Min (%)	-45.3050		-617.2469	

15/05/2022:

		IASI-b		IASI-c	
		Native	COX	Native	COX
Individual Pixels		561032	560366	563670	563089
Common Pixels		559883 (99.80%)		562634 (99.82%)	
Correlation	Mean	0.9996±0.0016		0.9996±0.0020	
	Max	1.0000		1.0000	
	Min	0.6292		0.5607	
Total Column Differences	Mean (10^{19} mol/cm^2)	0.0047±0.0049		0.0047±0.0054	
	Max (10^{19} mol/cm^2)	0.1784		0.3505	
	Min (10^{19} mol/cm^2)	-1.0613		-1.3840	
Total Column Relative Differences	Mean (%)	2.6424±1.7852		2.6383±2.1232	
	Max (%)	39.2032		45.8762	
	Min (%)	-426.8984		-516.6661	

15/06/2022:

		IASI-b		IASI-c	
		Native	COX	Native	COX
Individual Pixels		569771	568637	564493	563699
Common Pixels		568225 (99.73%)		563221 (99.77%)	
Correlation	Mean	0.9995±0.0017		0.9995±0.0017	
	Max	1.0000		1.0000	
	Min	0.6567		0.7092	
Total Column Differences	Mean (10^{19} mol/cm^2)	0.0046±0.0044		0.0045±0.0041	
	Max (10^{19} mol/cm^2)	0.8747		0.5960	
	Min (10^{19} mol/cm^2)	-1.0642		-0.7305	
Total Column Relative Differences	Mean (%)	2.6742±1.3153		2.6660±1.3850	
	Max (%)	69.0660		65.3881	
	Min (%)	-48.3578		-321.9923	

Figure 7.29 – Figure 7.34 show the correlation plots for total column between COX data and FORLI-CO for each platform. No critical deviation was found for these dates.

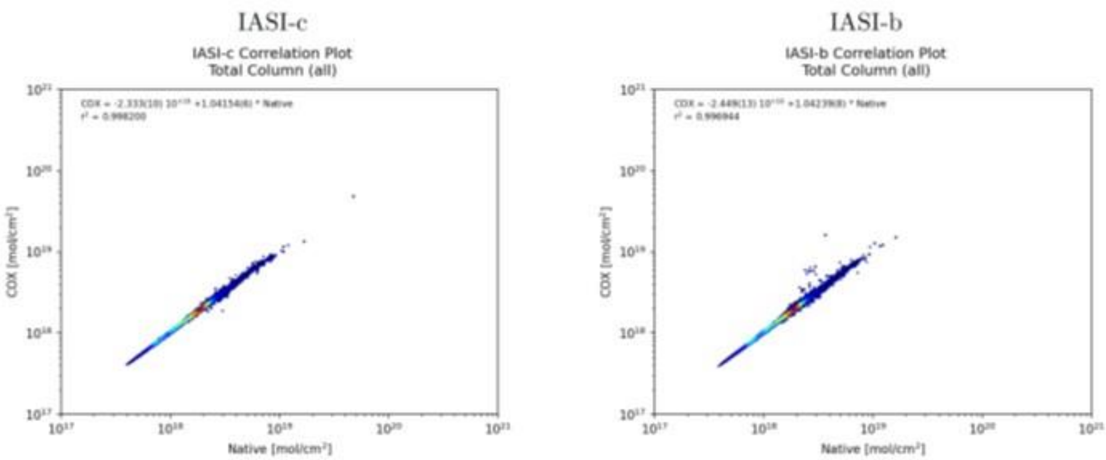

Figure 7.29. Correlation plots for total column between COX data and FORLI-CO for each platform for 15/01/2022. X-axis corresponds to native data (mol/cm^2) and Y-axis corresponds to COX data (mol/cm^2).

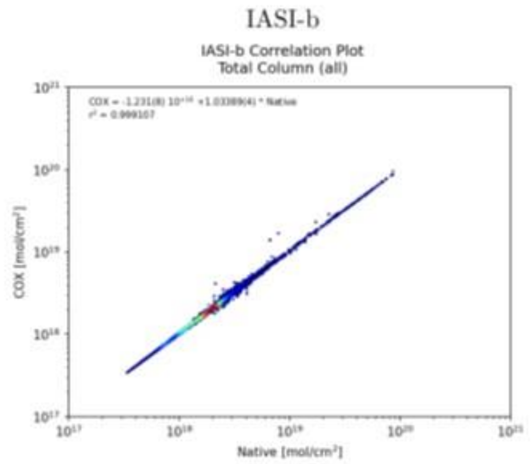

Figure 7.30. Same as Figure 7.29 but for 15/02/2022.

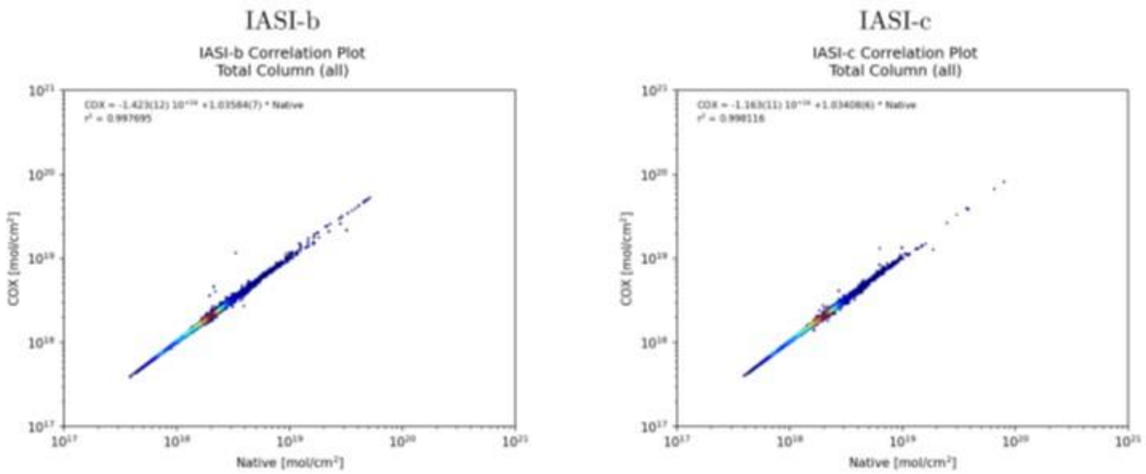

Figure 7.31. Same as Figure 7.29 but for 15/03/2022.

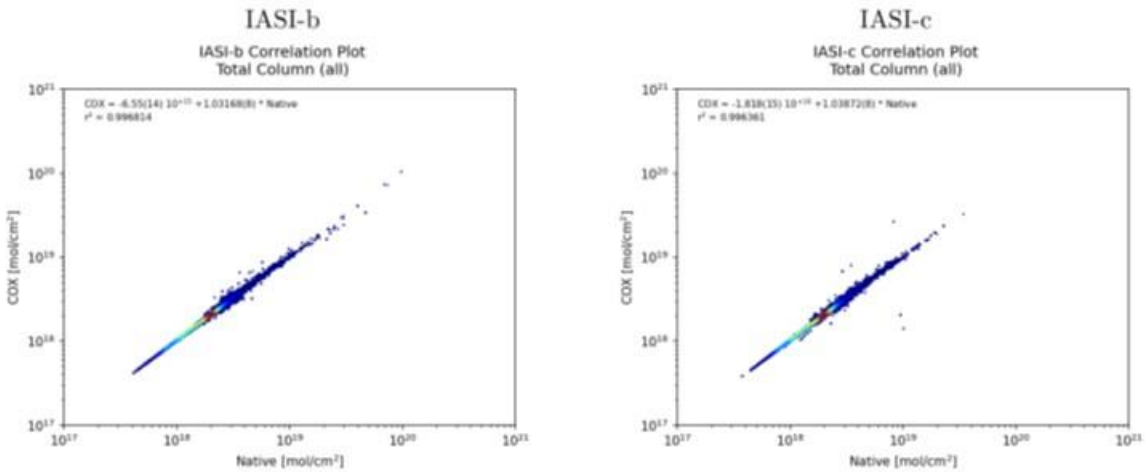

Figure 7.32. Same as Figure 7.29 but for 15/04/2021.

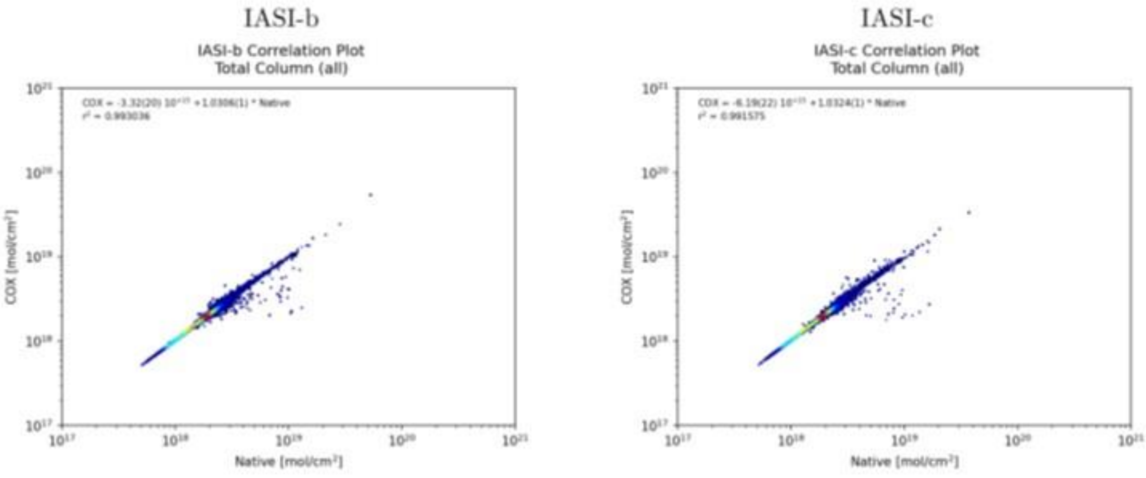

Figure 7.33. Same as Figure 7.29 but for 15/05/2022.

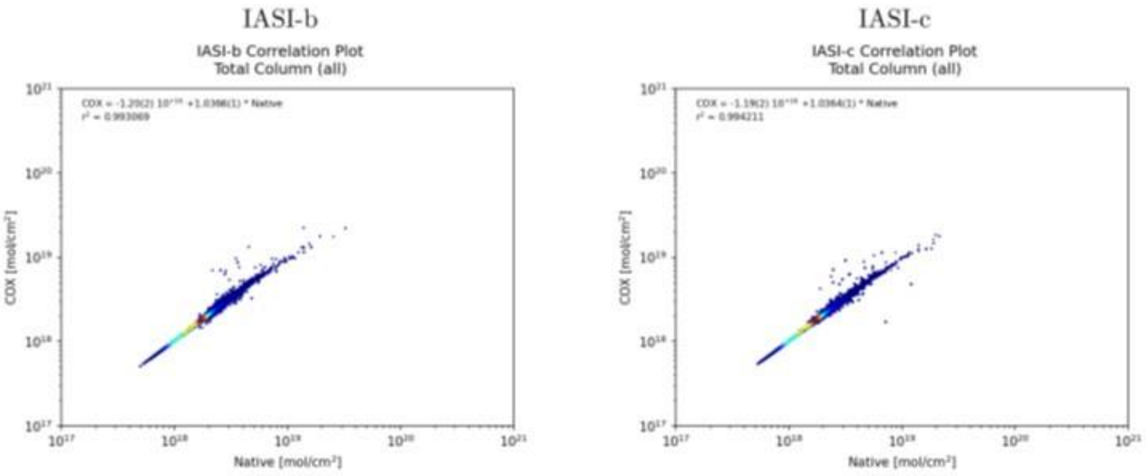

Figure 7.34. Same as Figure 7.29 but for 15/06/2022.

Note that a frequency distribution of the correlation coefficients (separated for each platform) will be provided when EUMETSAT will update the IASI CO retrieval algorithm at the EUMETSAT facilities. (In response to Action 3 (OR-9)).

IASI SO2:

The IASI BRESCIA SO2 retrieval algorithm has been implemented in the PPF v6.3 at EUMETSAT (operational release on 18/04/2018). Here we compare the EUMETSAT product disseminated by EUMETCast in BUFR format (SO2 EUMET) with the native product produced at ULB (SO2 ULB) for 6 days between January and April 2022, for Metop-B and Metop-C. We choose to study 20/01/2022, 21/01/2022, 22/01/2022, 22/02/2022, 16/03/2022 and 21/04/2022.

For each of the six days, scatterplots for the different estimated altitudes (7, 10, 13, 16 and 25 km) are presented (Figure 7.35 – Figure 7.40). The data have been filtered following the recommendations of the Product User Manual (Section 5.2.2, i.e. we kept the pixels in the neighbourhood (± 10 degrees) of SO2_BT_DIFFERENCE > 1K pixels, and did not use the pixels with a SO2_BT_DIFFERENCE < 0.4K.

We recall here that when the IASI L2 pressure and temperature profiles are not available, ECMWF forecasts (3h, interpolated in time and space) data are used in the EUMETSAT API. These pixels are flagged with SO2_QFLAG = 11, and are not part of the comparison.

Correlation coefficients (in blue) are ~1.

So far, the discrepancies are found within the numerical errors inherent to the use of different IT infrastructure.

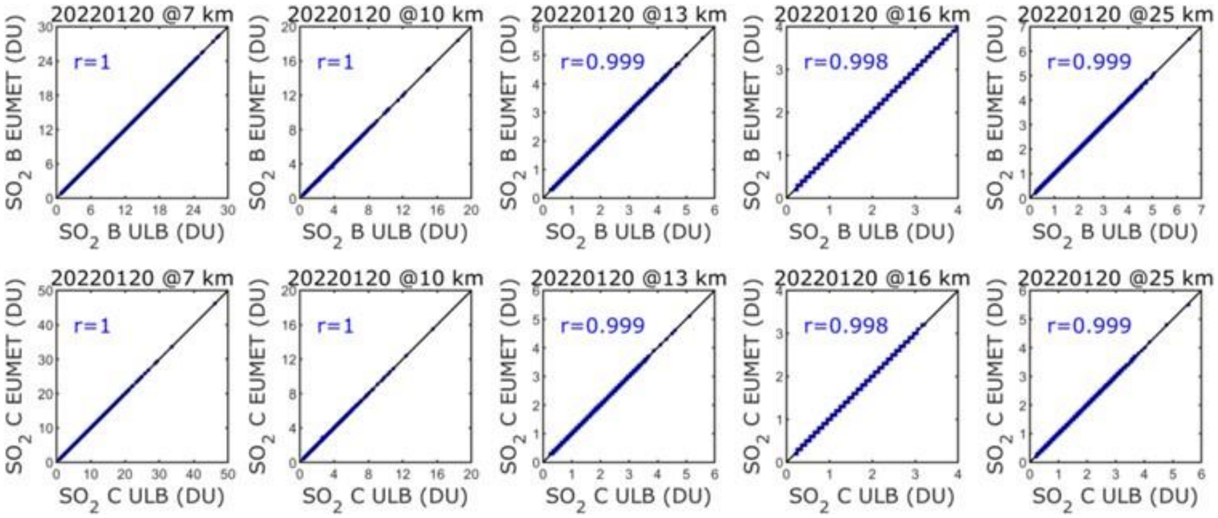

Figure 7.35. Scatterplots for Metop-B (top) and Metop-C (bottom): SO2 EUMET versus SO2 ULB for 20/01/2022, for the 5 estimated altitudes (7, 10, 13, 16 and 25 km).

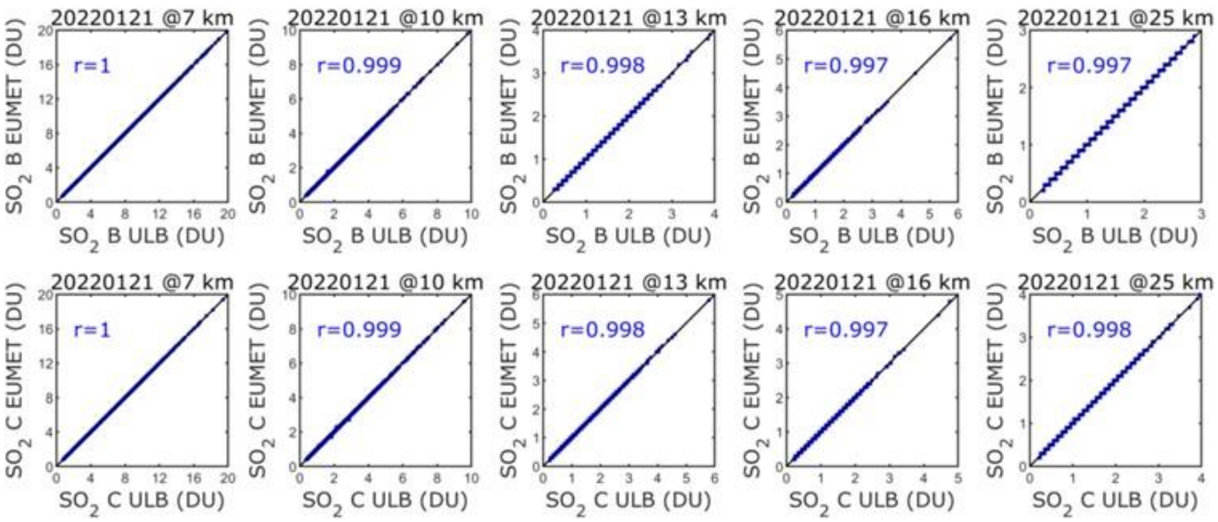

Figure 7.36. Same as Figure 7.35 but for 21/01/2022.

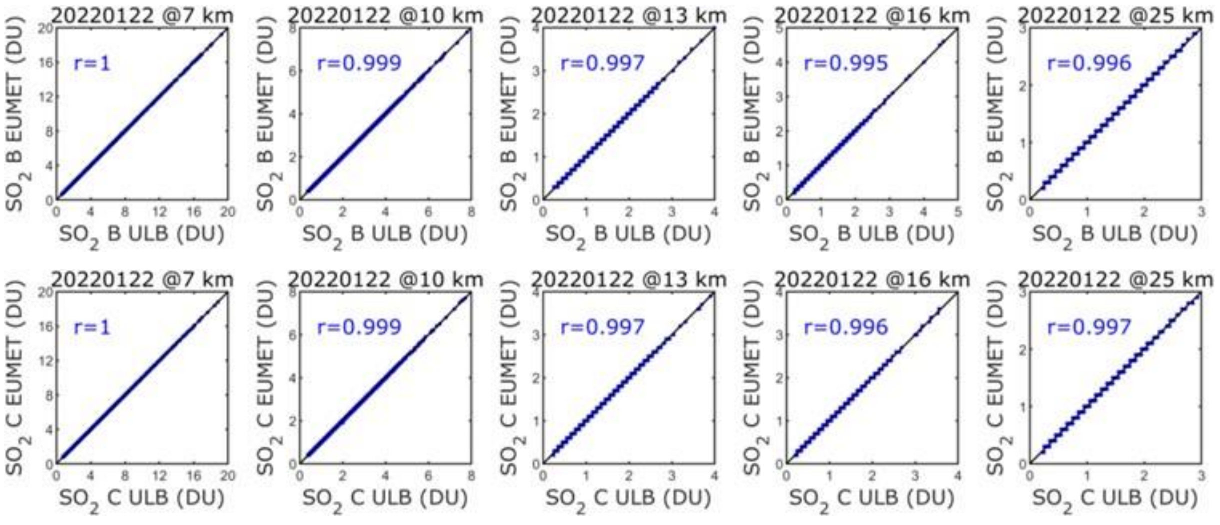

Figure 7.37. Same as Figure 7.35 but for 22/01/2022.

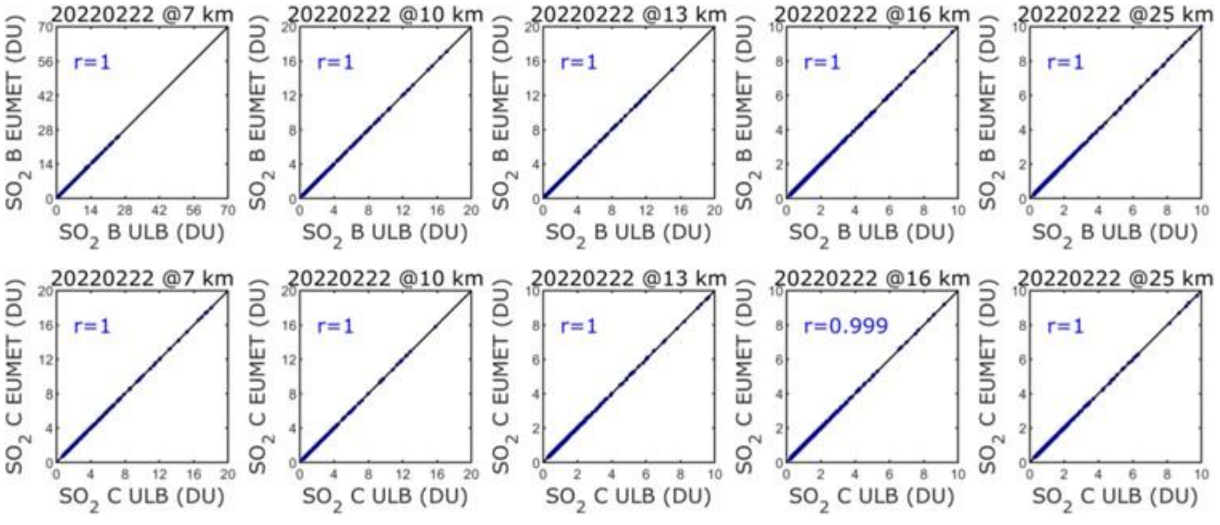

Figure 7.38. Same as Figure 7.35 but for 22/02/2022.

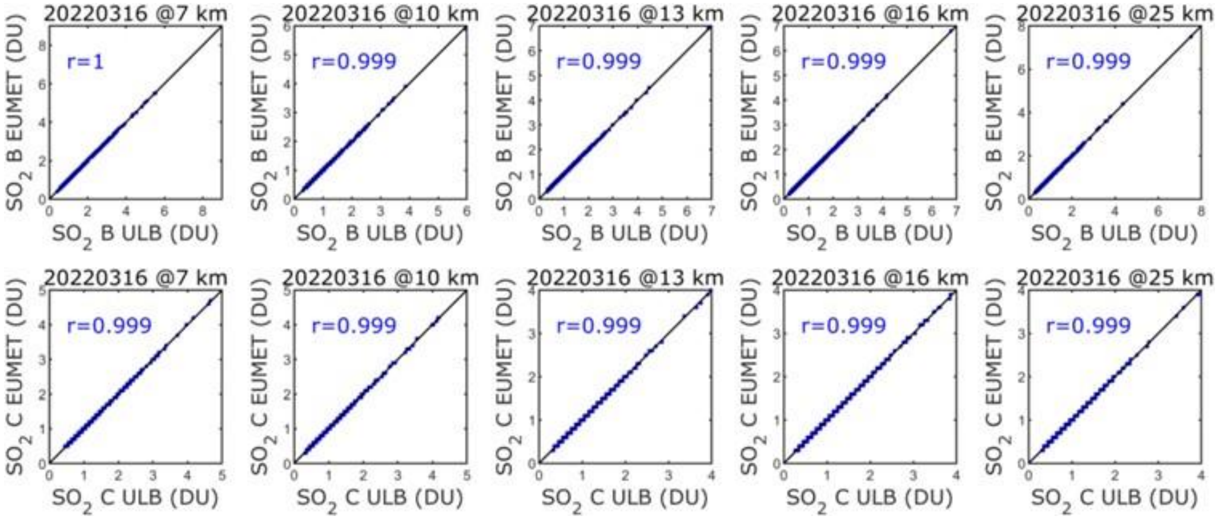

Figure 7.39. Same as Figure 7.35 but for 16/03/2022.

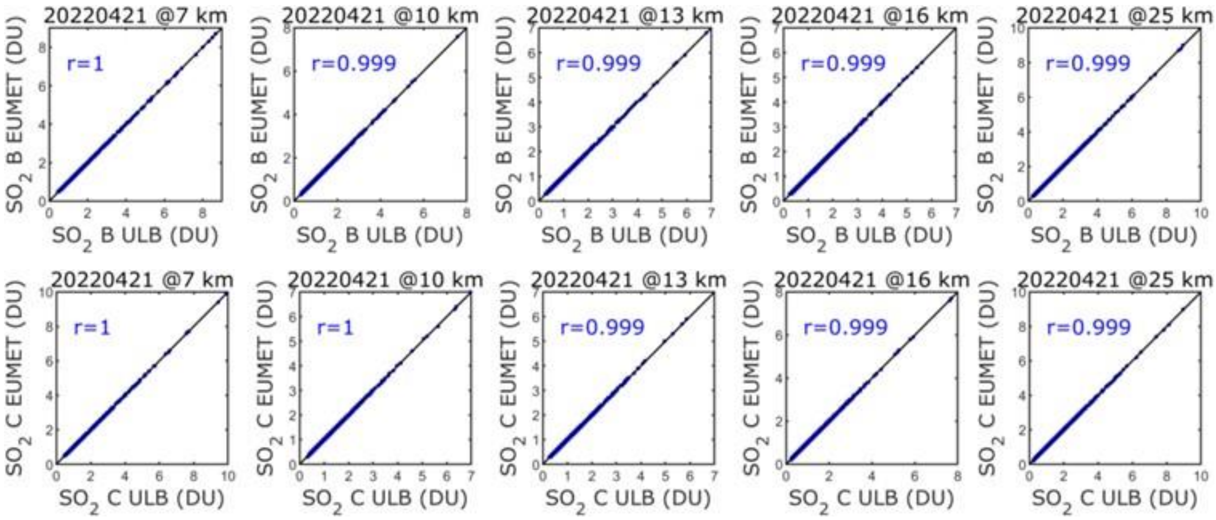

Figure 7.40. Same as Figure 7.35 but for 21/04/2022.

IASI O3:

The IASI NRT O3 product (v6.5) has been released as operational 18 May 2022. Here we present statistical results when comparing the EUMETSAT product disseminated by EUMETCast in BUFR format (OZO) with the native product produced at ULB (FORLI-O3 v20191122) for 6 days representative of 6 months: January 15th, February 15th, March 15th, April 15th, May 15th and June 15th, 2022, for Metop-B and Metop-C. This allows monitoring if any discrepancy occurs between the two, EUMETSAT and native, products. The data have been filtered following the recommendations of the Product User Manual. Furthermore, data associated with DOFS>2 have also been filtered out.

O3 total and 0 – 6 km column are investigated. Detailed statistics for total column between OZO data and FORLI-O3 data (v20191122) for each of the 6 days are presented in Table 7.23. No critical deviation was found for these dates.

Table 7.23. Statistics for total column between OZO data and FORLI-O3 data for 6 days: January 15th, February 15th, March 15th, April 15th, May 15th and June 15th, 2022.

15 January 2022	IASI-C		IASI-B	
	Native	BUFR	Native	BUFR
Individual Pixels	404985	102968	414329	102136
Common Pixels	90442 (22.33%)		89497 (21.60%)	
Correlation	0.9996		0.9996	
Mean Total Column Differences (DU)	2.1281±1.5966		2.1721±1.4845	
Mean Total Column Relative Differences (%)	0.7520±0.5346		0.7650±0.5034	

15 February 2022	IASI-C		IASI-B	
	Native	BUFR	Native	BUFR
Individual Pixels	406931	96651	406843	97625
Common Pixels	85618 (21.04%)		86538 (21.27%)	
Correlation	0.9995		0.9995	
Mean Total Column Differences (DU)	2.0885±1.7356		2.0833±1.7456	
Mean Total Column Relative Differences (%)	0.7454±0.5765		0.7410±0.5749	

15 March 2022	IASI-C		IASI-B	
	Native	BUFR	Native	BUFR
Individual Pixels	384028	97922	392492	97614
Common Pixels	85610 (22.29%)		85700 (21.83%)	
Correlation	0.9995		0.9995	
Mean Total Column Differences (DU)	2.1119±2.2025		2.1664±2.1288	
Mean Total Column Relative Differences (%)	0.7595±0.6376%		0.7745±0.6130	

15 April 2022	IASI-C		IASI-B	
	Native	BUFR	Native	BUFR
Individual Pixels	363519	90418	366375	90541
Common Pixels	80472 (22.14%)		80358 (21.93%)	
Correlation	0.9997		0.9998	
Mean Total Column Differences (DU)	2.1845±1.7532		0.7703±0.5411	
Mean Total Column Relative Differences (%)	0.7703±0.5411		0.7724±0.5164	

15 May 2022	IASI-C		IASI-B	
	Native	BUFR	Native	BUFR
Individual Pixels	392221	98781	386797	96993
Common Pixels	87569 (22.33%)		85766 (22.17%)	
Correlation	0.9997		0.9997	
Mean Total Column Differences (DU)	2.2382±1.3189		2.2026±1.3124	
Mean Total Column Relative Differences (%)	0.7517±0.4482		0.7403±0.4465	

15 June 2022	IASI-C		IASI-B	
	Native	BUFR	Native	BUFR
Individual Pixels	395795	100878	400483	100865
Common Pixels	88239 (22.29%)		88150 (22.01%)	
Correlation	0.9995		0.9995	
Mean Total Column Differences (DU)	2.0732±1.4234		2.0702±1.3933	
Mean Total Column Relative Differences (%)	0.7132±0.4889%		0.7121±0.4786	

Figure 7.41 and Figure 7.42 show the correlation plots for total and 0 – 6 km columns, respectively, between OZO data and FORLI-O3 for each platform. Correlation coefficients (in blue) are ~1.

So far, the discrepancies are found within the numerical errors inherent to the use of different IT infrastructure.

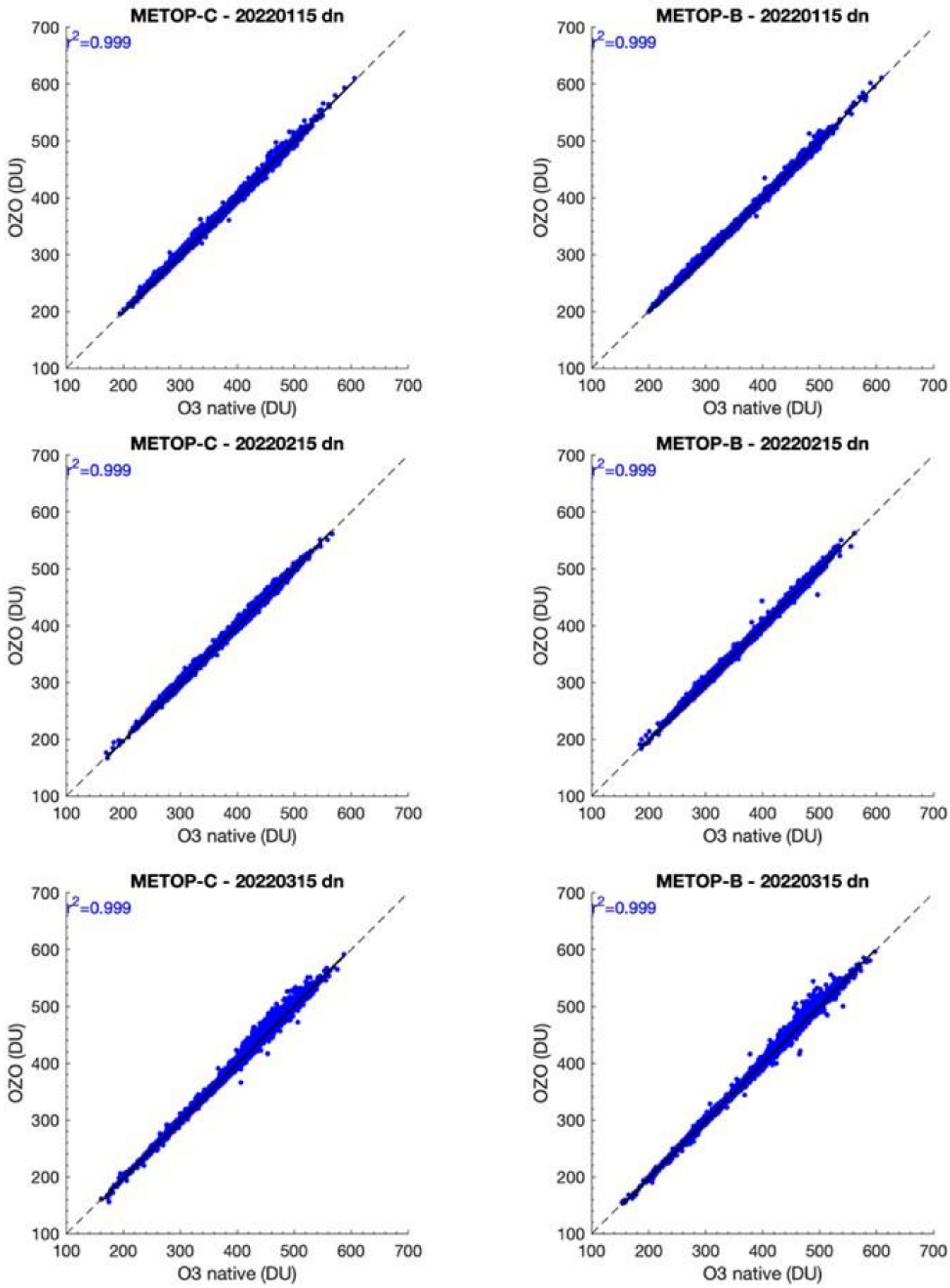
METOP-C - 20220115 dn
r^2=0.999
OZO (DU)
O3 native (DU)
METOP-B - 20220115 dn
r^2=0.999
OZO (DU)
O3 native (DU)
METOP-C - 20220215 dn
r^2=0.999
OZO (DU)
O3 native (DU)
METOP-B - 20220215 dn
r^2=0.999
OZO (DU)
O3 native (DU)
METOP-C - 20220315 dn
r^2=0.999
OZO (DU)
O3 native (DU)
METOP-B - 20220315 dn
r^2=0.999
OZO (DU)
O3 native (DU)

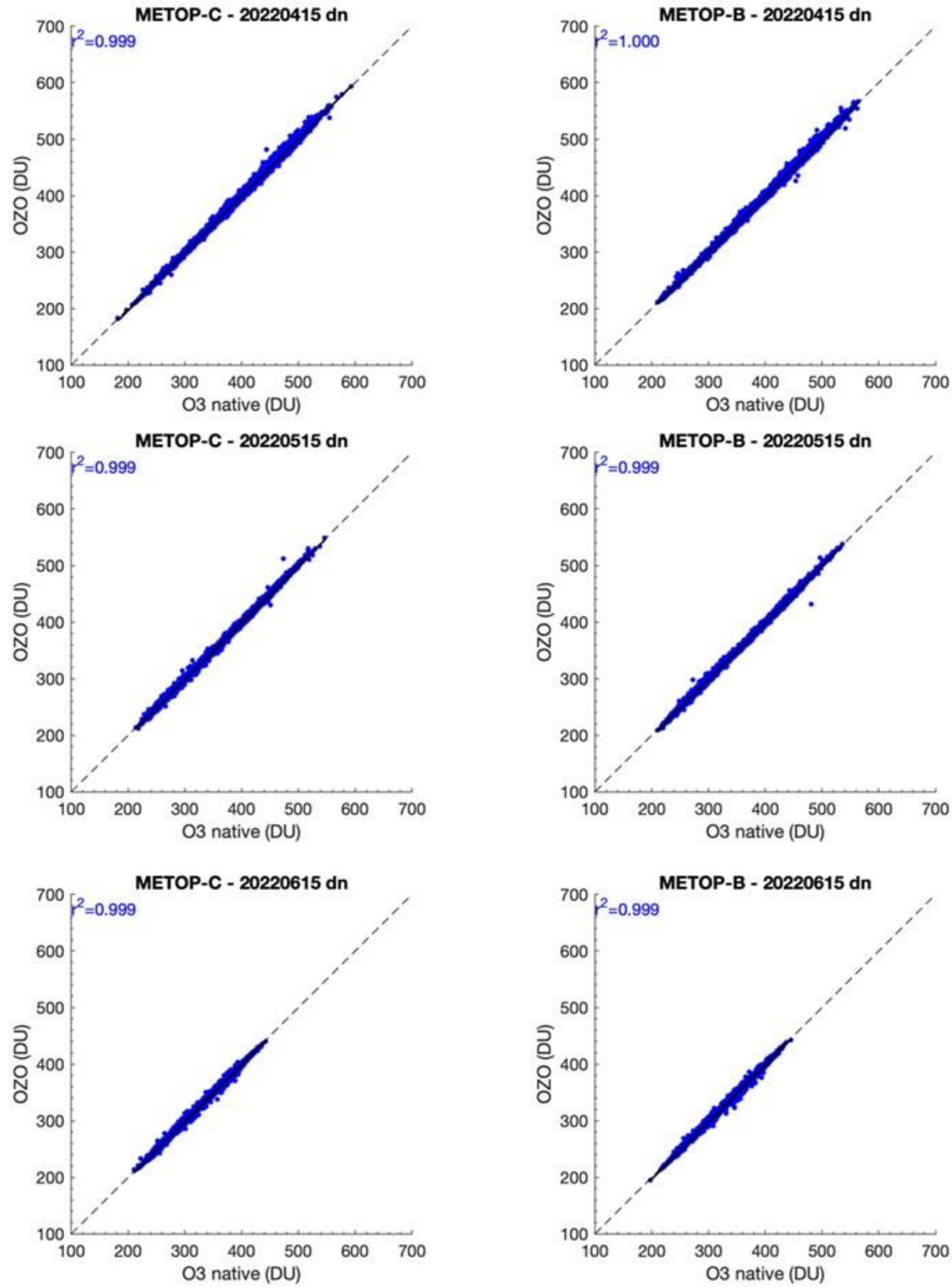

Figure 7.41. Correlation plots for total column between OZO and FORLI-O3 data for each platform for 6 days: January 15th, February 15th, March 15th, April 15th, May 15th and June 15th, 2022. X-axis corresponds to Native data (DU) and Y-axis corresponds to OZO data (DU).

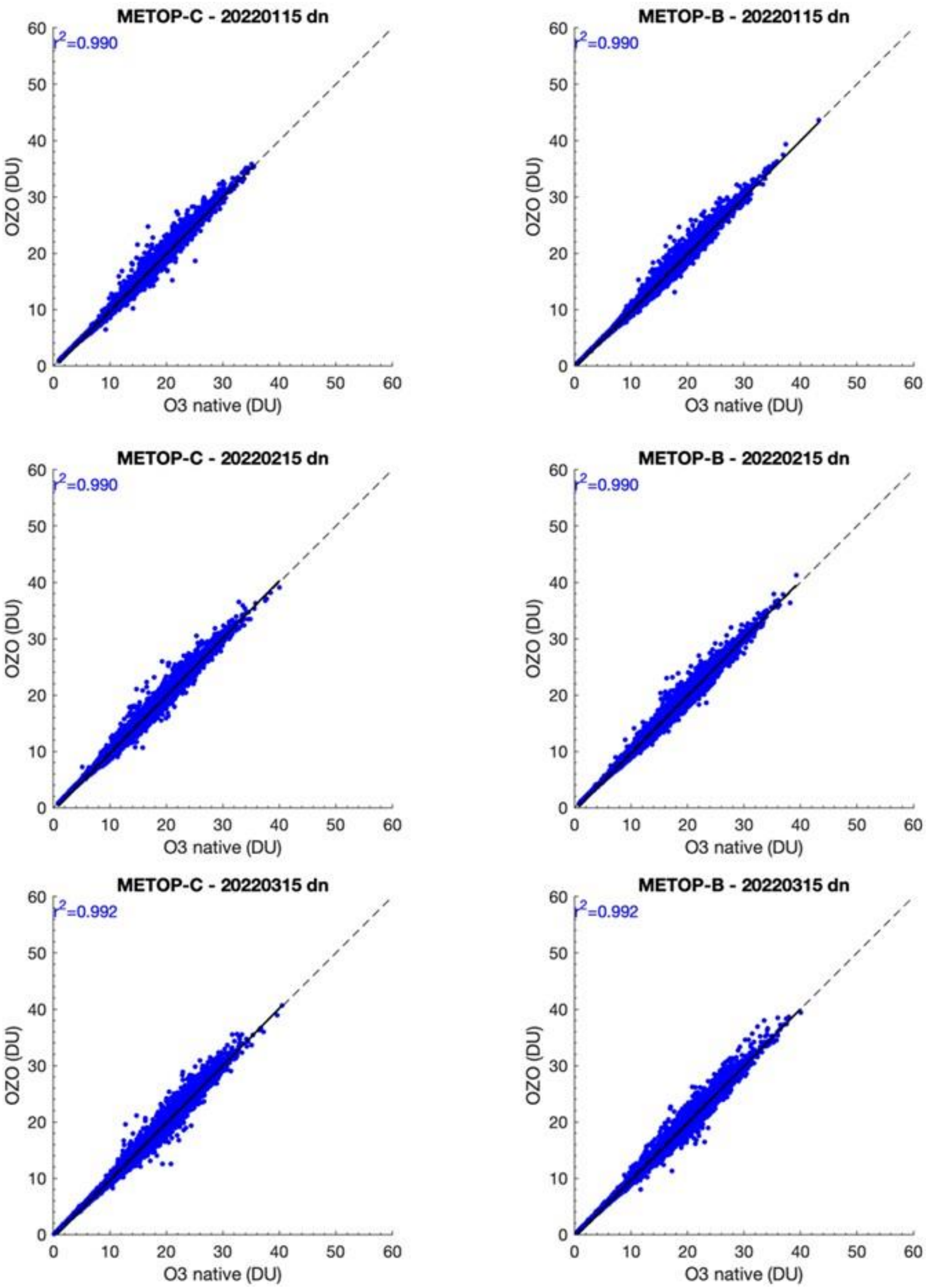
METOP-C - 20220115 dn
r^2=0.990
METOP-B - 20220115 dn
r^2=0.990
METOP-C - 20220215 dn
r^2=0.990
METOP-B - 20220215 dn
r^2=0.990
METOP-C - 20220315 dn
r^2=0.992
METOP-B - 20220315 dn
r^2=0.992
OZO (DU)
O3 native (DU)

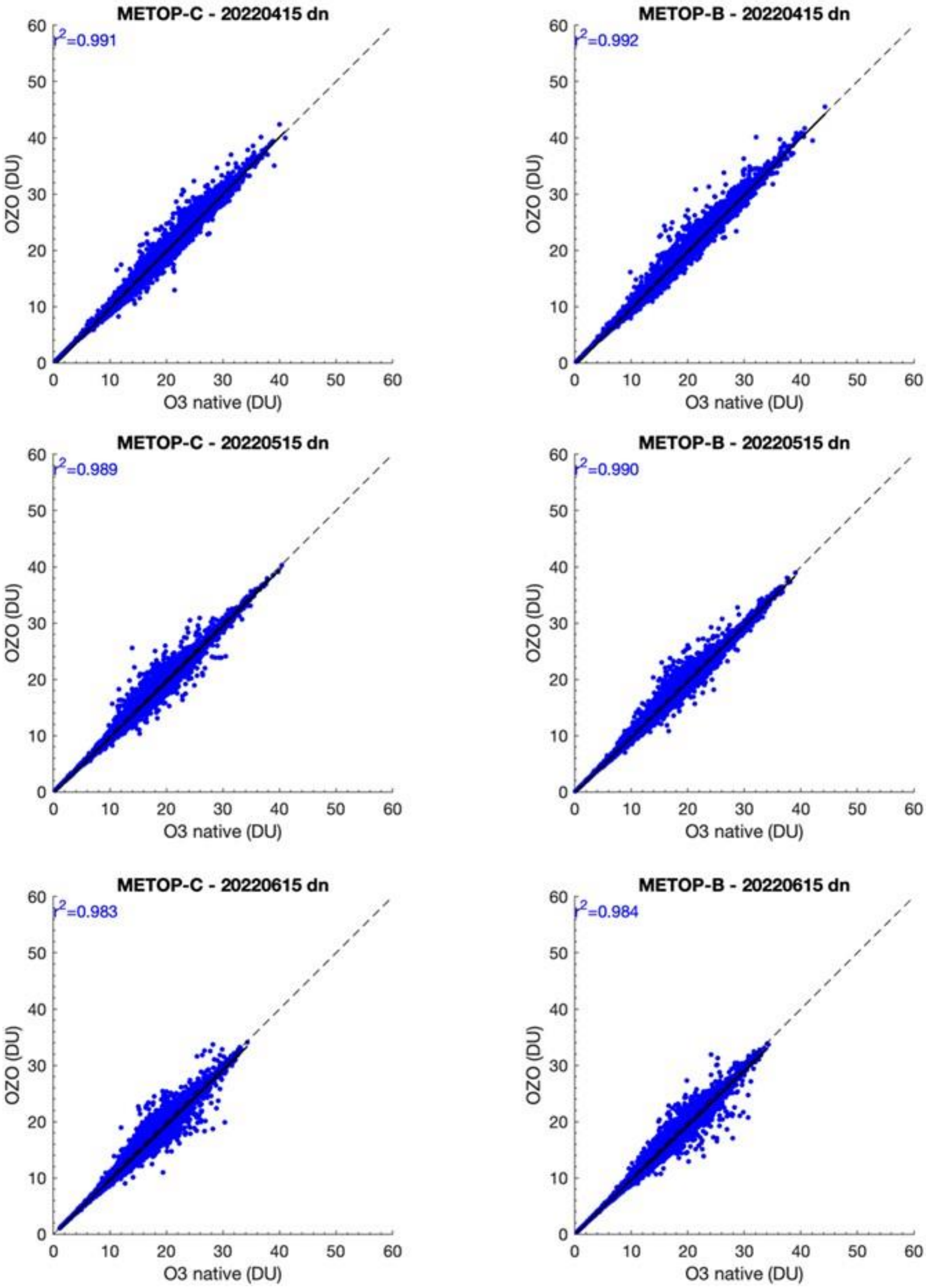

Figure 7.42. Correlation plots for 0-6km column between OZO and FORLI-O3 data for each platform for 6 days: January 15th, February 15th, March 15th, April 15th, May 15th and June 15th, 2022. X-axis corresponds to Native data (DU) and Y-axis corresponds to OZO data (DU).

IASI HNO3:

The IASI NRT HNO3 product (v6.5) has been released as operational 18 May 2022. Here we present statistical results when comparing the EUMETSAT product disseminated by EUMETCast in BUFR format (NAC) with the native product produced at ULB (FORLI-HNO3 v20191122) for 6 days representative of 6 months: January 15th, February 15th, March 15th, April 15th, May 15th and June 15th, 2022, for Metop-B and Metop-C. This allows monitoring if any discrepancy occurs between the two, EUMETSAT and native, products. The data have been filtered following the recommendations of the Product User Manual.

HNO3 total column is investigated. Detailed statistics for total column between NAC data and FORLI-HNO3 data (v20191122) for each of the six days are presented in Table 7.24. No critical deviation was found for these dates.

Table 7.24. Statistics for total column between NAC data and FORLI-HNO3 data for 6 days: January 15th, February 15th, March 15th, April 15th, May 15th and June 15th, 2022.

15 January 2022	IASI-C		IASI-B	
	Native	BUFR	Native	BUFR
Individual Pixels	281704	62831	283075	62678
Common Pixels	55956 (19.86%)		55628 (19.65%)	
Correlation	0.9998		0.9998	
Mean Total Column Differences (DU)	0.0074±0.0166		0.0073±0.0163	
Mean Total Column Relative Differences (%)	0.8761±1.3474		0.8733±1.3528	

15 February 2022	IASI-C		IASI-B	
	Native	BUFR	Native	BUFR
Individual Pixels	342683	63595	338558	62168
Common Pixels	57319 (16.73%)		56043 (16.55%)	
Correlation	0.9999		0.9998	
Mean Total Column Differences (DU)	0.0071±0.0158		0.0068±0.0172	
Mean Total Column Relative Differences (%)	0.8802±1.3130		0.8684±1.3817	

15 March 2022	IASI-C		IASI-B	
	Native	BUFR	Native	BUFR
Individual Pixels	304169	65993	304169	65993
Common Pixels	58561 (19.25%)		58279 (18.96%)	
Correlation	0.9998		0.9997	
Mean Total Column Differences (DU)	0.0076±0.0159		0.0076±0.0227	
Mean Total Column Relative Differences (%)	0.8944±1.3741		0.8953±1.4046	

15 April 2022	IASI-C		IASI-B	
	Native	BUFR	Native	BUFR
Individual Pixels	340964	69792	345351	70075
Common Pixels	62756 (18.41%)		62932 (18.22%)	
Correlation	0.9998		0.9997	
Mean Total Column Differences (DU)	0.0065±0.0188		0.0063±0.0204	
Mean Total Column Relative Differences (%)	0.7240±1.3502		0.7136±1.3158	

15 May 2022	IASI-C		IASI-B	
	Native	BUFR	Native	BUFR
Individual Pixels	332624	72825	326014	72879
Common Pixels	65703 (19.75%)		65842 (20.20%)	
Correlation	0.9946		0.9997	
Mean Total Column Differences (DU)	0.0071±0.0822		0.0071±0.0189	
Mean Total Column Relative Differences (%)	0.6749±1.3176		0.6740±1.2298	

15 June 2022	IASI-C		IASI-B	
	Native	BUFR	Native	BUFR
Individual Pixels	311569	74425	311173	74214
Common Pixels	67027 (21.51%)		66998 (21.53%)	
Correlation	0.9997		0.9997	
Mean Total Column Differences (DU)	0.0075±0.0193		0.0081±0.0183	
Mean Total Column Relative Differences (%)	0.6876±1.2632		0.7135±1.2308	

Figure 7.43 shows the correlation plots for total column, respectively, between NAC data and FORLI-HNO3 for each platform. Correlation coefficients (in blue) are ~1.

So far, the discrepancies are found within the numerical errors inherent to the use of different IT infrastructure.

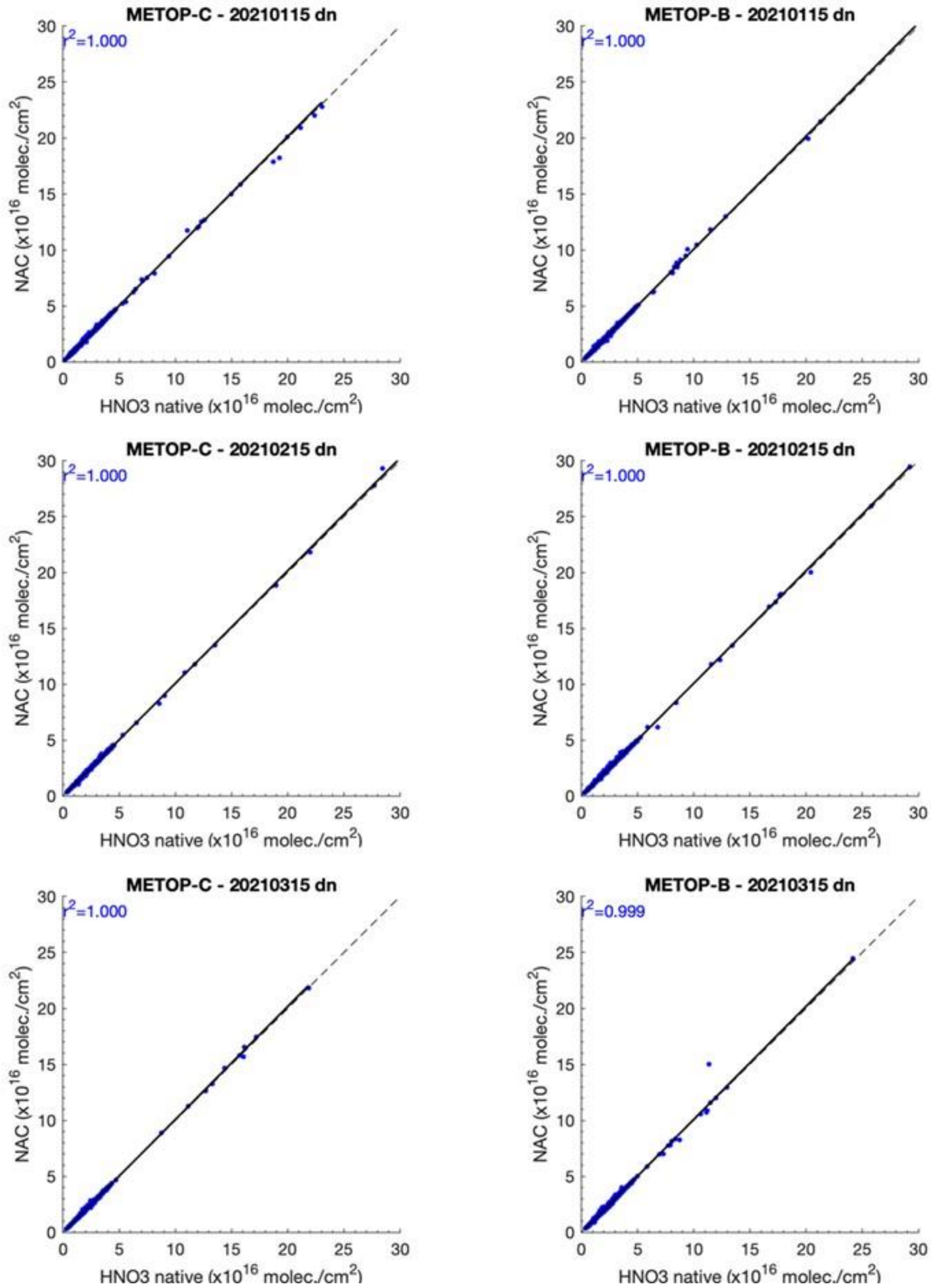
METOP-C - 20210115 dn
r2=1.000
METOP-B - 20210115 dn
r2=1.000
METOP-C - 20210215 dn
r2=1.000
METOP-B - 20210215 dn
r2=1.000
METOP-C - 20210315 dn
r2=1.000
METOP-B - 20210315 dn
r2=0.999
NAC (x10^16 molec./cm^2)
HNO3 native (x10^16 molec./cm^2)

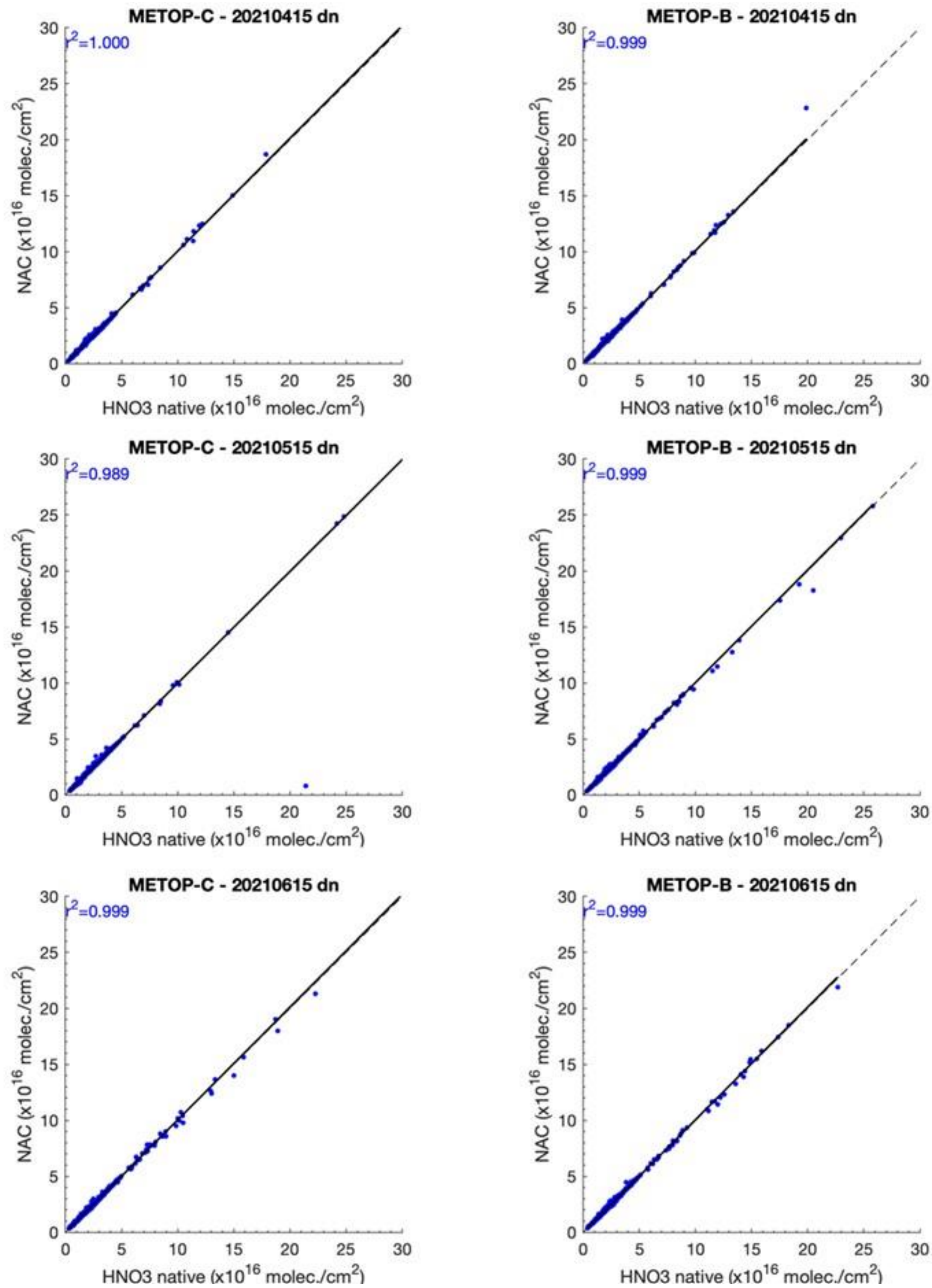

Figure 7.43. Correlation plots for total column between NAC and FORLI-HNO3 data for each platform for 6 days: January 15th, February 15th, March 15th, April 15th, May 15th and June 15th, 2022. X-axis corresponds to Native data (molec./cm^2) and Y-axis corresponds to NAC data (molec./cm^2).

Validation with CO FTIR ground-based data

This section presents the work of Bavo Langerock (BIRA-IASB) that compared the Metop-A/B/C IASI CO data against FTIR measurement data available from the NDACC (Network for the Detection of Atmospheric Composition Change). The Copernicus Atmosphere Monitoring Service

(CAMS) projects supports selected NDACC instruments and Pis for rapid delivery of quality measurements to the NDACC data host (contract CAMS27). Recent FTIR measurement data is now available for many more sites (in this study data from 22 sites is used).

These ground-based, remote-sensing instruments are sensitive to the CO abundance in the troposphere and lower stratosphere, i.e. between the surface and up to 20 km altitude. CO total columns are validated (from surface to 100 km). A description of the FTIR instruments and retrieval methodology can be found at https://nors.aeronomie.be. The typical uncertainty on the FTIR CO column is approximately 3%, which is also used in the color scale in Figure 7.45.

In this comparison each FTIR measurement is co-located to all IASI measurements within a time difference of 3 hours and within a distance of 50 km to the effective location of the FTIR measurement (this effective location is calculated along the line of sight of the FTIR measurement). The IASI *a priori* is substituted in the FTIR retrieval and subsequently the FTIR retrieved profile with the IASI *a priori* is smoothed using the IASI averaging kernel, as described in Rodgers *et al.*, 2003. In the plots the relative differences are calculated using the latter FTIR columns (smoothed with the IASI averaging kernels). This validation methodology is described in more detail in Ronsmans *et al.*, 2016. All figures for the individual stations can be browsed on https://cdop.aeronomie.be.

Table 7.25. Statistics between IASI-B/C and FTIR CO smoothed total columns for the entire time period January 2017 – May 2022 (the column "std" is the standard deviation of the local FTIR columns relative to the standard deviation of the IASI columns)

	Metop-B					Metop-C				
	# meas.	Std.	R	rel. Diff.	Std. Rel. Diff.	# meas.	Std.	R	rel. Diff.	Std. Rel. Diff.
Eureka	928	0.7	0.87	18.23	16.31					
Ny Ålesund	112	1.2	0.92	20.48	8.91	60	1.1	0.92	21.49	9.1
Thule	5283	0.8	0.84	5.49	11.11	2423	0.8	0.82	7.91	11.08
Kiruna	1004	1	0.82	-3.22	7.27	549	1	0.82	-2.9	7.07
Harestua	217	1.1	0.84	8.47	7					
St. Petersburg	926	0.8	0.88	7.36	6.46	265	0.9	0.81	8.83	6.3
Bremen	412	0.9	0.87	8.06	7.17	151	0.9	0.81	7.58	7.65
Garmisch	3028	0.9	0.86	2.35	7.44	1386	0.9	0.89	2.23	6.87
Zugspitze	2963	0.9	0.91	-1.45	6.16	1237	0.9	0.92	-1.57	5.78
Jungraujoch	874	0.9	0.95	0.01	4.61	552	0.9	0.95	-0.48	4.69
Toronto	1265	0.7	0.81	21.2	14.1	736	0.7	0.86	22.22	12.53
Rikubetsu	61	0.8	0.82	4.92	7.69	20	0.8	0.88	2.54	5.97
Boulder	3220	0.9	0.86	-1.75	8.38	2579	0.8	0.83	-1.34	10.71
Izana	977	1	0.94	-0.72	4.11	414	0.9	0.95	0.73	4.74
Mauna Loa	1425	1.1	0.98	-1.37	3.3	552	1.1	0.97	-2.59	3.84
Altzomoni	1127	1.1	0.95	4.35	4.37	536	1.1	0.96	3.87	4.51
Paramaribo	116	0.9	0.92	8.96	4.58	34	0.8	0.82	7.88	5.91
Porto Velho	278	0.9	0.98	9.82	6.63					
La Reunion Maido	2444	1	0.99	4.92	3.3	605	1	0.98	5.62	3.69
Wollongong	1822	0.8	0.94	6.93	7.8	917	0.8	0.93	6.54	8.28
Lauder	2645	0.9	0.96	9.31	5.69	1591	0.9	0.96	8.72	5.56
Arrival Heights	411	0.9	0.95	16.52	7.23	285	0.9	0.93	15.4	7.55

Average for all sites		0.9	0.9	6.77	7.26		0.87	0.85	6.25	7.63

The correlation coefficients of the Taylor diagrams (Figure 7.44 and Table 7.25) are generally ranging from ~0.8 to nearly 1, showing a very good agreement between the IASI and FTIR data, for Metop-B and Metop-C. However, some sites are special:

1. Rikubetsu, Ny Ålesund, Kiruna and Harestua have only few co-located measurements and are statistically less relevant
2. Toronto has a low correlation although the site has many co-locations. This may be due to some co-locations where the IASI concentration is much higher than observed by the FTIR and probably related to false co-locations during fire events. The FTIR time-series seems to suffer from outliers being too low.
3. At Kiruna, Thule and Eureka the satellite underestimates the CO columns by up to 30 % during the early spring weeks and is related to a reduced sensitivity of the IASI CO product during local spring.

The Taylor diagrams in Figure 7.44 and statistics in Table 7.25 also show that the standard deviations of the FTIR columns values are smaller compared the satellite standard deviation probably due to higher noise on the satellite time-series. Almost all site points are shifted left of the satellite reference, typically with a factor of 0.8 to 1 of the standard deviation of the satellite CO columns.

Figure 7.45 shows the time-series of bi-weekly mean relative differences for the time period January 2017 – May 2022. Red indicates a positive bias (IASI > NDACC) while blue indicates an underestimation of the satellite retrievals. The chosen color scale is based on the FTIR typical uncertainty. The IASI retrieval uncertainty should be added (typically around 4%), so only biases above 5% are to be considered significant. In the Northern Hemisphere a seasonal changing bias is observed: overestimation during summer and underestimation during winter months. A similar seasonal dependence but less pronounced is observed in the Southern Hemisphere. A longer time period is required to study this seasonal dependence in more detail.

We can conclude that for most of the 22 stations included in the comparison, mean relative differences, or biases, are less than 10 % (see the individual station plots at https://cdop.aeronomie.be/ under Validation Results). For the Eureka, Ny Ålesund and Arrival Heights stations, located at high latitudes, biases are larger. A similar bias is found by Buchholz *et al.* (2017) when comparing with MOPITT data. When looking at the stations between -60° and 60°, the Toronto station shows the largest biases (mean bias ±20 %) which seems to be due to outliers.

The IASI data are generally overestimating with the overall bias of approx 6.5 % being off the same order as the reported combined total uncertainty of 5 % (Table 7.25).

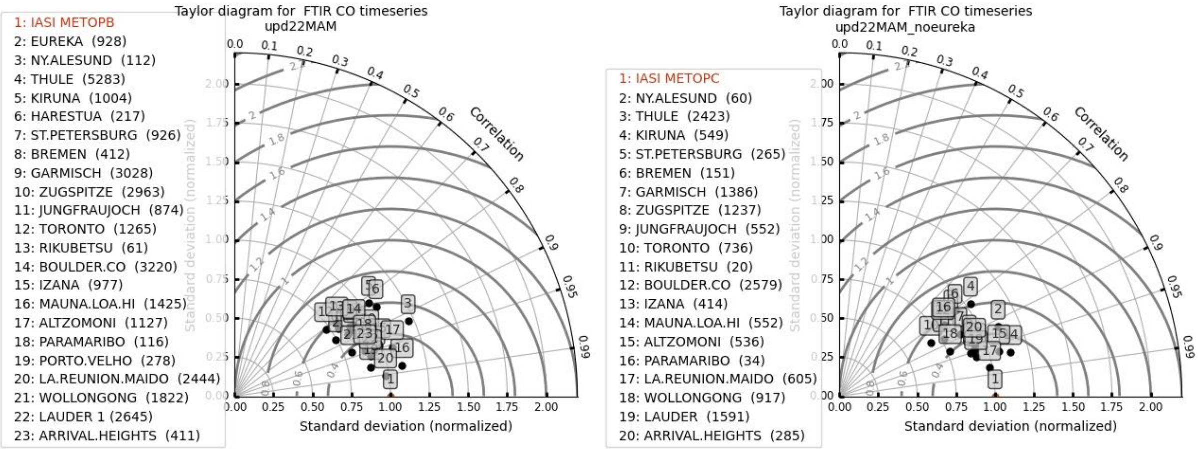

Figure 7.44. Correlation plots for IASI-B (left) and IASI-C (right) CO total columns against 22 NDACC FTIR sites. The stations are slightly shifted to the left, indicating that the satellite time-series has a higher standard deviation (more noisy).

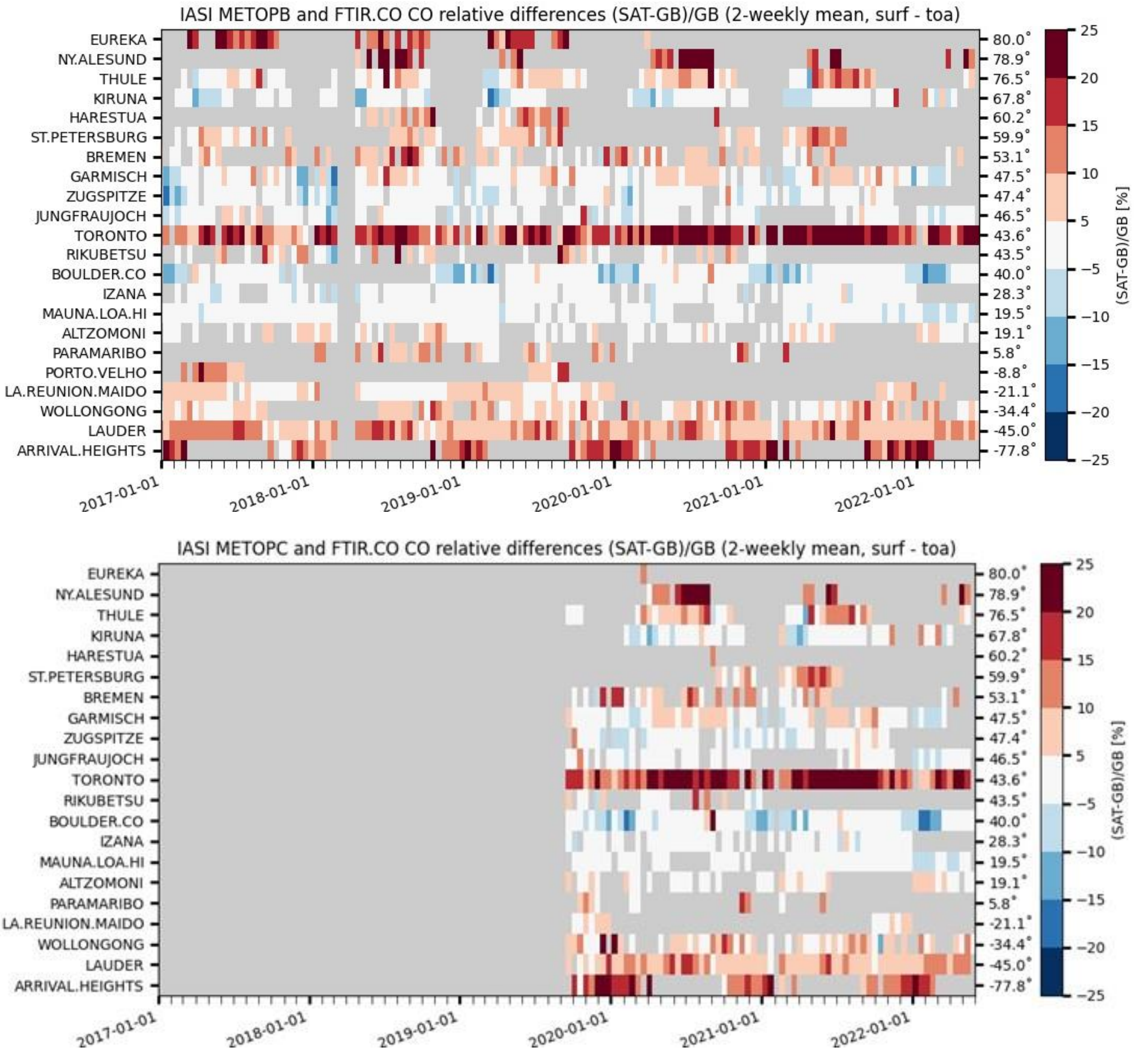

Figure 7.45. Time-series of bi-weekly relative difference for IASI-B (top) and IASI-C (bottom). Not all stations have co-locations with the Metop-C satellite. The Metop-C relative bias time-series seems to correspond closely to the Metop-B time-series.

Acknowledgements: The data used in this publication were obtained as part of the Network for the Detection of Atmospheric Composition Change (NDACC) and are publicly available. Rapid delivery of NDACC data is partly supported by the CAMS-27 data procurement service contracted by ECMWF for the validation of the Copernicus Atmospheric Monitoring Service (CAMS).

References:

Buchholz, R. R., Deeter, M. N., Worden, H. M., Gille, J., Edwards, D. P., Hannigan, J. W., Jones, N. B., Paton-Walsh, C., Griffith, D. W. T., Smale, D., Robinson, J., Strong, K., Conway, S., Sussmann, R., Hase, F., Blumenstock, T., Mahieu, E., and Langerock, B.: Validation of MOPITT carbon monoxide using ground-based Fourier transform infrared spectrometer data from NDACC, Atmos. Meas. Tech., 10, 1927-1956, 2017. https://doi.org/10.5194/amt-10-1927-2017

Ronsmans, G., Langerock, B., Wespes, C., Hannigan, J. W., Hase, F., Kerzenmacher, T., Mahieu, E., Schneider, M., Smale, D., Hurtmans, D., De Mazière, M., Clerbaux, C., and Coheur, P.-F.: First

characterization and validation of FORLI-HNO_3 vertical profiles retrieved from IASI/Metop, Atmos. Meas. Tech., 9, 4783-4801,2016.
https://doi.org/10.5194/amt-9-4783-2016

8. List of AC SAF users

The institutes of registered users of AC SAF products are listed below.

8.1. FMI archive

Europe:

Armenia:
- ICHD

Austria:
- Central Institute for Meteorology and Geodynamics
- Private individual
- Sistema GmbH
- University of Veterinary Medicine
- University of Vienna (2 users)

Belarus:
- National Academy of Sciences
- State University

Belgium:
- BIRA-IASB
- Ghent University (10 users)
- Karel de Grote University College
- KMI (3 users)
- KU Leuven
- ULB (3 users)

Bulgaria:
- Bulgarian Academy of Science
- Space Research and Technology Institute (2 users)

Croatia:
- J. J. Strossmayer University of Osijek

Czech Republic:
- Czech Hydrometeorological Institute (4 users)
- Global Change Research Institute

Denmark:
- Aarhus University (2 users)
- DMI (2 users)

Estonia:
- Estonian Environment Agency
- Intertrust

Finland:
- FMI (10 users)
- Häme University of Applied Sciences
- University of Helsinki (3 users)

France:
- AERIS/ICARE
- Aix-Marseille University
- CNRS (3 users)
- Grenoble Alpes University
- Laboratory of Atmospheric Optics
- Lasem
- LATMOS
- LISA (2 users)
- LISA-CNRS
- LPC2E-CNRS
- LSCE-IPSL-CNRS
- Météo France (5 users)
- Mines Paristech
- Open University
- Private Individual
- Reuniwatt
- Sistema
- University of La Reunion
- University of Lille
- University of Paris Est Creteil

Germany:
- ask – Innovative Visualisierungslösungen GmbH
- Datiaperti
- DLR (2 users)
- DWD (4 users)
- EUMETSAT (19 users)
- Federal Office for Radiation Protection
- Forschungszentrum Jülich GmbH (4 users)
- Fraunhofer Institute
- Gymnasium Olching
- Oldenburg University
- Private individual
- Max Planck Institute for Chemistry (6 users)
- Sabrina Szeto Consulting
- Technical University of Munich
- University of Bremen (4 users)
- University of Cologne
- University of Konstanz
- University of Münster
- University of Potsdam
- University of Rostock

Greece:
- AUTH (4 users)
- Hellenic Centre for Marine Research

- National Technical University of Athens (2 users)
- Private Individual
- University of Athens
- University of the Aegean
- University of Crete (2 users)

Hungary:
- Eötvös Loránd University (2 users)
- Hungarian Academy of Sciences
- Hungarian Meteorological Service (2 users)
- Individual
- University of Szeged

Ireland:
- National University of Ireland Galway
- Trinity College Dublin

Italy:
- ARPA Valle d'Aosta
- B-Open Solutions S.r.l. (2 users)
- CNR-ISAC
- European Space Agency
- fabbricadigitale
- IFAC-CNR (2 users)
- Julia Wagemann Consulting
- LaMMA Consortium (2 users)
- MEEO
- National Institute for Astrophysics
- Parthenope University of Naples
- Private Individual
- Regional Environmental Protection Agency Calabria
- University of Bologna (2 users)
- University of Florence
- University of Milan
- University of Modena and Reggio Emilia
- University of Venice

Lithuania:
- Lithuanian National Meteorological Service
- Vilnius University (3 users)

Malta:
- University of Malta

Moldova:
- Academy of Sciences

The Netherlands:
- BESSR
- ESA

- KNMI (5 users)
- S[&]T Corporation
- Wageningen University & Research (2 users)

Norway:
- Norwegian Institute for Air Research (2 users)
- UiT The Arctic University of Norway

Poland:
- CloudFerro
- Institute of Environmental Protection (2 users)
- Institute of Geodesy and Cartography
- Military University of Technology
- University of Warsaw

Portugal:
- Instituto Dom Luiz
- Instituto Português do Mar e da Atmosfera (4 users)
- University of Aveiro
- University of Lisbon
- University of Trás-os-Montes and Alto Douro (2 users)

Republic of North Macedonia:
- Hydrometeorological Service

Romania:
- Babes-Bolyai University (3 users)
- Global Top Systems
- INCAS
- INOE (3 users)
- National Meteorological Administration (3 users)
- University of Galați (3 users)
- Politehnica University of Bucharest

Russia:
- Altai State University
- Daghestan Scientific Centre of Russian Academy of Sciences
- Federal Research Center Krasnoyarsk Scientific Center of the Siberian Branch of the RAS (2 users)
- Fedorov Institute of Applied Geophysics
- Institute of Atmospheric Physics
- Institute of Computational Modeling of the Siberian Branch of the RAS
- Institute of Global Climate and Ecology
- Irkutsk State Transport University
- Moscow State University
- Planeta (2 users)
- Research Center of Ecological Safety
- Roscosmos
- St. Petersburg State University
- Tomsk State University of Control Systems and Radioelectronics

Serbia:
- Geographical institute “Jovan Cvijic”, SASA

Slovakia:
- Private Individual

Slovenia:
- Bide-san, s.p.

Spain:
- Autonomous University of Barcelona
- Barcelona Supercomputing Center
- Basque Meteorology Agency
- CREAF-CSIC-UAB
- GREA
- I.E.S. Punta del Verde
- Modeliza
- Pablo de Olavide University
- Polytechnic University of Catalonia (2 users)
- State Meteorological Agency
- University of Alicante
- University of Barcelona (2 users)
- University of Extremadura
- University of Granada
- University of Málaga
- University of Valencia (3 users)
- University of Valladolid (2 users)

Sweden:
- NBI/Handelsakademin
- SMHI (5 users)
- The Swedish Defence Research Agency

Switzerland:
- Swiss Federal Laboratories for Materials & Technology

Turkey:
- Hacettepe University
- Istanbul University
- Middle East Technical University
- Turkish State Meteorological Service (2 users)

Ukraine:
- Scientific Centre for Aerospace Research of the Earth
- Taras Shevchenko National University of Kyiv
- UHMC
- Ukrainian Hydrometeorological Institute (2 users)

United Kingdom:
- Airbus S.A.S.
- ECMWF (2 users)

- ESA
- IDEMS International
- London School of Hygiene and Tropical Medicine
- Office of National Statistics
- Private individual
- Rutherford Appleton Lab
- Satavia Ltd. (2 users)
- Satellite Applications Catapult
- Science and Technology Facilities Council (2 users)
- siHealth Ltd.
- University College London
- University of Birmingham
- University of Edinburgh
- University of Leeds (3 users)
- University of Leicester
- University of Oxford
- University of York

Asia:

Bangladesh:
- Institute of Forestry and Environmental Sciences
- Stamford University
- University of Dhaka

China:
- Anhui Institute of Optics and Fine Mechanics
- Anhui Institute of Meteorological Sciences
- Beijing Municipal Environmental Monitoring Center
- Beijing Normal University (2 users)
- China Academy of Sciences (6 users)
- China Meteorological Administration (2 users)
- China University of Mining and Technology (6 users)
- Chinese Academy of Meteorological Sciences (2 users)
- Fudan University
- HTHJ
- Institute of Atmospheric Physics (2 users)
- Institute of Earthquake Forecasting
- Institute of Remote Sensing and Digital Earth (3 users)
- Jiangsu Meteorological Observatory
- Jiangsu Normal University (2 users)
- Lanzhou University (2 users)
- Lanzhou Jiaotong University
- Nanjing University
- Nanjing University of Information Science & Technology (6 users)
- National Satellite Meteorological Center
- National University of Defense Technology
- Northeast Normal University

- Peking University (3 users)
- School
- Shandong University
- Shanghai University
- Shenzhen University
- Southern University of Science and Technology
- State Environmental Protection Key Lab of Satellite Remote Sensing
- Sun Yat-Sen University
- The Chinese University of Hong Kong (2 users)
- The Institute of Atmospheric Physics (3 users)
- Tsinghua University (3 users)
- (unknown) (2 users)
- University of Science and Technology (2 users)
- Xiamen University
- Zhejiang University (2 users)

India:

- Anna University
- Aryabhatta Research Institute of Observational Sciences
- Banaras Hindu University
- Birla Institute of Technology
- Bose Institute
- Council of Scientific and Industrial Research
- CSIR-NIO
- CSIR-NPL
- Dibrugarh University
- “Education”
- IIT KGP
- Indian Institute of Remote Sensing
- Indian Institute of Science Education and Research
- Indian Institute of Technology Kharagpur (4 users)
- Indian Institute of Technology Roorkee (2 users)
- Indian Institute of Tropical Meteorology (3 users)
- Indian Space Research Organization (2 users)
- Jawaharlal Nehru Technological University, Kakinada
- Jawaharlal Nehru University
- Malaviya National Institute of Technology Jaipur
- Mangalore University
- MSRIT
- National Atmospheric Research Laboratory (3 users)
- National Centre for Medium Range Weather Forecasting
- National Remote Sensing Centre
- Savitribai Phule Pune University (2 users)
- School of Planning and Architecture, Bhobal
- SIG
- University of Calcutta
- University of Hyderabad

- University of Kalyani
- Vikram Sarabhai Space Centre (2 users)
- Vindhyan Ecology and Natural History Foundation

Indonesia:
- Meteorology, Climatology, and Geophysical Agency (2 users)
- National Institute for Aeronautics and Space
- Sumatera Institute of Technology

Japan:
- Chiba University
- Japan Meteorological Agency
- Kyushu University
- National Institute for Environmental Studies
- Waseda University

Malaysia:
- Science University of Malaysia
- Malaysian Space Agency
- National University of Malaysia (5 users)
- University Malaysia Sabah

Myanmar:
- Yangon Technological University

Nepal:
- International Centre for Integrated Mountain Development (2 users)
- Institute for Advanced Sustainability Studies
- Institute of Tibetan Plateau Research
- Institute of Engineering

Pakistan:
- University of the Punjab
- National University of Sciences & Technology

Philippines:
- Manila Observatory

Singapore:
- National University of Singapore (2 users)

South Korea:
- Chungnam National University (2 users)
- Gwangju Institute of Science and Technology (2 users)
- Korea Polar Research Institute
- National Institute of Environmental Research (2 users)
- National Meteorological Satellite Center (3 users)
- Yonsei University (3 users)
- Kongju National University
- Seoul National University

Sri Lanka:
- Central Environmental Authority

Taiwan:
- Academia Sinica
- National Central University (2 users)
- Research Center for Environmental Changes

Thailand:
- Asian Institute of Technology
- King Mongkut’s Institute of Technology Ladkrabang

Vietnam:
- University of Science (2 users)

Middle East:

Iran:
- Islamic Azad University
- University
- Atmospheric Science & Meteorological Research Center

Iraq:
- Al Iraqia University
- Mustansiriyah University

Israel:
- Israel Institute for Biological Research
- University of Tel Aviv (2 users)

Oman:
- Sultan Qaboos University

Saudi Arabia:
- King Abdullah University of Science and Technology
- Private individual

United Arab Emirates:
- Khalifa University
- Masdar Institute
- Uruk Engineering & Contracting

North America:

Canada:
- Dalhousie University

United States of America:
- Caltech
- Colorado State University
- Florida State University
- Hampton University
- Harvard-Smithsonian Center for Astrophysics
- Intertek

- Joint Center for Satellite Data Assimilation
- Massachusetts Institute of Technology
- Michigan Technological University (4 users)
- Mote Marine Laboratory
- NASA (2 users)
- Naval Research Laboratory
- NOAA
- Princeton University
- Private Individual
- SpaceKnow Inc.
- Texas A&M University
- The Aerospace Corporation
- Trinity Consultants Inc.
- University of Alabama in Huntsville
- University of Alaska (2 users)
- University of California (2 users)
- University of Central Florida
- University of Colorado Boulder
- University of Maryland
- University of Washington
- Unknown
- USGS
- U.S. Environmental Protection Agency

South America:

Argentina:

- Universidad Nacional de Córdoba
- Universidad Nacional de Rosario

Brazil:

- APAC
- Federal University of Western Pará
- LAPIS
- Universidade Federal de Alagoas

Colombia:

- Universidad EAFIT

Ecuador:

- Universidad San Francisco de Quito (2 users)

Guatemala:

- Ambente
- INSIVUMEH

Mexico:

- Ibero Puebla
- Instituto Politecnico Nacional

Paraguay:
- Universidad San Carlos

Uruguay:
- Universidad de la República

Australia / New Zealand:

- Australian National University
- Bureau of Meteorology
- University of Canterbury (3 users)
- University of Melbourne (2 users)
- University of Southern Queensland (2 users)
- University of Sydney

Africa:

Algeria:
- Meteo Algeria

Cameroon:
- African Institute for Mathematical Sciences

Egypt:
- Egyptian Meteorological Authority (2 users)
- National Research Institute of Astronomy and Geophysics

Eritrea:
- Department of Environment

Ethiopia:
- Addis Ababa University

Ghana:
- Ghana Meteorological Agency
- University of Energy and Natural Resources

Morocco:
- Abdelmalek Essaadi University
- EM5D
- Maroc Météo
- University of Hassan II Casablanca

Nigeria:
- Abdou Moumouni University
- Federal University Lafia

South Africa:
- South African Weather Service (2 users)
- Stellenbosch University
- University of KwaZulu-Natal
- University of Pretoria
- University of the Witwatersrand

Registered users: **577**

8.2. DLR archive

Europe:

Austria:
- University of Innsbruck
- University of Veterinary Medicine
- University of Vienna

Belarus:
- National Academy of Sciences

Belgium:
- BIRA-IASB (6 users)
- Ghent University (6 users)
- KMI (2 users)
- ULB (2 users)

Bulgaria:
- Space Research and Technology Institute (2 users)

Czech Republic:
- Charles University
- Czech Hydrometeorological Institute (5 users)
- Global Change Research Institute

Denmark:
- Aarhus University (2 users)

Estonia:
- Estonian Environment Agency
- Intertrust

Finland:
- FMI (7 users)
- Häme University of Applied Sciences
- University of Helsinki (2 users)

France:
- AERIS/ICARE
- Aix-Marseille University
- CNRS (3 users)
- Grenoble Alpes University
- Institute of Environmental Geosciences
- Laboratory of Atmospheric Optics
- Lasem
- LATMOS (3 users)
- LISA
- LISA-CNRS
- LSCE-IPSL-CNRS
- LPC2E-CNRS
- Météo France (4 users)

- Mines Paristech
- Open University
- Reuniwatt
- Sistema
- University of La Reunion

Germany:

- ask – Innovative Visualisierungslösungen GmbH
- Datiaperti
- DLR (4 users)
- DWD (2 users)
- EUMETSAT (18 users)
- Forschungszentrum Jülich GmbH (2 users)
- Fraunhofer Institute
- Gymnasium Olching
- Heidelberg University
- Karlsruhe Institute of Technology
- Max Planck Institute for Chemistry (5 users)
- Private individual
- Sabrina Szeto Consulting
- Technical University of Munich
- University of Bremen (7 users)
- University of Cologne (2 users)
- University of Hannover
- University of Münster

Greece:

- AUTH (4 users)
- Hellenic Centre for Marine Research
- National Technical University of Athens (2 users)
- Private Individual
- University of Athens
- University of Crete (2 users)

Hungary:

- Hungarian Meteorological Service (2 users)
- Individual
- University of Szeged

Iceland:

- Private individual

Ireland:

- National University of Ireland Galway
- Trinity College Dublin

Italy:

- B-open Solutions S.r.l. (2 users)
- CNR-ISAC
- fabbricadigitale

- IFAC-CNR
- Italian National Research Council
- Julia Wagemann Consulting
- LaMMA Consortium
- MEEO
- National Institute of Geophysics and Volcanology
- Private Individual
- Regional Environmental Protection Agency Calabria
- University of Bologna
- University of Florence
- University of Modena and Reggio Emilia
- University of Venice

Lithuania:
- Lithuanian National Meteorological Service

Malta:
- University of Malta

The Netherlands:
- BESSR
- KNMI (6 users)
- S[&]T Corporation
- Wageningen University & Research (2 users)

Norway:
- UiT The Arctic University of Norway

Poland:
- CloudFerro
- Institute of Environmental Protection (2 users)
- Institute of Geodesy and Cartography
- Institute of Meteorology and Water Management-NRI
- Military University of Technology
- University of Warsaw

Portugal:
- Instituto Dom Luiz (2 users)
- Instituto Português do Mar e da Atmosfera (3 users)
- University of Tras-os-Montes and Alto Douro

Romania:
- Babes-Bolyai University (3 users)
- Global Top Systems
- INOE (4 users)
- National Meteorological Administration (2 users)
- University of Galați (3 users)
- Politehnica University of Bucharest

Russia:
- Altai State University

- Institute of Computational Modeling of the Siberian Branch of the RAS
- Institute of Global Climate and Ecology
- Irkutsk State Transport University
- Planeta

Serbia:
- Geographical institute “Jovan Cvijic”, SASA

Slovakia:
- Private Individual

Slovenia:
- Bide-san, s.p.

Spain:
- Autonomous University of Barcelona
- CREAF-CSIC
- GREA
- Modeliza
- Pablo de Olavide University
- Polytechnic University of Catalonia (2 users)
- State Meteorological Agency
- Universitat Politècnica de València
- University of Alicante
- University of Barcelona (2 users)
- University of Granada (2 users)
- University of Extremadura (2 users)
- University of Oviedo
- University of Valencia (3 users)
- University of Valladolid

Sweden:
- SMHI (4 users)
- The Swedish Defence Research Agency (3 users)

Switzerland:
- Swiss Federal Laboratories for Materials & Technology
- WMO

Turkey:
- Hacettepe University
- Kastamony University
- Middle East Technical University
- Turkish State Meteorological Service (2 users)

Ukraine:
- Scientific Centre for Aerospace Research of the Earth
- UHMC
- Ukrainian Hydrometeorological Institute

UK:
- Airbus S.A.S.

- ECMWF (4 users)
- ESA
- IDEMS International
- Hibarcus
- London School of Hygiene and Tropical Medicine
- Private individual
- Satavia Ltd. (2 users)
- Satellite Applications Catapult
- Science and Technology Facilities Council (2 users)
- siHealth Ltd.
- University of Birmingham
- University of Leeds (2 users)
- University of Leicester (2 users)
- University of York

Asia:

Bangladesh:
- Institute of Forestry and Environmental Sciences
- University of Dhaka

China:
- Anhui Institute of Meteorological Sciences University of Dhaka
- Anhui Institute of Optics and Fine Mechanics (2 users)
- Anhui University
- Beijing Municipal Environmental Monitoring Center
- Beijing Normal University
- Chinese Academy of Meteorological Sciences
- China Academy of Sciences (7 users)
- China Meteorological Administration
- China University of Mining and Technology (6 users)
- HTHJ
- Institute of Atmospheric Physics
- Institute of Geographic Sciences and Natural Resources Research, China Academy of Sciences
- Institute of Remote Sensing and Digital Earth
- Jiangsu Meteorological Observatory
- Jiangsu Normal University (2 users)
- Jinan University
- Lanzhou University
- Nanjing University (2 users)
- Nanjing University of Information Science & Technology (3 users)
- National Satellite Meteorological Center
- Northeast Normal University
- Peking University (2 users)
- School
- Shandong University
- Shanghai University
- Shenzhen University

- Southern University of Science and Technology
- State Environmental Protection Key Lab of Satellite Remote Sensing
- The Chinese University of Hong Kong (2 users)
- The Institute of Atmospheric Physics (2 users)
- Tsinghua University (2 users)
- University of Science and Technology (2 users)
- (unknown) (3 users)
- Wuhan University of Technology
- Zhejiang Academy of Agricultural Sciences
- Zhejiang University

India:
- Anna University
- Aryabhatta Research Institute of Observational Sciences
- Banaras Hindu University
- Birla Institute of Technology
- Bose Institute
- Central University of Hyderabad
- CSIR-NIO
- Dibrugarh University (2 users)
- “Education”
- IIT KGP
- Indian Institute of Remote Sensing
- Indian Institute of Science Education and Research
- Indian Institute of Technology Kharagpur (2 users)
- Indian Institute of Technology Roorkee (2 users)
- Indian Institute of Tropical Meteorology (3 users)
- Indian Space Research Organization (2 users)
- Jawaharlal Nehru University
- Malaviya National Institute of Technology Jaipur
- MSRIT
- National Atmospheric Research Laboratory
- National Centre for Medium Range Weather Forecasting
- Savitribai Phule Pune University (2 users)
- School of Planning and Architecture, Bhobal
- SIG
- University of Calcutta
- University of Hyderabad
- University of Kalyani
- Vikram Sarabhai Space Centre

Indonesia:
- Meteorology, Climatology, and Geophysical Agency (2 users)
- National Institute for Aeronautics and Space
- Sumatera Institute of Technology

Japan:
- Chiba University

- Japan Meteorological Agency
- Kyushu University (4 users)
- National Institute for Environmental Studies
- Remote Sensing Technology Center of Japan
- Waseda University

Malaysia:
- Malaysian Space Agency
- National University of Malaysia (4 users)
- University Malaysia Sabah

Myanmar:
- Yangon Technological University

Nepal:
- Institute for Advanced Sustainability Studies
- Institute of Engineering
- International Centre for Integrated Mountain Development (2 users)

Pakistan:
- National University of Sciences and Technology
- University of the Punjab

Singapore:
- National University of Singapore (2 users)

South Korea:
- Chungnam National University (2 users)
- Gwangju Institute of Science and Technology (2 users)
- Korea Polar Research Institute
- National Institute of Environmental Research (2 users)
- National Meteorological Satellite Center (3 users)
- Seoul National University (4 users)
- Ulsan National Institute of Science and Technology
- Yonsei University (5 users)

Sri Lanka:
- Central Environmental Authority

Taiwan:
- National Central University

Thailand:
- King Mongkut’s Institute of Technology Ladkrabang

Vietnam:
- University of Science (2 users)

Middle East:

Iran:
- Khavaran Institute of Higher Education
- University
- University of Tehran

Iraq:

- Al Iraqia University
- Mustansiriyah University

Israel:

- Ben-Gurion University

Saudi Arabia:

- King Abdulaziz City for Science and Technology
- Private individual

United Arab Emirates:

- Khalifa University
- Masdar Institute
- Uruk Engineering & Contracting

North America:

Canada:

- Environment and Climate Change Canada (4 users)

USA:

- Arizona State University
- Caltech
- Colorado State University
- Florida State University
- Johns Hopkins University
- Hampton University
- Harvard University (3 users)
- Intertek
- Joint Center for Satellite Data Assimilation
- Massachusetts Institute of Technology
- Michigan Technological University (2 users)
- NASA (7 users)
- NOAA (3 users)
- Princeton University
- Private Individual
- Smithsonian Astrophysical Observatory
- SpaceKnow Inc.
- Texas A&M University
- Trinity Consultants Inc.
- University of Alabama in Huntsville
- University of Alaska (2 users)
- University of California (3 users)
- University of Central Florida
- University of Colorado Boulder
- University of Houston
- University of Illinois
- University of Maryland (3 users)

- University of North Carolina at Chapel Hill
- University of Washington (2 users)
- University of Wisconsin-Madison
- Unknown
- USGS
- U.S. Environmental Protection Agency
- Utah State University

South America:

Argentina:
- Argentine Air Force
- Universidad Nacional de Rosario

Brazil:
- APAC
- LAPIS
- Universidade Federal de Alagoas
- University of São Paulo

Colombia:
- Universidad EAFIT

Ecuador:
- Universidad San Francisco de Quito

Guatemala:
- Ambente
- INSIVUMEH

Mexico:
- Ibero Puebla
- Instituto Politecnico Nacional

Paraguay:
- Universidad San Carlos

Uruguay:
- Universidad de la República

Australia / New Zealand:

- Environmental Systems & Services
- University of Canterbury (2 users)
- University of Melbourne (2 users)
- University of Southern Queensland
- University of Wollongong

Africa:

Algeria:
- Meteo Algeria

Cameroon:
- African Institute for Mathematical Sciences

Egypt:

- Egyptian Meteorological Authority (2 users)
- National Research Institute of Astronomy and Geophysics

Eritrea:

- Department of Environment

Ghana:

- Ghana Meteorological Agency

Morocco:

- Abdelmalek Essaadi University
- EM5D
- Maroc Météo
- National Center for Meteorological Research
- University of Hassan II Casablanca

Nigeria:

- Federal University Lafia

South Africa:

- South African Weather Service
- Stellenbosch University
- University of Pretoria
- University of the Witwatersrand
- Ware Jacob Enterprises

Registered users: **514**

8.3. DMI (NUV product via FTP)

- Meteorological Institute of Romania
  ⇒ Several commercial companies obtain the data from MIR
- Danish Meteorological Institute, Denmark
- TrygFonden, Denmark
- Department for Health, Greenland Homerule
- The Danish Cancer Society, Denmark
- Libraries of Hjørring Community
- SunSense AS, Norway
- Richard McKenzie, New Zealand
- Elian Wolfram, Laser Research Center and Applications, Argentina
- KMI, Belgium

Registered users: **10**

8.4. KNMI (unofficial NRT AAI via FTP)

- FMI, Finland
- William B. Hanson Center for Space Science, USA
- University of Leicester, UK

Registered users: **3**

8.5. Known international projects that use EUMETCast or WMO/GTS

- MACC project
- SACS service
- Temis WWW service
- ESA GlobVapour
- ESA CCI Ozone project

8.6. EUMETCast

Albania	4	Iceland	1	Portugal	5
Algeria	4	India	1	Qatar	3
Angola	1	Iran, Islamic Republic of	32	Reunion	1
Armenia	1	Iraq	2	Romania	10
Austria	19	Ireland	7	Russian Federation	7
Azerbaijan	3	Israel	4	Rwanda	2
Belgium	10	Italy	281	San Marino	1
Benin	1	Jordan	1	Saudi Arabia	3
Bosnia and Herzegovina	1	Kazakhstan	6	Senegal	5
Botswana	4	Kenya	6	Serbia	2
Brazil	3	Kuwait	2	Seychelles	1
Bulgaria	6	Kyrgyzstan	1	Slovakia	6
Burkina Faso	1	Latvia	1	Slovenia	1
Cameroon	2	Lebanon	4	South Africa	5
Canada	1	Lesotho	2	South Sudan	1
China	4	Liberia	1	Spain	43
Congo	1	Libya	1	Sudan	1
Congo, Democratic Republic of	1	Lithuania	2	Sweden	5
Croatia	1	Luxembourg	1	Switzerland	15
Cyprus	1	Madagascar	3	Syrian Arab Republic	1
Czech Republic	20	Malawi	2	Tajikistan	1
Denmark	5	Mali	1	Tanzania, United Republic of	3
Egypt	3	Malta	2	Togo	1
Estonia	3	Mauritania	3	Tunisia	3
Eswatini	2	Mauritius	2	Turkey	7
Ethiopia	5	Moldova, Republic of	1	Turkmenistan	1
Finland	5	Morocco	5	Uganda	2
France	56	Mozambique	2	Ukraine	3
Gabon	1	Namibia	1	United Arab Emirates	3
Georgia	1	The Netherlands	21	United Kingdom	112
Germany	104	Niger	2	United States	1
Ghana	5	Nigeria	6	Uzbekistan	1
Greece	18	Norway	4	Vietnam	1
Guinea-Bissau	2	Oman	2	Yemen	1
Hong Kong	1	Pakistan	1	Zambia	3
Hungary	10	Poland	12	Zimbabwe	2
TOTAL (January 2022)	**999**				

9. Updates during the reporting period

Listed below are the major configuration updates concerning operational data processing and archiving. If new versions of relevant AC SAF documents are released during the reporting period, they should be listed here also.

9.1. Software updates

28 February	DLR: DIMS update (version 2.8.0)

9.2. Hardware updates

12 May	FMI: Size of the AC SAF data archive increased 50 TB → 75 TB

9.3. Documentation updates

3 February	FMI: AC SAF Product Requirements Document (issue 1.9.1)
18 February	KNMI: Algorithm Theoretical Basis Document for near real-time, offline and reprocessed vertical ozone profiles and tropospheric ozone column (issue 2.1.2)
25 February	KNMI: Product User Manual for near real-time, offline and reprocessed vertical ozone profiles and tropospheric ozone column (issue 2.5.1)
28 February	RMI/DWD/AUTH: Validation Report for IASI NRT total O3 and O3 profiles (issue 2/2022)
28 February	DLR: DIMS Software Release Note (issue 2.8.0)
28 February	FMI: AC AF System Version Document (issue 1.13)
7 April	FMI: AC SAF Operations Report (issue 2/2021 rev. 1)
26 April	BIRA-IASB: Validation Report for IASI NRT HNO3 (issue 1/1)
28 April	ULB/LATMOS: Product User Manual for IASI NRT HNO3 (issue 1.1)
28 April	ULB/LATMOS: Algorithm Theoretical Basis Document for IASI NRT total O3 and O3 profiles (issue 1.1)
20 June	EUMETSAT: EUMETSAT - AC SAF JOP/OICD (issue v2G)
22 June	FMI: AC SAF Service Specification (issue 1.6)

10. Changes and usage statistics of the web portal

Listed below are the major changes in the appearance and content on the AC SAF main web pages. Additionally some web page usage statistics gathered by Google Analytics are listed.

10.1. Changes in appearance and content

Table 10.1. Changes in appearance and content of the main AC SAF web pages during the reporting period

Date	Description
	Nothing to report.

In addition to updates above, following routine updates are conducted whenever necessary:

- The links to public AC SAF user documents are updated whenever new documents or new versions of existing documents become available
- The "top story" on the front page is updated
- News list on the front page is updated

10.2. Web page statistics

Google Analytics tracking service continuously monitors AC SAF web portal usage. Following diagrams and tables present some statistics gathered during the reporting period.

Note: Google Analytics was updated to version 4 in 18 May. Not all previous information was available after that.

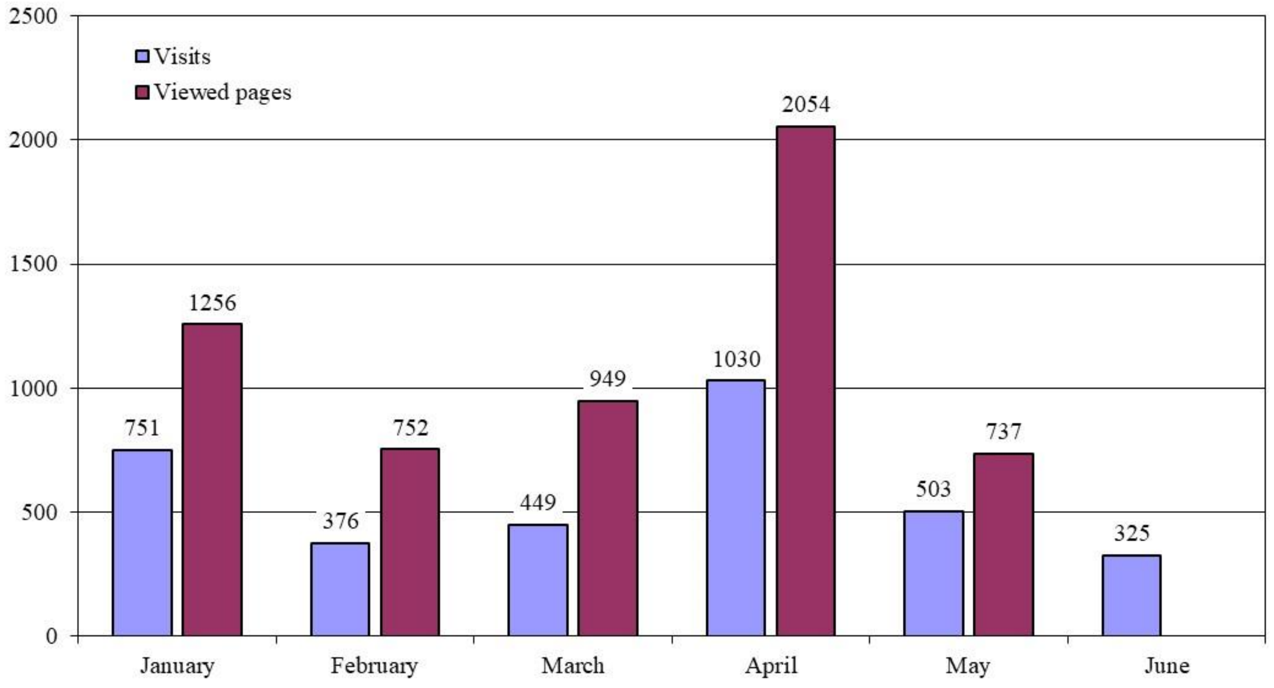

Figure 10.1. Individual visits to the web portal and number of viewed pages

Table 10.2. TOP 5 visiting countries (number of visits in brackets)

January	USA (142)	UK (108)	Australia (64)	Germany (33)	China (32)
February	Belgium (33)	USA (32)	China (25)	Germany (21)	Finland (12)
March	Belgium (60)	China (41)	USA (38)	Germany (31)	Finland (15)
April	USA (93)	China (52)	Belgium (38)	Germany (29)	Brazil (28)
May	Belgium (92)	China (43)	Germany (41)	USA (36)	Finland (29)
June	Belgium (113)	China (43)	USA (28)	Germany (17)	France (15)
Σ	USA (357)	Belgium (336)	China (232)	UK (166)	Germany (153)

Table 10.3. TOP 5 pages (number of views in brackets)

January	index (590)	products/nto_so2 (146)	nrt_access (74)	offline_access (42)	datarecord_access (39)
February	index (295)	offline_access (39)	nrt_access (28)	products/nto_so2 (23)	datarecord_access (21)
March	index (357)	offline_access (80)	datarecord_access (49)	nrt_access (30)	products/oto_no2 (26)
April	index (1765)	publications (35)	offline_access (32)	registration_form (24)	datarecord_access (18)
May	index (469)	nrt_access (71)	offline_access (57)	datarecord_access (45)	registration_form (39)
June	index (322)	nrt_access (31)	offline_access (27)	datarecord_access (22)	datarecords_brotropo (19)
Σ	index (3798)	offline_access (277)	nrt_access (239)	datarecord_access (194)	products_nto_so2 (191)

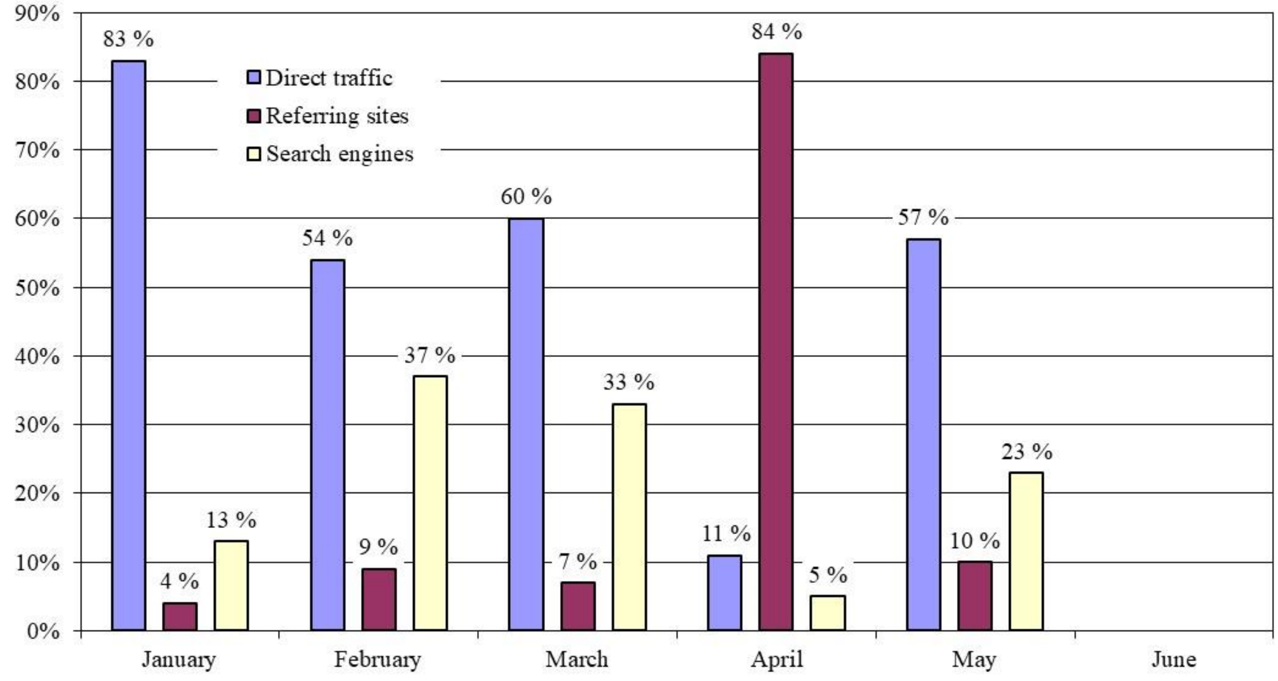

Figure 10.2. Traffic sources by type

Note: high value for referring sites in April is due to visits from “supertraffic.xyz”, which is a commercial web traffic generating “service”

APPENDIX 1

Table A.1 presents the overall summary of orders from AC SAF archive at FMI, sorted by product types, during the reporting period

Table A.2 presents a detailed summary of product orders from AC SAF archive at FMI during the reporting period.

Table A.1. Overall summary of product orders, by product type, during the reporting period

Product type	Number of orders	Number of users	Number of products	Total size
OOP-A	1	1	2	94.5 MB
OOP-B	1	1	1	33.0 MB
OHP-A	9	6	456	115 GB
OHP-B	6	4	440	109 GB
OHP-C	6	4	875	217 GB
ARS-A	3	2	10506	10.5 GB
ARS-B	4	1	11508	11.5 GB
ARS-C	5	1	8791	8.95 GB
ARP-A	3	2	10715	73.9 GB
ARP-B	17	5	45316	299 GB
ARP-C	14	3	7366	50.2 GB
OUV-A	15	3	22003	1.30 GB
OUV-B	19	4	16280	1.21 GB
OUV-AB	19	4	25069	1.96 GB
OUV-BC	18	4	9899	369 MB
LER-MSC-AB	0	-	-	-
LER-PMD-AB	0	-	-	-

Table A.2. More detailed summary of product orders during the reporting period

JANUARY			
Product type	**Number of products**	**Order size**	**Institute / company**
OUV-A OUV-AB OUV-B OUV-BC	Time series for 4383 days Selected subset: ERYDD, VITDD, UVADD, UVBDD, ERYDR, VITDR, UVADR, UVBDR, UVI Location: 2.02E 41.39N (1.52 MB in total)		University of Barcelona, Spain

OUV-A OUV-AB OUV-B OUV-BC	Time series for 4383 days Selected subset: ERYDD, VITDD, UVADD, UVBDD, ERYDR, VITDR, UVADR, UVBDR, UVI Location: 16.50W 28.31N (1.52 MB in total)		University of Barcelona, Spain
OUV-A OUV-AB OUV-B OUV-BC	Time series for 4383 days Selected subset: ERYDD, VITDD, UVADD, UVBDD, ERYDR, VITDR, UVADR, UVBDR, UVI Location: 3.72W 40.45N (1.52 MB in total)		University of Barcelona, Spain
OUV-A OUV-AB OUV-B OUV-BC	Time series for 4383 days Selected subset: ERYDD, VITDD, UVADD, UVBDD, ERYDR, VITDR, UVADR, UVBDR, UVI Location: 3.72W 40.45N (1.52 MB in total)		University of Barcelona, Spain
OUV-A OUV-AB OUV-B OUV-BC	Time series for 4383 days Selected subset: ERYDD, VITDD, UVADD, UVBDD, ERYDR, VITDR, UVADR, UVBDR, UVI Location: 8.42W 43.37N (1.52 MB in total)		University of Barcelona, Spain
OUV-A OUV-AB OUV-B OUV-BC	Time series for 4383 days Selected subset: ERYDD, VITDD, UVADD, UVBDD, ERYDR, VITDR, UVADR, UVBDR, UVI Location: 41.39E 36.50N (1.52 MB in total)		University of Barcelona, Spain
OUV-A OUV-AB OUV-B OUV-BC	Time series for 5114 days Selected subset: ERYDD, VITDD, UVADD, UVBDD, ERYDR, VITDR, UVADR, UVBDR, UVI Location: 6.29W 2.02N (758 kB in total)		University of Barcelona, Spain
ARP-B ARP-C	70 70	963 MB	FMI, Finland
OHP-B	2	503 MB	University of Valencia, Spain
FEBRUARY			
Product type	**Number of products**	**Order size**	**Institute / company**
ARP-B ARP-C	85 86	1.19 GB	FMI, Finland
ARP-A ARP-B	1180 1318	17.4 GB	AUTH, Greece
OHP-B OHP-C	4 5	2.23 GB	IFAC-CNR, Italy

OHP-C	1	251 MB	Sistema, France
ARP-B ARP-C	56 54	758 MB	FMI, Finland
MARCH			
Product type	**Number of products**	**Order size**	**Institute / company**
OHP-A OHP-B	5 4	2.15 GB	IFAC-CNR, Italy
OHP-B	6	1.49 GB	IFAC-CNR, Italy
OHP-A OHP-C	6 5	2.71 GB	IFAC-CNR, Italy
OHP-A	4	983 MB	IFAC-CNR, Italy
OHP-A	1	246 MB	IFAC-CNR, Italy
ARP-B ARP-C	29 28	395 MB	FMI, Finland
ARP-B ARP-C	43 42	589 MB	FMI, Finland
ARP-B ARP-C	14 15	200 MB	FMI, Finland
OUV-AB OUV-B	Time series for 456 days Selected subset: ERYDD, DNADD, PLADD, UVADD, UVBDD, ERYDR, DNADR, PLADR, UVADR, UVBDR, UVI Location: 56.62W 64.20S (78.4 kB in total)		FMI, Finland
OUV-AB OUV-B	Time series for 456 days Selected subset: ERYDD, DNADD, PLADD, UVADD, UVBDD, ERYDR, DNADR, PLADR, UVADR, UVBDR, UVI Location: 60.96W 64.20S (189 kB in total)		FMI, Finland
OUV-AB OUV-B	Time series for 456 days Selected subset: ERYDD, DNADD, PLADD, UVADD, UVBDD, ERYDR, DNADR, PLADR, UVADR, UVBDR, UVI Location: 59.00W 64.20S (78.4 kB in total)		FMI, Finland

OUV-AB OUV-B	Time series for 456 days Selected subset: ERYDD, DNADD, PLADD, UVADD, UVBDD, ERYDR, DNADR, PLADR, UVADR, UVBDR Location: 60.75W 64.00S (73.4 kB in total)		FMI, Finland
APRIL			
Product type	**Number of products**	**Order size**	**Institute / company**
ARP-B ARP-C	63 71	921 MB	FMI, Finland
OUV-A OUV-AB OUV-B OUV-BC	4018 Selected subset: UVADD, UVBDD Region: global (4.82 GB in total)		Intertek, USA
ARS-C	6497	6.63 GB	AUTH, Greece
ARS-C	76	78.2 MB	AUTH, Greece
ARS-A ARS-B	4506 6508	11.0 GB	AUTH, Greece
OUV-A OUV-AB OUV-B OUV-BC	Time series for 5114 days Selected subset: UVI Location: 54.73W 2.41S (307 kB in total)		Federal University of Western Pará, Brazil
OUV-A OUV-AB OUV-B OUV-BC	Time series for 5114 days Selected subset: UVI Location: 54.73W 2.41S (307 kB in total)		Federal University of Western Pará, Brazil
OUV-A OUV-AB OUV-B OUV-BC	Time series for 5114 days Selected subset: UVI Location: 32.50W 5.77S (307 kB in total)		Federal University of Western Pará, Brazil
OUV-A OUV-AB OUV-B OUV-BC	Time series for 5114 days Selected subset: UVI Location: 45.00W 22.60S (307 kB in total)		Federal University of Western Pará, Brazil
OUV-A OUV-AB OUV-B OUV-BC	Time series for 5114 days Selected subset: UVI Location: 58.37W 62.10S (307 kB in total)		Federal University of Western Pará, Brazil
OUV-A OUV-AB OUV-B OUV-BC	Time series for 5114 days Selected subset: UVI Location: 70.91W 53.10S (307 kB in total)		Federal University of Western Pará, Brazil

OUV-A OUV-AB OUV-B OUV-BC	Time series for 5114 days Selected subset: UVI Location: 53.81W 29.60S (307 kB in total)		Federal University of Western Pará, Brazil
OHP-A	1	373 MB	Shenzhen University, China
OOP-B	1	33 MB	Shenzhen University, China
OOP-A	2	94.5 MB	National Remote Sensing Centre, India
OHP-A	1	372 MB	National Remote Sensing Centre, India
ARP-B ARP-C	14 14	192 MB	FMI, Finland
ARP-B ARP-C	13 12	171 MB	FMI, Finland
OUV-BC	Time series for 85 days Selected subset: UVI Location: 24.90E 60.10N (5.67 kB in total)		FMI, Finland
OUV-BC	Time series for 57 days Selected subset: UVI Location: 22.90E 40.60N (4.00 kB in total)		FMI, Finland
OUV-BC	Time series for 57 days Selected subset: UVI Location: 5.10E 52.10N (3.99 kB in total)		FMI, Finland
MAY			
Product type	**Number of products**	**Order size**	**Institute / company**
ARS-B ARS-C	354 354	726 MB	AUTH, Greece
ARS-A ARS-B ARS-C	4303 4303 1520	10.1 GB	AUTH, Greece
OHP-C	14	3.51 GB	Forschungszentrum Jülich GmbH, Germany
OHP-A	14	5.23 GB	Karel de Grote University College, Belgium
ARS-A	1697	1.68 GB	China University of Mining and Technology, China
OHP-C	425	105 GB	University of Science and Technology, China
OHP-A OHP-B OHP-B	423 423 425	314 GB	University of Science and Technology, China
ARP-B ARP-C	56 55	752 MB	FMI, Finland
ARP-B ARP-C	14 14	192 MB	FMI, Finland
ARP-A ARP-B ARP-C	4506 6857 6849	124 GB	AUTH, Greece

ARP-A ARP-B	5029 5165	70.9 GB	AUTH, Greece
OHP-B	1	252 MB	China University of Mining and Technology, China
ARP-B ARP-C	43 42	582 MB	FMI, Finland
ARS-B ARS-C	343 344	708 MB	AUTH, Greece
ARP-B	45981	297 GB	King Abdullah University of Science and Technology, Saudi Arabia
JUNE			
Product type	**Number of products**	**Order size**	**Institute / company**
ARP-B ARP-C	14 14	192 MB	FMI, Finland
OHP-A	1	242 MB	Institute of Atmospheric Physics, China

APPENDIX 2

Table A.3 presents a detailed summary of failed product orders from AC SAF archive at FMI during the reporting period. The middle column indicates whether the failure was related to problems with AC SAF archive and/or ordering system or was the problem on the user's side.

Table A.3. Summary of failed product orders during the reporting period

Date	Error type	Failure description and details
		Order ID: User institute: Order contents: Ordering log error message: ‘’ Failure description: Corrective action: Final outcome: